Investigation of the impacts of emissions on the trace gas budgets in the troposphere by using global climate chemistry model simulations

Eleni Eugenia Tsati

München 2014

Investigation of the impacts of emissions on the trace gas budgets in the troposphere by using global climate chemistry model simulations

Eleni Eugenia Tsati

Dissertation
an der Fakultät für Physik
der Ludwig–Maximilians–Universität
München

vorgelegt von
Eleni Eugenia Tsati
aus Athen, Griechenland

München, Juli 2014

Erstgutachter: Prof. Dr. Martin Dameris
Zweitgutachter: Prof. Dr. Bernhard Mayer
Tag der mündlichen Prüfung: 24.09.2014

Contents

Kurzfassung

Ozon ist eine der wichtigsten chemischen Komponenten der Atmosphäre, die Luftqualität, die Oxidationskapazität der Atmosphäre und den Strahlungstransport beeinflussen. Troposphärisches Ozon entsteht durch die Emission der Vorläufersubstanzen Kohlendioxid, Methan und Nicht-Methan Kohlenwasserstoffe in Anwesenheit von Stickoxiden. Diese Spurengase werden durch anthropogene Aktivitäten und natürliche Quellen, z.B. Biomasseverbrennung, Blitze und Bodenemissionen, emittiert. Um den Beitrag und die Relevanz dieser individuellen Quellen und chemischen Reaktionswege zur beobachteten Ozonkonzentration abschätzen zu können, wird ein effizientes und geeignetes Konzept benötigt. Die hier vorgestellte Tagging Methode bietet ein Konzept zur Unterscheidung und zur quantitativen Bestimmung individueller Beiträge für eine Anzahl von unterschiedlichen Emissionsquellen. Zur Nachverfolgung der individuellen Reaktionswege und Quellen, wurde die Tagging-Methode in das globale Atmosphären-Chemiemodel EMAC integriert.

Die vorliegenden Arbeit ist die Erste, welche den Beitrag von nichtlinear konkurrierenden Substanzen und Gruppen (NO_y, CO, NMHC) zur Konzentration troposphärischen Ozons und HO_x quantifiziert. Um dieses Ziel zu erreichen, wurde ein Ansatz Ozon und HO_x zu taggen ausgearbeitet und im globalen Klima-Chemie Modell EMAC-TAGGING implementiert. Im ersten Teil dieser Studie wird erstmalig daher der Beitrag der oben genannten konkurrierenden Substanzen zur Ozonkonzentration abgeleitet. Dies bildete die Grundlage für ein chemisches Taggingschema, das die Hauptwege der troposphärischen HO_x Chemie beschreibt. Es ist das Erste und einzige seiner Art, welches in einem globalen Klima-Chemie Modell angewendet wurde. Die entwickelte HO_x Tagging Methode lieferte auch einen wichtigen Beitrag im REACT4C Projekt, das den Beitrag des Flugverkehrs auf das Klima untersucht.

Die durchgeführten Untersuchungen deuten auf einen substantiellen Einfluss von Methan und Blitzaktivität auf troposphärisches Ozon hin. In den Tropen beträgt deren Beitrag im Mittel 14% bzw. 22%. Anthropogene Quellen beeinflussen die Nordhalbkugel (NH) und ihr gesamter Beitrag zur Ozonmasse beträgt etwa 38%. Der Industriesektor beeinflusst die NH in den mittleren Breiten mit Werten von 23%. Die gesamte Ozonmasse, die von anthropogenen Emissionen produziert wird beträgt in der Simulation 138 Mt, jene aus dem Blitzsektor mit 115 Mt. Die wichtigste Reaktion zur Ozonproduktion ist die von NO_y Vorläufersubstanzen und dem HO_2 Radikal, da deren Beitrag um 50% höher ist als all jene von NO_y mit der Familie der NMHC (RO_2). Zusammenfassend, in dieser Arbeit wurde eine Taggingmethode entwickelt, mit der der Beitrag emittierter Spurenstoffe auf die Ozonkonzentration erstmalig abgeschätzt werden konnte unter der Berücksichtigung ihrer Konkurrenz in der Ozonproduktion und des Ozonverlustes.

Abstract

Ozone is one of the key chemical components in atmospheric composition relevant for air quality, oxidizing capacity and radiative transfer. Tropospheric ozone is produced by emissions of the precursors, carbon monoxide, methane and non-methane hydrocarbons in the presence of nitrogen oxides. These trace species are emitted by both anthropogenic activities and natural sources e.g. biomass burning, lightning and soils. In order to estimate the contribution importance of individual sources and chemical reaction channels for observed global tropospheric ozone concentrations, an efficient and appropriate concept is required. Here, the tagging approach offers a concept to distinguished and to quantify individual contributions simultaneously for a set of individual emission sources. For this purpose tagging is included in the chemical scheme of the global atmospheric chemistry model EMAC, in order to follow individual reaction pathways and account for individual contributions.

In the present study and for the first time, the quantification of the contributions of non-linearly competing species and families (NO_y, CO, NMHC), to the tropospheric ozone and HO_x concentration has been accomplished. This has come to fruition with the development and implementation of ozone and an HO_x tagging approach in the global atmospheric chemistry climate model EMAC-TAGGING. The first step of this study is to determine the contributions of the competitive species and families NO_y, CO, and NMHCs, to the ozone concentration which has been developed for the first time. Furthermore, a chemical tagged scheme, which describes the main principles of the tropospheric HO_x chemistry has been developed and constitutes the only existing implementation in a global chemistry-climate model. An application of tagged HO_x chemistry with respect to aviation emission sector has been used in as an important contribution, for the REACT4C project.

This investigation shows a major contribution of methane and lightning to tropospheric ozone in the tropics reaching global mean values around 14% and 22%, respectively. Anthropogenic sources affect the Northern Hemisphere (NH) and their total contribution to ozone mass is around 38%. Industry emissions are found to affect the NH at mid-latitudes reaching values around 23%. Also, the total ozone mass produced by anthropogenic emissions is simulated to be around $138\ Mt$ while the lightning is around $115\ Mt$. The leading chemical reaction for ozone production is attributed to NO_y pre-cursors with HO_2 radical since it is 50% higher than the total average of NO_y with NMHC chemical families (RO_2). To summarise, a tagging method has been developed with which the contribution of emitted species to the ozone concentration was estimated for the first time, including their competition in the ozone production and loss.

Chapter 1

Introduction

The Earth's atmosphere is a dynamical and chemical complex system. It is distinguished into layers which are based on the vertical temperature profile. The troposphere is the lowest layer, characterized by decreasing temperature with altitude and extends from the surface to 10 - 17 km above it. The chemical composition includes gases, of which 99% are nitrogen gas (N_2) and oxygen gas (O_2), as well as trace gases covering 1%. A part of 1% is covered by greenhouse gases (e.g. CO_2, O_3, N_2O, CH_4) which are characterized by the increase of the tropospheric temperature once infrared radiation has been absorbed (greenhouse effect).

Tropospheric ozone is produced by the emissions of the precursors, carbon monoxide, methane and non-methane hydrocarbons in the presence of nitrogen oxides. The photochemical (interaction between sunlight and photo-labile molecules) cycle of tropospheric ozone formation is shown in Fig. 1.1. The radicals NO (nitric oxide) and HO_2 (hydroperoxil) react and produce NO_2 (nitrogen dioxide) and OH (hydroxide). Now, the ozone is produced via the photolysis of NO_2 (Crutzen et al., 1999). Nitrogen oxides (NO_x) and non-methane hydrocarbon (NMHC) lead to ozone formation via solar radiation ($h\nu$) (Finlayson-Pitts and Pitts, 1997; Fowler et al., 1998). The carbon compounds, CO (carbon monoxide), CH_4 (methane) and NMHC, produce HO_2 which reacts with nitric oxide and produce ozone. However, the OH and HO_2 radicals also react fast with other trace gases removing them from the atmosphere. This mechanism is the so-called oxidation capacity of the troposphere.

The emissions of the trace gases, such as NMHC, CO and NO_x, can be both natural (e.g. biomass burning, soils) and anthropogenic (e.g. industry, aviation). The increase of the trace gas budget in the troposphere, by man-made sources, leads to increasing greenhouse gases (GHG) concentrations and hence to climate change. It is crucial to investigate firstly, the chemical mechanism which leads to greenhouse gases formation and secondly, the significance of contribution to chemical sectors [1].

[1] Chemical sectors: emission sources divided to natural and man-made categories such as lightning, soils, aviation, industry etc.

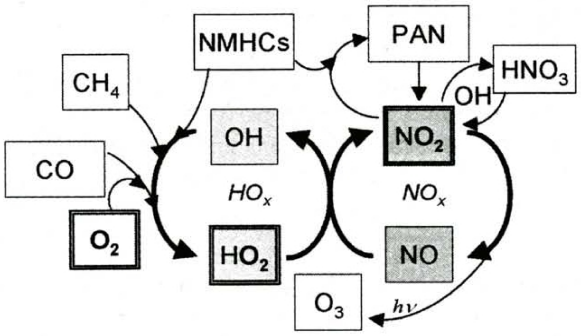

Figure 1.1: Chemical cycle of tropospheric ozone formation, from Grewe (2009)

1.1 State of the art

Considerable attention has been paid to photochemical pollution, such as tropospheric ozone, in relation to global warming from emitted man-made greenhouse gases and in general, in reference to climate change. The radiative forcing (RF) is a measure of how the components of the atmosphere influence the energy balance of the Earth-atmosphere system (Forster et al., 2007). In principle, radiative forcing is used to examine the potential of climate change by the contribution of several drivers (IPCC, 2013). Numerous studies have focused on effect of greenhouse gases and tropospheric ozone to radiative forcing (Hoor et al., 2009; Hansen et al., 2005; Lacis et al., 1990; Myhre et al., 2011; Stevenson et al., 2013). Hansen and Lacis (1990) estimated that radiative forcing due to greenhouse gases will increase by 2-2.5 Wm^{-2}, reaching 4-5 Wm^{-2}, by the middle of this century (RF > 0 corresponds to warming, RF < 0 to cooling). A year later, Wang et al. (1991) calculated these changes of radiative forcing which were due to changes of the concentration of tropospheric ozone. The radiative forcing caused by tropospheric ozone, with respect to the latest (2013) Intergovernmental Panel of Climate Change (IPCC) report is 0.40 Wm^{-2} (IPCC, 2013; Stevenson et al., 2013).

Observations have shown that tropospheric ozone has increased in regions of the Northern Hemisphere (NH), such as United States and western Europe, where emissions of NO_x, CO, CH_4 and NMHC are dominant (Bojkov, 1988; Crutzen, 1973, 1979, 1974; Feister and Warmbt, 1987; Janach, 1989; London and Lui, 1992; Staehelin and Schmid, 1991; Wege et al., 1989; Kley et al., 1993; Karnosky et al., 2007; Finlayson-Pitts and Pitts, 1997; Fowler et al., 1998). There is evidence that for the time period between 1970 to 2000, tropospheric ozone has increased by up to 30% (Oltmans et al., 2006, 1998; Logan et al., 1981; Vingarzan, 2004; IPCC, 2001). In order to investigate the impact of several sectors such as land transportation, industry, aviation and shipping to tropospheric ozone concentration, numerous studies have been done (e.g. (Granier and Brasseur, 2003; Hoor et al., 2009; Myhre et al., 2010; Matthes et al., 2007; Dahlmann et al.,

2011; Grooß et al., 1998; Grewe et al., 2002a,b; Grewe, 2007; Koffi et al., 2010; Dameris et al., 1998)). In 2011, Dahlmann et al. (2011) quantified the global mean ozone column [DU] [2], split by trends (road traffic, aviation, shipping etc), from 1960 to 2019 years period. They found that lightning and aviation cause the highest ozone production, compared to the ground level sources (Lightning: one molecule of NO_x produces 100 molecules of O_3. Aviation: 50 molecules of O_3 per molecule NO_x. Road traffic, shipping and industry: 10 to 30 molecules of O_3 per molecule NO_x). This is explained by the higher amount of UV radiance at higher altitudes as well as the longer life time of ozone at higher altitudes. However, many studies have focused only on the impact of emissions from aviation, to atmospheric composition (e.g. (Dameris et al., 1998; Schumann and Wurzel, 1994; Schumann, 1997; Denman et al., 2007; Johnston et al., 1989)). Schumann (1997) demonstrated that a local increase of up to 10% of the tropospheric ozone concentration (maximized during the summer months) is caused by air traffic.

In 2007, Grewe investigated the contribution of nitrogen oxide emissions to the increase of tropospheric ozone concentration, which is caused by several sectors both natural (lightning, biomass burning, soils, stratosphere) and anthropogenic (industry, land transportation, ships, aviation), using a climate-chemistry model simulations. Grewe showed that the evolution of tropospheric ozone concentration is caused (up to 70% and 40% for NO_y and ozone, respectively) in the tropics and Southern Hemisphere (SH) by lightning (natural sources). In contrast, in the NH where anthropogenic sources are dominant, industry and land transportation cause the major increase in ozone formation (Grewe, 2007).

Later in 2009, Hoor et al., investigated the impact of traffic emissions (including air, ship and land transportation) on ozone and OH. It was found that in the lower troposphere the ozone was sensitive firstly to ship emissions ($50,6\% \pm 10,9\%$), secondly to road emissions ($36,7\% \pm 9,3\%$) and lastly to aviation emissions ($12,7\% \pm 2,9\%$) especially during summertime (low zenith angle). However, in the upper northern troposphere the ozone from air traffic NO_x emissions, exhibits a maximum reaching roughly 70%. In these altitudes the ozone perturbation is higher because of the longer lifetime of NO_x and its reservoir peroxyacyl nitrates (PAN) (Hoor et al., 2009).

To summarize all the above investigations, it is concluded that the anthropogenic emissions in last decades have changed the chemical composition of the troposphere and therefore they played an important role in changing , first the climate variability and second, the air quality mostly in the NH (were mostly man-made emissions occurred).

In the present study and for the first time the contributions of the non-linearly competing species and families NO_y, CO, NMHCs are analyzed in order to quantify the contribution of tropospheric ozone and HO_x by ten different emitting sources via the tagging method (see section 4.3).

[2] 1 Dobson Unit: number of molecules of ozone required to create a 0.01 millimeters thick column of ozone at $0°C$ and 1000 hPa. 1 DU is equivalent to $2.69 \cdot 10^{20}$ ozone molecules per m^2.

1.2 The aim of this investigation

The scientific aim of this study is to quantify the role and the importance of individual emission sources to global atmospheric concentration. Specifically, for this purpose the following questions are addressed:

1. How can the contributions from different emissions sources to concentrations of trace gases be quantified?
2. How important are the contributions from anthropogenic emission sources versus natural ones and which is the main contributor for tropospheric ozone concentration?
3. What is the importance of individual production and loss rates to ozone concentration?
4. How the individual transport emitting sources influence the HO_x chemistry?

First, in order to provide a method for quantifying individual contributions to global distribution of trace gas concentrations, the TAGGING sub-model has been developed which connects to the global climate-chemistry model EMAC and is based on the tagging method Grewe et al. (2010). Tagging method means to quantify the contributions of specific emissions sources to the global atmospheric concentrations, by following the chemical reaction pathways.

Second, this novel tagging method has been applied within the global modular atmospheric model EMAC to ten different emission sources, comprising natural and anthropogenic ones. In detail individual sources are: aviation, shipping, road traffic, industry, biomass burning, soils, lightning, stratosphere, methane (CH_4) and nitrous oxide (N_2O). For the first time, results are shown from applying the tagging method to ozone (O_3), nitrous oxides (NO_y), peroxyacetyl nitrate (PAN), carbon monoxides (CO), non-methane hydrocarbons (NMHC) and hydroxyl radical (HO_x) chemistry in a global chemistry-climate model.

Third, for the first time, a sensitivity study was performed in order to investigate the role of the HO_x chemistry for the individual transport emitting sources. For this purpose, the tropospheric HO_x chemistry is tagged and is additionally included in the previous tagged chemical scheme. This constitutes the only existing implementation in a global chemistry-climate model. Results for the contribution from shipping and aviation emissions on global concentrations of HO_2 and OH are shown. However, large uncertainties in these estimates remain, due to the two basic characteristics of HO_x chemistry are firstly, the short life time (seconds) of these radicals (OH and HO_2) and secondly, the strong interaction between them.

Therefore, two different approaches are contemplated. The first investigation is applied to the system without the tagged HO_x chemistry, when the second one is considered as a whole system [3].

[3] For the first approach the chemical mechanism includes the tagged species: NO_x, NMHC, O_3, CO and PAN. However, the rest of the species or families, such as HO_x, are calculated via background chemistry.

My thesis is organized in the following chapters: The second chapter provides the basic overview of the theoretical background of tropospheric chemistry as well as the main notions which are required for this study. The description of the global climate chemistry model, EMAC, which is used in this study, is presented in third chapter.

The fourth chapter describes the theoretical background of the tagging method which is used to answer the question 1. The model configuration for production results and their characteristics are provided in chapter five. The sixth chapter presents the results of the first approach, without including the HO_x chemistry.

Chapter seven demonstrates the tagging implementation to HO_x chemistry and its results of the sensitivity study based on the individual transport sectors.

Finally, the conclusion of this study and its outlook for further analysis are provided in the eighth chapter.

Chapter 2

An introduction to tropospheric chemistry

Throughout the last decades the tropospheric chemical composition has been changed because of increasing emissions of greenhouse gases and their precursors (Oltmans et al., 2006, 1998; Logan et al., 1981; Vingarzan, 2004; IPCC, 2001, 2013; Crutzen, 1973, 1979; Karnosky et al., 2007). The primary air pollutants are emitted to the troposphere directly from the sources of chemical species (e.g. nitrogen oxides (NO_x), carbon monoxide (CO), non-methane hydrocarbon (NMHC), methane (CH_4). The secondary air pollutants are formed when the primary ones act in the presence of solar radiation ($h\nu$) (e.g. ozone (O_3), peroxyacyl nitrates (PAN)) and eventually lead to the photochemical pollution.

Tropospheric chemistry plays a key role in our understanding of the climate and its evolution. In order to understand the main notions and chemical interactions required for this study, a short summary of the main tropospheric chemical compounds and its basic chemistry is introduced in the following sections (Atkinson, 1990; Atkinson et al., 2003; Olson et al., 2006; Seinfeld and Pandis, 2006).

2.1 Inorganic chemistry

2.1.1 The HO_x family

The HO_x family includes the hydroxyl (OH) and hydroperoxil (HO_2) molecules. These radicals are characterized by fast reactions with trace gases and consequently a short life time (seconds). Figure 2.1, illustrates the chemical cycle of the HO_x family and shows production and loss terms for the hydroxyl and hydroperoxyl. The situations of low (solid lines) and high (dashed lines) NO_x concentration, are taken into consideration so as to reflect the different chemical regimes stemming from different NO_x levels.

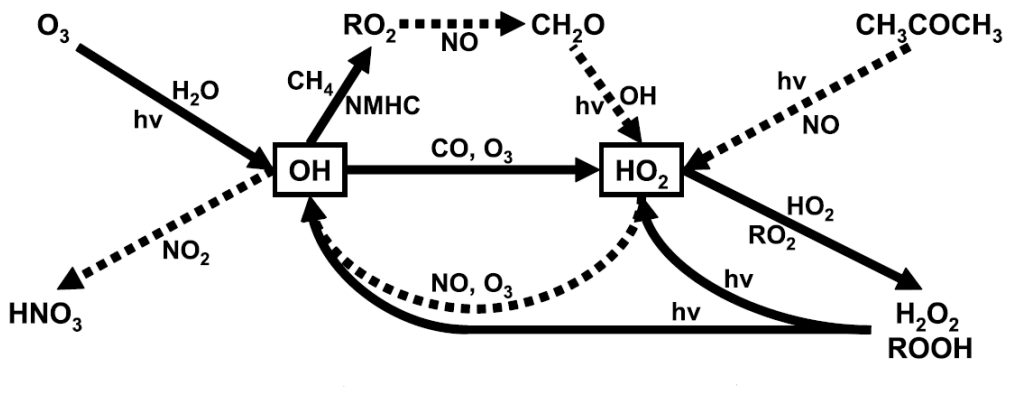

Figure 2.1: Chemical reactions for HO_x family - production and loss pathways. Two different cases are taken into account. Solid lines: low NO_x concentration and dashed lines: high NO_x concentration (Olson et al., 2006).

HO_x chemistry with respect to low NO_x concentration

OH chemistry

The production of hydroxyl radicals starts with the photolysis ($h\nu$) of ozone which occurs for the wavelengths shorter than $319\,\text{nm}$ (Fig. 2.1), with respect to the minimum energy needed to break the potent chemical bond of ozone:

$$O_3 + h\nu \rightarrow O_2 + O(^1D). \tag{2.1}$$

The excited oxygen atom $O(^1D)$ (an atom whose electrons have a higher energy than that of the ground state) reacts with the water vapor by being the source for OH through the reaction:

$$H_2O + O(^1D) \rightarrow 2OH. \tag{2.2}$$

The above gas-phase reaction is the only reaction in troposphere able to break the H-O bond in H_2O. The production of the OH radical is fundamental to the entire troposphere (Monks, 2005).

The second mechanism of OH formation occurs via the photolysis of acids with the general chemical formula ROOH where R stands for organic compounds with hydrogen (general formula: C_vH_{2v+1}) (see also section 2.2). One example is the photolysis with acetic acid:

$$CH_3OOH + h\nu \rightarrow CH_3O + OH. \tag{2.3}$$

However, the depletion of hydroxyl occurs with carbon compounds, methane (CH_4) and non-methane hydrocarbons (NMHC):

$$OH + CH_4 \rightarrow CH_3 + H_2O, \tag{2.4}$$

$$OH + C_2H_6 + O_2 \rightarrow C_2H_5O_2 + H_2O. \tag{2.5}$$

HO_2 chemistry

The most important source of hydroperoxyl is described by the following reaction:

$$CO + OH \rightarrow CO_2 + H. \tag{2.6}$$

The hydrogen atom reacts fast with oxygen and creates one molecule of HO_2:

$$H + O_2 + M \rightarrow HO_2 + M, \tag{2.7}$$

$$Net : CO + OH \rightarrow CO_2 + HO_2. \tag{2.8}$$

The second mechanism for HO_2 formation, is via ozone:

$$OH + O_3 \rightarrow HO_2 + O_2. \tag{2.9}$$

However, the depletion of hydroperoxyl is occurred also via hydroperoxyl or carboxylic acid (RO_2):

$$HO_2 + HO_2 \rightarrow H_2O_2 + O_2, \tag{2.10}$$

$$RO_2 + HO_2 \xrightarrow{O_2} CH_3OOH. \tag{2.11}$$

To conclude, the above chemical equations, it is summarized: first, the formation of OH is taking place via the photolysis of ozone, in the presence of water vapor, as well as via the photolysis of carboxylic acid. Second, the production of HO_2 occurs from the depletion of OH by carbon monoxide or ozone. Third, HO_2 is depleted via itself or via RO_2 (see Fig. 2.1).

HO_x chemistry with respect to high NO_x concentration

As the concentration of nitric oxide increases, changes of hydroxyl and hydroperoxyl concentrations occur (Fig. 2.1, dashed lines).

HO_2 chemistry

Acetone (CH_3COCH_3) is one of HO_x precursors. It is chemically produced at low altitudes and it can be transported to the upper troposphere by deep convection (Folkins and Chatfield, 2000). The chemical equation (2.12) describes the photolysis of acetone (CH_3COCH_3) via nitric oxide, which produces hydroperoxyl:

$$CH_3COCH_3 + h\nu \xrightarrow{2O_2} CH_3C(O)OO + CH_3O_2, \tag{2.12}$$

$$CH_3O_2 + NO \xrightarrow{O_2} HCHO + NO_2 + HO_2. \tag{2.13}$$

Now, the oxidation of HCHO via OH produce an other HO_2 molecule (note that the depletion of OH leads to HO_2 production):

$$HCHO + OH + O_2 \rightarrow HO_2 + CO + H_2O. \tag{2.14}$$

A second mechanism for the HO_2 production is the reaction of OH with methane:

$$OH + CH_4 \rightarrow CH_3O_2 + H_2O, \tag{2.15}$$

$$CH_3O_2 + NO + O_2 \rightarrow CH_2O + HO_2 + NO_2, \tag{2.16}$$

$$CH_2O + OH \rightarrow HO_2 + CO + H_2O. \tag{2.17}$$

The depletion of hydroperoxil radical is described by the following equations:

$$HO_2 + O_3 \rightarrow OH + 2O_2, \tag{2.18}$$

$$HO_2 + NO \rightarrow OH + NO_2. \tag{2.19}$$

OH chemistry

The OH formation is shown on the chemical equations: (2.18) and (2.19). The OH depletion is placed via the chemical equations (2.14), (2.15), (2.17) as well as from the following, with M denoting a collision partner:

$$OH + NO_2 + M \rightarrow HNO_3 + M. \tag{2.20}$$

In case of high NO_x concentrations, the production of OH is taking place via the depletion of HO_2. The HO_2 production is via the photolysis of acetone as well as via the OH depletion (Fig. 2.1).

As far as all the above chemical equations are concerned, in both cases the production of HO_x radicals is most prevalent in tropical regions where high solar energy ($h\nu$) takes place (Fig. 2.2) and influences the ozone chemistry (see Fig. 2.1). The chemical equation (2.2) describes the main source of HO_x radicals. The increase of HO_2 concentrations leads to tropospheric ozone production by reaction (2.19) (see also methane and carbon oxidation chains, section of tropospheric ozone 2.1.3). As long as, the H_2O concentration is low (decreases with the altitude) that leads also to OH loss. However, in upper troposphere, the production of HO_x precursors include acetone and methyl hydroperoxide (CH_3OOH) (Folkins and Chatfield, 2000).

Figure 2.2 shows the annual and zonal mean concentrations of OH and HO_2 radicals as calculated with the EMAC atmospheric chemistry model. High concentrations are simulated in tropical regions at lower altitudes. Also, higher OH concentrations found in the upper tropical troposphere. This is attributed to the NO_x production by lightning which therefore lead to higher OH concentration (see chemical reaction 2.19). A similar zonal mean distribution for the OH concentration is shown in Von Kuhlmann (2001) (similar frames: maxima in the northern tropical regions at lower altitudes). However, no observation data exists for HO_x chemistry so that to compare them with the model results (see the evaluation of the model section 3.4).

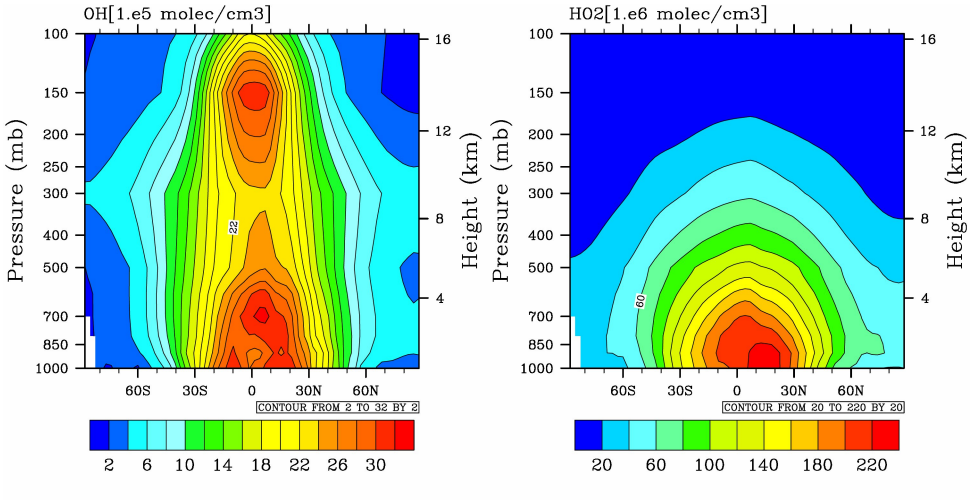

Figure 2.2: Annual zonal mean for OH [10^5 molecules/cm^3] and HO_2 [10^6 molecules/cm^3] concentrations, calculated with the EMAC atmospheric chemistry model.

2.1.2 Nitrogen oxides NO_x

The chemical family of nitrogen oxides includes the two molecules, nitrogen monoxide (NO) and nitrogen dioxide (NO_2). Nitrogen oxides are emitted from combustion, lightning, industry etc. (McConnell and Jin, 2008): The tropospheric chemical cycle is illustrated in Fig. 2.3. The chemical characteristics of nitrogen oxides are different during daytime and night-time. During daytime, and for wavelengths shorter than 400 nm, the photolysis of NO_2 is taking place through the reactions:

$$NO_2 + h\nu \rightarrow NO + O, \tag{2.21}$$

$$O + O_2 + M \rightarrow O_3 + M. \tag{2.22}$$

Ozone reacts with NO through the reaction:

$$O_3 + NO \rightarrow NO_2 + O_2. \tag{2.23}$$

The conversion of NO_2 to nitric acid occurs via the reaction with hydroxyl radical, with M denoting a collision partner:

$$OH + NO_2 + M \rightarrow HNO_3 + M. \tag{2.24}$$

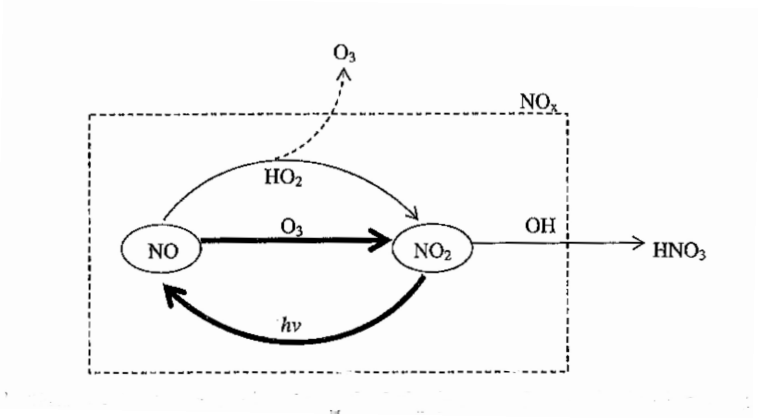

Figure 2.3: Chemical cycle for NO_x family (Seinfeld and Pandis, 2006).

During night-time, almost all of nitrogen oxides convert into NO_3 because NO_2 reacts rapidly with O_3:

$$NO_2 + O_3 \rightarrow NO_3 + O_2. \tag{2.25}$$

Nitrogen oxides are converted into PAN (peroxyacyl nitrates), which is an important reservoir of NO_x. The general chemical formula of PAN is $RC(O)OONO_2$ and the first two compounds are the peroxyacetyl ($CH_3C(O)OONO_2$) and peroxypropionyl nitrate ($CH_3CH_2C(O)OONO_2$). PAN is not confined only to urban areas but it can be transported over long distances in the upper troposphere. It has been identified as one of the most abundant reactive nitrogen-contain species (Roberts, 1990).

$$C_xH_yO_3 + NO_2 \rightleftharpoons C_xH_yO_3NO_2 \tag{2.26}$$

The chemical lifetime of NO_x is short, only few hours, close to the surface. The lifetime increases to a few days or even weeks at higher altitudes. During wintertime, the lifetime is generally longer compared to summertime.

Figure 2.4 shows the annual zonal mean mixing ratio for NO_x (pptv) as calculated with the EMAC atmospheric chemistry model. Maximum distribution simulated in tropical regions at upper troposphere, reaching 520 pptv, results from longer life time of NO_x in conjunction to higher solar radiation. Also, high values simulated, in the northern hemisphere lower troposphere, results from anthropogenic activities (e.g. emissions from industry, road traffic, shipping etc. See Appendix C). A similar zonal mean distribution for NO_x mixing ratio is shown in Kraus et al. (1996) (similar frames: maxima in the northern mid-latitudes due to anthropogenic emission sources, at lower altitudes. Also, maxima mixing ratios in the tropical regions at higher altitudes due to solar radiation).

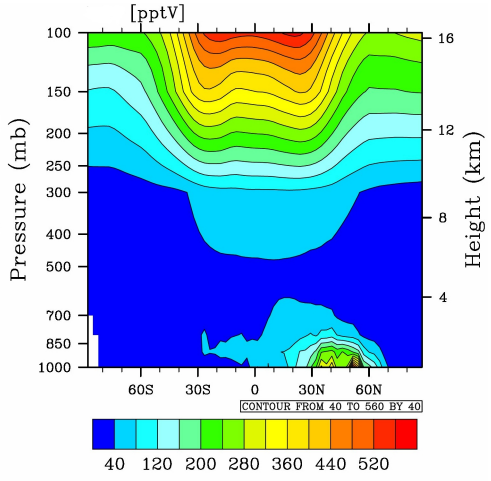

Figure 2.4: Annual zonal mean for NO_x mixing ratios (pptv) as calculated with the EMAC atmospheric chemistry model.

2.1.3 Tropospheric ozone

The tropospheric ozone is produced during the day, via methane (CH_4), carbon monoxide (CO) photochemical oxidation chain in the presence of nitrogen oxides:

Methane oxidation chain:

$$CH_4 + OH + O_2 \rightarrow CH_3O_2 + H_2O \tag{2.27}$$

$$CH_3O_2 + NO \rightarrow CH_3O + NO_2 \tag{2.28}$$

$$CH_3O + O_2 \rightarrow HCHO + HO_2 \tag{2.29}$$

$$HO_2 + NO \rightarrow OH + NO_2 \tag{2.30}$$

$$NO_2 + h\nu \rightarrow NO + O \tag{2.31}$$

$$O + O_2 + M \rightarrow O_3 + M \tag{2.32}$$

$$Net : CH_4 + 4O_2 + 2h\nu \rightarrow HCHO + 2O_3 + H_2O. \tag{2.33}$$

Carbon monoxide oxidation chain:

$$CO + OH \rightarrow CO_2 + H \tag{2.34}$$

$$H + O_2 + M \rightarrow HO_2 + M \tag{2.35}$$

$$HO_2 + NO \rightarrow OH + NO_2 \tag{2.36}$$

$$NO_2 + h\nu \rightarrow NO + O \tag{2.37}$$

$$O + O_2 + M \rightarrow O_3 + M \tag{2.38}$$

$$Net : CO + 2O_2 \rightarrow O_3 + CO_2. \tag{2.39}$$

The ozone concentration in the troposphere depends on the concentration of the precursors NO_x and HO_x. Figure 2.5 shows a typical ozone isopleth in relation to VOCs (volatile organic compounds includes NMHC, CO etc species) and NO_x concentrations which are based on a field campaign in Atlanta, USA (Jeffries and Crouse, 1990) combined with box model calculations.

A hypothetical well mixed box is transposed from the ground, in the city center (a region of most intense sources emissions), to maximum mixing height of 1500 m and for a time period over 14 hours. In order to generate this plot, systematically different initial concentrations of VOCs and NO_x were given to the model and run with the same scenario. The dot point in the figure represents the base case and for initial NO_x and VOCs concentrations equal to 1000 ppb and 600 ppb, respectively. The region above the ridge line corresponds to the low VOCs : NO_x ratio ("*NO_x saturated*" region) and below the ridge line to high VOCs : NO_x ratio ("*NO_x limited*" region). Above the ridge line, as long as VOCs concentration is stable and NO_x concentration decreasing, these two factors lead to an increase in the ozone concentration. The ozone

concentration is depleted whenever, for constant VOCs concentration, either NO_x concentration increases above the ridge line or decreases below that line. Finally, the ozone ridge lines correspond to ozone maximum concentrations which can be achieved from different initial VOCs and NO_x concentrations.

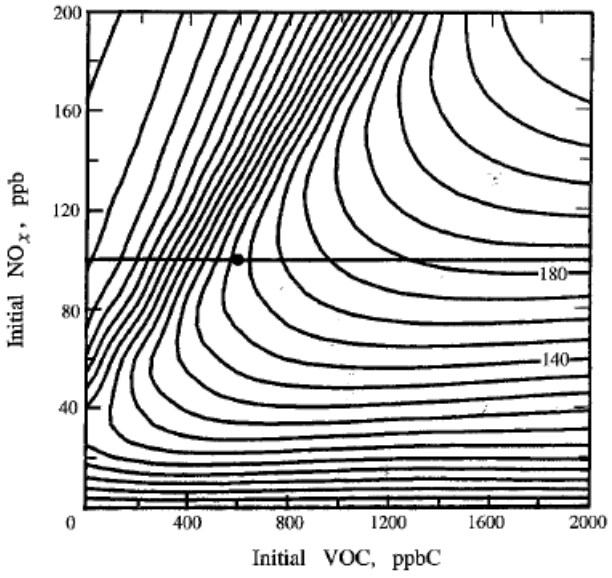

Figure 2.5: Ozone isopleth plot based on simulations of chemistry along air trajectories in Atlanta (Jeffries and Crouse, 1990). Each isopleth is 10 ppb higher in O_3 as one moves upward and to the right (Seinfeld and Pandis, 2006).

However, in higher altitudes (tropopause) the tropospheric ozone concentration owe from the Brewer-Dobson circulation (BDC) (Dobson et al., 1927; Dobson, 1956; Brewer, 1949) in conjunction with ozone production in stratosphere (photolyzed of oxygen molecules O_2) as well as from the stratospheric-tropospheric exchange (STE) (Holton et al., 1995).
The BD circulation is a dynamical process which describes the global meridional and vertical transport and mixing of ozone with other gases in the troposphere and stratosphere regions. In particular, it explains how the air masses move from tropospheric tropical regions in to the stratosphere. In the tropospheric tropic regions, air masses rise vertically into the stratosphere. In the stratosphere, these air masses are moving meridionally to the winter poles. In general, the gravity and the Rossby waves are crucial for the Brewer-Dobson circulation. The Rossby waves owe their origin to the rotation (Coriolis force) and sphericity of the Earth as well as due to a combination of meridional temperature gradients (Rossby, 1939; Blinova, 1943). The Rossby waves are originate in the lower troposphere where are forced to propagate vertically by the deference of adiabatic heating (land-sea) as well as the orography.

In smaller scale, the tropopause folds increase partly the tropospheric ozone concentration by

stratospheric-tropospheric exchange (Holton et al., 1995). The transport of ozone in the troposphere is controlled by these dynamical processes.

Conclusively, the main factors which control the variability of ozone with respect to season, latitude and altitude, are chemical and dynamical (transportation of air masses) processes. The lifetime of ozone is influenced by these two factors. For instance, the lifetime of ozone in tropical boundary layer is only some days, whereas in upper troposphere-lower stratosphere (UTLS) it is between months to a year (IPCC, 2013; Stevenson et al., 2013). However, models show a decrease in ozone lifetime due to climate change (Stevenson et al., 2013).

Figure 2.6 shows the annual tropospheric ozone mixing ratio (ppbv) as calculated with the EMAC atmospheric chemistry model. Large concentration is simulated in the UTLS (upper troposphere-lower stratosphere) polar regions. Also, in the northern hemisphere and lower troposphere is simulated significant ozone contribution by man-made sources (see analysis of tropospheric ozone contribution in chapter 6). However, the shorter life time of ozone at these altitudes leads to less ozone mixing ratios. A similar zonal mean distribution of tropospheric ozone mixing ratios, is shown in Crutzen and Zimmermann (1991); Jöckel et al. (2006). Also the evaluation of the model with respect to ozone chemistry is showing in the section 3.4.

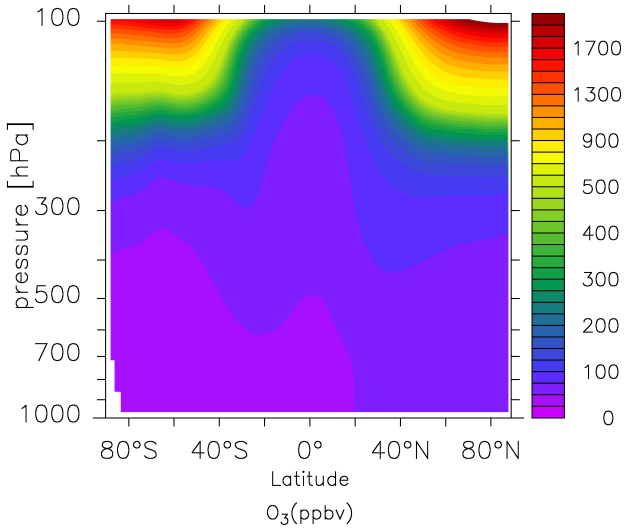

Figure 2.6: Annual zonal mean mixing ratios for O_3 (ppbv) as calculated with the EMAC atmospheric chemistry model.

2.2 Organic chemistry

In the previous sections, the basics of inorganic chemistry have been presented, which nicely demonstrate the principles of tropospheric chemistry. In this section, reactions from the organic chemistry will be elaborated, which influence the chemical composition, such as ozone (photochemical production in the presence of NO_x and light via VOCs) in troposphere. Also, organic compounds such as isoprene (CH_2=C(CH_3)CH=CH_2), which is emitted by photosynthesis, are very important elements for the chemistry in the troposphere (Lerdau and Keller, 1997).

The chemical compounds that include carbon, are called organic compounds (except: carbon monoxide (CO), carbon dioxide (CO_2), carbon acid (H_2CO_3) and carbonates). The organic compounds are classified in different categories which are dubbed homologous series (Table 2.1). The homologous series constitute a specific category of organic compounds and have the following characteristics:

I) They have the same chemical features because they belong to the same chemical function group.

II) Every member which belongs to the same chemical group differs from the next one with the factor of -CH_2-, methylene.

Large quantities of organic compounds are coming from biogenic and anthropogenic emissions. The organic compounds (RH) react with hydroxyl (see chemical reaction 2.40) and nitrate radicals (see chemical reaction 2.41) hence playing a key role in lower tropospheric chemistry (Atkinson, 1990; Atkinson et al., 2003). With R is defined as C_vH_{2v+1}. The general chemical reactions are the following:

$$OH + RH \rightarrow H_2O + R \tag{2.40}$$

$$NO_3 + RH \rightarrow HNO_3 + R \tag{2.41}$$

$$RO_2 + NO \rightarrow RONO_2 \tag{2.42}$$

$$RO_2 + NO \rightarrow RO + NO_2. \tag{2.43}$$

The general chemical formula (2.43) applies to the chemical equation (2.28). The chemical equation (2.28) is the pathway for the chemical reaction (2.30) with the last one to produce ozone in the presence of solar radiation.

This was an overview of the theoretical background for tropospheric chemistry, covering the main characteristics and impacts of inorganic and organic chemistry.

Name	Function group	General formula	
Alkanes	$C-C$	RH or C_vH_{2v+2}	(v $\geq$ 1)
	Example:	CH_3-CH_2-CH_3	
Alkenes	$C=C$	RH or C_vH_{2v}	(v $\geq$ 2)
	Example:	CH_3-CH=CH_2	
Alkynes	$C\equiv C$	RH or C_vH_{2v-2}	(v $\geq$ 2)
	Example:	CH_3-$C\equiv C$H	
Alcohols	$C-OH$	ROH or C_vH_{2v+2}O	(v $\geq$ 1)
	Example:	CH_3-CH_2OH	
Etheres	$C-O-C$	R-O-R' or C_vH_{2v-2}	(v $\geq$ 2)
	Example:	CH_3-CH_2-O-CH_2-CH_3	
Aldehydes	$CH=O$	RCH=O or C_vH_{2v}O	(v $\geq$ 1)
	Example:	CH_3-CH=O	
Ketones	$C-C(=O)-C$	R-C(=O)-R' or C_vH_{2v}O	(v $\geq$ 3)
	Example:	CH_3-C(=O)-CH_3	
Carboxylic acids	$O=C-OH$	RCOOH or C_vH_{2v}O	(v $\geq$ 1)
	Example:	CH_3COOH	

Table 2.1: Groups of some homologous series (McMurry, 1984).

Chapter 3

The EMAC atmospheric chemistry model

The global atmospheric chemistry-climate model EMAC is a numerical simulation system. In general, the model allows to describe the chemistry and the meteorological processes in the troposphere and the middle atmosphere and their interactions with the ocean, land and human influences (Jöckel et al., 2006) using sub-models. The EMAC model consists of two parts, the base model (Roeckner et al., 2003) and the standard interface models. The base model is the general circulation model ECHAM5 (version echam5.3.01). It solves the primitive equations of radiation, moisture, temperature, motion etc. The MESSy (Modular Earth Submodel System) interface model (version 1.10) (Jöckel et al., 2005) couples all the processes among the sub-models (modular entities which are describe the chemical, physical and biological processes) as well as their simulations to ECHAM5.

In this chapter, first, a short description of the atmospheric general circulation model ECHAM and second, of MESSy interface model, are given.

3.1 The atmospheric general circulation model, ECHAM

The atmospheric general circulation model, ECHAM, is developed from the spectral weather prediction model of the European Centre for Medium-Range Weather Forecasts, ECMWF (Simmons et al., 1989). The current version, ECHAM5, was developed at the Max Planck Institute for Meteorology, Hamburg (Roeckner et al., 2003). ECHAM5 is a spectral model which solves the atmospheric primitive equations (differential equations for momentum, temperature etc.) horizontally (Roeckner et al., 2003). It includes five prognostic variables: vorticity (ξ), divergence (D), temperature (T) logarithm of the surface pressure (p_s) and specific humidity (q). These variables are represented in spherical harmonics, except for the specific humidity which is calculated in the grid point space. The horizontal resolution is formulated in spectral space and divided in several harmonics.

In order to define the pressure levels, the model uses hybrid coordinates (A_i and B_i) which are

defined in a way that follows the orography close to surface (lower troposphere) and represents pressure levels at higher altitudes. The pressure of a layer center p_i, at the time t, is defined as:

$$p_i(\lambda, \varphi, t) = A_i + B_i p_s(\lambda, \varphi, t) \tag{3.1}$$

where λ describes the longitude and φ the latitude ($\lambda \in [0°, 360°]$, $\varphi \in [-90°, 90°]$). The lowest pressure is represented by the factor p_1 (level 1).

The time step of the model is dependent on the horizontal and vertical resolution. The Courant-Friedrich-Lewy criterion,($\frac{u\Delta t}{\Delta x} < 1$, with *u* being the velocity, Δx and Δt the grid length and the time step, respectively) must be satisfied for any particular solution. The Courant-Friedrich-Lewy criterion demands that the time an air parcel needs to travel through a grid cell, to be longer than the time step of the model.

3.2 The Modular Earth Sub-model System MESSy

The modular Earth sub-model system, MESSy has been developed at the Max Planck Institute for Chemistry, Mainz (Jöckel et al., 2006). The purpose is to investigate the interactions among physical, chemical and biological processes covering different domains such as land, ocean, atmosphere etc. (Jöckel et al., 2005). The idea was to develop one model code for all projects covering all contributions which will be independent of the base model, (general circulation models, GCM such as ECHAM5). Figure 3.1 illustrates the general structure of this interaction. Each specific physical, chemical or biological processes is a separate and independent modular entity and is described by a sub-model. The MESSy interface model is the connecting link, first between the base model (in this study ECHAM5) and several sub-models, and second, among the sub-models. In general, the user has the flexibility to switch on/off sub-models depending the purpose of his study. The MESSy base model has been applied to the general circulation model ECHAM5 and to numerous box-models (Jöckel et al., 2005).

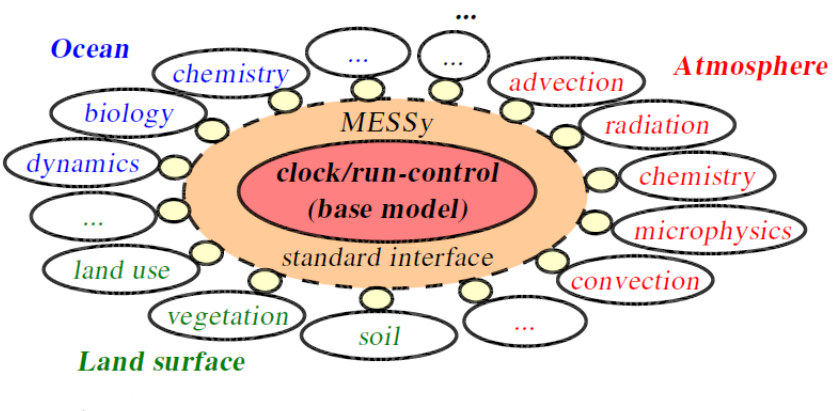

Figure 3.1: Several physical, chemical and biological modular entities connected via the interface (Jöckel et al., 2005).

MESSy is separated into four layers:

⋆ *The Base Model Layer, (BML):* This is ECHAM5 (Fig. 3.1, red color).

⋆ *The Base Model Interface Layer, (BMIL):* It controls the data exchange between the sub-models interface layer and the base model (Fig. 3.1, orange color).

⋆ *The sub-model Interface Layer, (SMIL):* It handles all informations from BMIL and transfers them to sub-model core layer (SMCL). Also, it is responsible for the coupling between different sub-models (Fig. 3.1, yellow color).

⋆ *The sub-model Core Layer, (SMCL):* is independent of the base model and contains the

core routines for a sub-model such as physics, chemical integrations, diagnostic calculations etc (Fig. 3.1, white color).

3.3 The EMAC model set-up: T42L41DLR simulation

3.3.1 The ECHAM set-up

In this study (ECHAM version echam5.3.01), the T42 resolution is used, which corresponds to a grid of 64 cells along the latitude and 128 along the longitude (width of each cell approximately $2.8^\circ \times 2.8^\circ$ (latitude $\times$ longitude) (Roeckner et al., 2003)). The vertical resolution, for this study, is L41DLR where the upper layer is centered at 5 hPa. The atmosphere is divided in not equidistant vertical layers up to 5 hPa. The time step of this simulation is fifteen minutes and the output is set to produce instantaneous values with an interval of five hours.

3.3.2 The MESSy set-up

The MESSy (version 1.10) sub-models are divided in three main categories, which are: emissions, physics and chemistry. The new TAGGING sub-model is a part to the chemistry and it detailed description is presented in chapters 4 and 5. In this study the following sub-models are used:

Emissions

• **OFFLEM** sub-model provides emissions to the model from IPCC Lamarque et al. (2010) and QUANTIFY Borken et al. (2007); Lee et al. (2005) (see detailed description Appendix C). It reads surface, multi-layer and volume emissions from data files via the MESSy interface (Jöckel et al., 2006; Kerkweg et al., 2006).

• **ONLEM** sub-model calculates the tracer tendencies due to online emissions emissions for gas-phase tracers such as biogenic emissions, CH_4, N_2O and stratosphere (see detailed description Appendix C). The flux of these emissions are characterized by the dependence of the actual state of the model in the atmosphere such as wind speed, season, etc. For this reason, these emissions have to be calculated for every time step during the simulations (Kerkweg et al., 2006; Jöckel et al., 2006).

• **LNOx** sub-model calculates the production of NO_x from lightning for every timestep. It is also depending on the current atmospheric conditions as ONLEM (Jöckel et al., 2006).

Physics

- **JVAL** sub-model calculates the photolysis rate coefficients (Landgraf and Crutzen, 1998), (Jöckel et al., 2006).

- **CLOUD** sub-model calculates the precipitation (Roeckner et al., 2006; Jöckel et al., 2006).

- **CONVECT** sub-model calculates the convection and the convective transport of the chemical species (Tost et al., 2006; Tost, 2006; Jöckel et al., 2006).

- **HETCHEM** sub-model calculates heterogeneous reaction rates of species reacting on particles, in the troposphere region (Jöckel et al., 2006).

- **PSC** sub-model calculates the reaction rates coefficients (Kirner et al., 2010).

- **RAD4ALL** sub-model calculates the radiative transfer and provides heating rates (Roeckner et al., 1996; Jöckel et al., 2006).

- **SCAV** sub-model calculates the processes of wet deposition (Tost et al., 2006; Tost, 2006; Jöckel et al., 2006).

- **TROPOP** sub-model calculates the altitude as well as the height of the planetary boundary layer (Jöckel et al., 2006).

  Chemistry

- **MECCA** (Module Efficiently Calculating the Chemistry of the Atmosphere) sub-model contains the tropospheric chemical reactions. The included 62 chemical reactions consist the chemical schemes of HO_x, NO_x, methane, ozone, non methane hydrocarbons (NMHC). The reaction rates depend on atmospheric parameters such as temperature, pressure, radiation etc. (Jöckel et al., 2006; Sander et al., 2005).

- **TAGGING** sub-model contains the tagging method (see section 4.3). It quantifies the concentration of contribution of chemical species by following the reactions path-ways. The chemical species or families which were implemented: NO_y, O_3, PAN, NMHC and CO. The new version also includes the HO_x chemistry and quantifies the tropospheric ozone contribution by including also NMHC and CO concentrations. (detailed description in chapters 4, 5 and 7).

3.4 Evaluation of the model

Since the distribution of ozone and hydroxyl radicals in the troposphere is one of the main themes of this thesis, in this section basic results of the reference model configuration are evaluated.

In order to evaluate an atmospheric-chemistry general circulation model, the comparison between the model results with observations and other model studies is required. Jöckel et al. (2006) presented the evaluation of the EMAC model (version MESSy1.1 and echam5.3.01) with respect to tropospheric chemistry on the distributions of ozone, hydroxyl radicals, carbon monoxide and reactive nitrogen compounds. The inter-comparison of both model results and observations covers the time period between 1998 and 2005 (Jöckel et al., 2006). The model reference simulation has been performed for the spectral T42 horizontal and L90MA-layer vertical resolutions with explicit middle atmospheric (MA) dynamics. However, in the present study the simulations have been performed by using the T42L41DLR resolution (see section 3.1). Since there are no available studies investigating the evaluation of the model by using this vertical resolution, in this section the comparison between the T42L90MA (MA: middle atmosphere; up to 0.01 hPa) and the T42L41DLR (up to 5 hPa) simulations is shown. Nevertheless, it has to be emphasised it that the different input emission datasets (e.g. emissions from aviation in (Jöckel et al., 2006): Schmitt and Brunner (1997), present study: Lee et al. (2005)), which have been used in the two different simulations, lead to quantitative differences. Also, the different tropospheric NO_x budget from lightning per year (Jöckel et al. (2006) is 2.19 Tg(N)/year; present study 4.7 Tg(N)/year) is the cause of larger OH concentration in the tropical UTLS region.

Ozone

Figure 3.2 shows the zonal mean of ozone (ppbv) in the troposphere for the T42L90MA and the T42L41DLR resolutions, respectively.

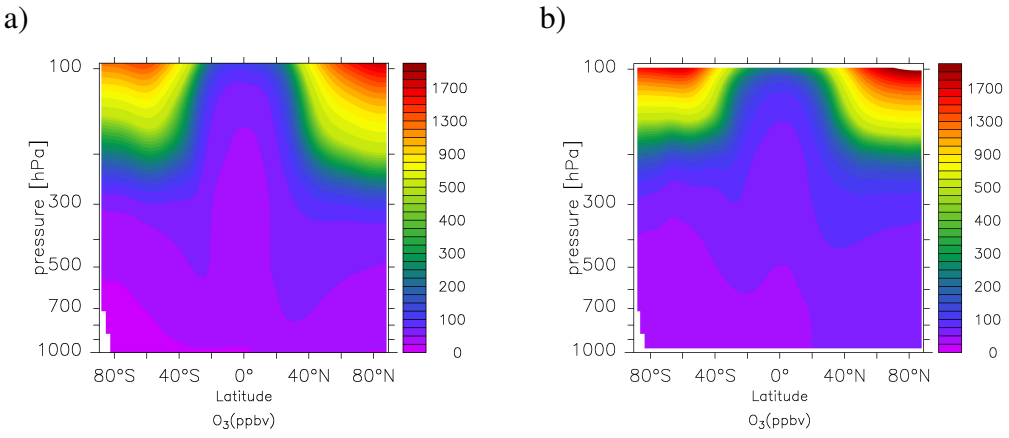

Figure 3.2: Zonal mean of ozone (ppbv) mixing ratios for **a)** 2000 to 2004 by using the T42L90MA simulation (for details of the simulation, see Jöckel et al., 2006) and **b)** 2001 to 2002 by using the T42L41DLR simulation.

For Fig. 3.2a) the time period covers five simulation years, between 2000 and 2004 (for details of the simulation, see Jöckel et al., 2006). In comparison, Fig 3.2b) represents the two simulation years between 2001 to 2002. Both figures show the maximum mixing ratios of above 1700 ppbv in the polar stratosphere close to 100 hPa. In the lower troposphere the range of the mixing ratios is between around 20 to 120 ppbv.

For the T42L90MA resolution (Fig 3.2a), the tropospheric distribution exhibits a symmetry according to the equator for values around 50 ppbv. In contrast, a similar symmetry with respect to the equator exhibits higher values, around 100 ppbv, the T42L41DLR (Fig 3.2b) simulation. This difference can be attributed to the different simulation periods.

Hydroxyl radical

Figures 3.3 and 3.4 show the seasonal zonal averages of OH (10^6 cm^{-3}) with respect to the T42L90MA and T42L41DLR resolutions, respectively. Although, Fig. 3.3 was averaged over five simulations years, between 2000 to 2004, since Fig. 3.4 was averaged over two years (2001 to 2002), only. The maximum concentrations of OH are found in the NH at mid latitudes during MAM and JJA in the lower troposphere. This is attributed to the fact that the OH formation depends on the solar energy (hv) and water vapor (H_2O) (see chemical reaction 2.2). Furthermore, the secondary formation of OH depend on the NO_x concentration (see section 2.1.1). Since the NH is more polluted than the SH more NO_x emissions lead to larger OH concentrations (see chapter 6.1.1).

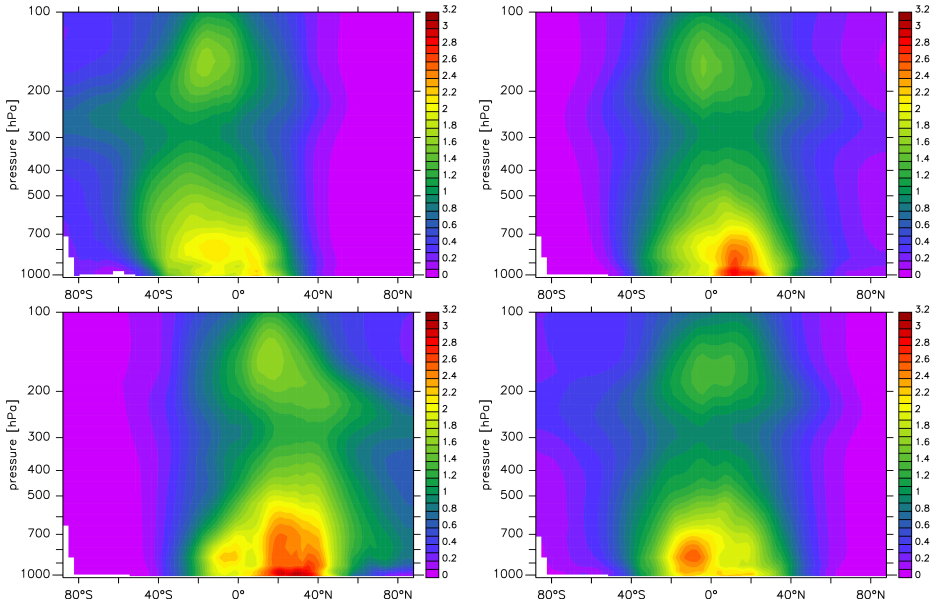

Figure 3.3: Zonal mean of OH (10^6 cm^{-3}) concentration averaged over the five simulation years: DJF (up left), MAM (up right), JJA (down left) and SON (down right) (Jöckel et al., 2006).

Figure 3.4 shows the OH concentration averaged over the two simulation years from 2001 to 2002, by using the T42L41DLR resolution. One difference compared to the T42L90MA resolution, is that the local maximum in the tropical UTLS (upper troposphere - lower stratosphere) region is larger. This is attributed to the stronger NO_x production by lightning which therefore lead to higher OH concentration. Another difference is that in the lower troposphere in the NH at mid latitudes and for DJF (December January February) and SON (September October November), maxima of the OH concentration are found. This is also attributed to the secondary OH formation due to enhanced NO_x concentrations arising from to the more polluted NH.

Since the additional vertical layers in the T42L90MA resolution compared to the T42L41DLR resolution are located mainly in the stratosphere, the differences in the troposphere are the results of different emission datastes as well as of different budgets of NO_x formation by lightning. Additionally, it has to be emphasized that qualitatively the results match between the two simulations. All in all, the conclusion can be drawn, that despite the quantitative differences in O_3 and HO_2, between the simulations, the T42L41DLR resolution can be used for tropospheric chemistry analysis as well as for predicting of the actual tropospheric chemical composition.

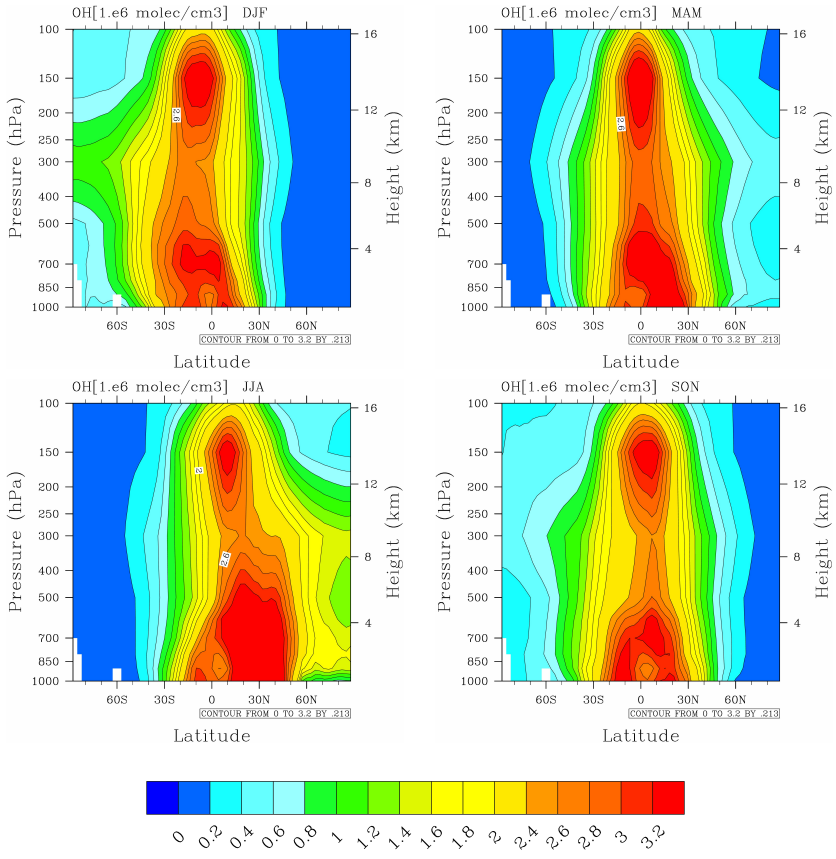

Figure 3.4: Zonal mean of OH (10^6 cm^{-3}) concentration averaged over the two simulation years: DJF (upper left), MAM (upper right), JJA (down left) and SON (down left).

Chapter 4

Methods to estimate the contribution of emissions to atmospheric concentrations

In this chapter, a summary of the perturbation and the tagging methods is presented. The perturbation method determines the changes of a concentration due to a perturbation of an emission. This concentration change is then taken as the contribution of the respective emission to the this concentration. In comparison, the tagging method estimates the concentration of individual species by the contribution of individual sectors by following reaction pathways. The goal of using these two methodologies is to understand how a specific emission (natural or anthropogenic) sector influences the tropospheric chemical composition. This present study is focusing on the importance of understanding the contribution of an emission category on the chemistry.

The perturbation method is based on the difference between two simulations, the base case (all emissions) and the perturbation case which refers to a simulation were the emissions of the respective category are perturbed (e.g. (Fuglestvedt et al., 2008; Wang et al., 2009; Hoor et al., 2009)). On the other hand, the tagging method is based on one simulation only and analyses the contribution of emissions to concentrations by following reaction pathways. Several tagging methods have been published (e.g. (Gromov et al., 2010; Horowitz and Jacob, 1999; Butler et al., 2011; Emmons et al., 2012)) using different designs but have in common the use of tagged species. Grewe et al. (2010) first focused on tagging an entire chemical system (tagged the competitive chemical species and families NO_y, CO etc to the ozone concentration) and not only one sub-species, compared to previous tagging methodologies. The tagging method (Grewe et al., 2010) follows the reaction pathways and quantifies the attribution of a specific emissions category. Additionally, it should be emphasized that using this tagging method, the non-linearity of a chemical system is taken into account.

In order to clarify the difference between the perturbation and tagging method, the following example can be used: A car in Munich city-center emits NO. Through the chemical process the local NO_y concentration will increase. Thereby, the ozone production will start increasing too. However, the ozone loss rates will increase also, due to high NO_y concentration (see chemical

equation 2.25) in this area and thus will lead to low ozone concentrations. The NO_y molecules will be transported by the wind far from the emitting source. Roughly, 30 km west far, at the DLR area, the background of NO_y concentration will increase. Since in this area no NO emissions occur, the ozone loss rates compared to te city-center will be low. This now leads to the increase of local ozone concentration. This example shows explicitly how the ozone contribution of a car emission, can be quantified by following the reaction pathways as the tagging method does.

Now, an example for the perturbation method: back to the city-center the car start emitting NO to the local area additionally to the background. As before, the NO_y molecules will be transported by the wind to the DLR area. However, there is a case where the local ozone concentration at DLR will be unchanged, despite of the increase of NO_y concentration (see Fig. 2.5, ozone isopleth lines: case where the efficiency of NO_y molecules to reduce-increase ozone, decreases). In this case the car contribution to the ozone concentration, at the DLR area, is calculated to be zero even though NO is emitting, to the atmosphere, which taking part of the ozone formation. Since the perturbation method can estimate the car contribution due to the changes of ozone concentration, this leads to the conclusion that this method is not enough to describe the contribution of the emitting sources, to the atmospheric concentrations.

The purpose of this section is to present a short summary of the tagging method (see analytical description in Grewe et al. (2010)). For this reason, the main formulas which comprise the theoretical background of this method as well as used for its implementation in EMAC model, are presented. The comparison between the perturbation and the tagging method is required so that the main advantages of the tagging method are properly manifested (see sections 4.3 and 4.4). The analytical solutions of these methods are applied to non-linear simple chemical systems which are adequate to investigate the basic principles of the tagging mechanism in a framework similar to the tropospheric ozone chemistry. Thereby, the analysis can proceed much more easily.

First, a short description for both systems is presented. Subsequently, the two methodologies, perturbation and the tagging are explained, applied to both chemical systems and an analytical solution is derived.

4.1 Ozone tagging chemical scheme

In this section, the determination of the ozone tagging chemical scheme is presented. Tagging a chemical scheme means to specify the origins of the chemical compounds with respect to emission sources (e.g. NO emitted from road traffic, aviation etc).

Figure 4.1a) simply shows chemical compounds which constitute a part of the tropospheric chemistry. The tropospheric chemistry is too complex to tag every individual species. For this reason only those species are tagged which are relevant to tropospheric ozone chemistry. The tagged species are combined into different chemical families such as NMHC, NO_y, HO_x and PAN (see Fig. 4.1b)).

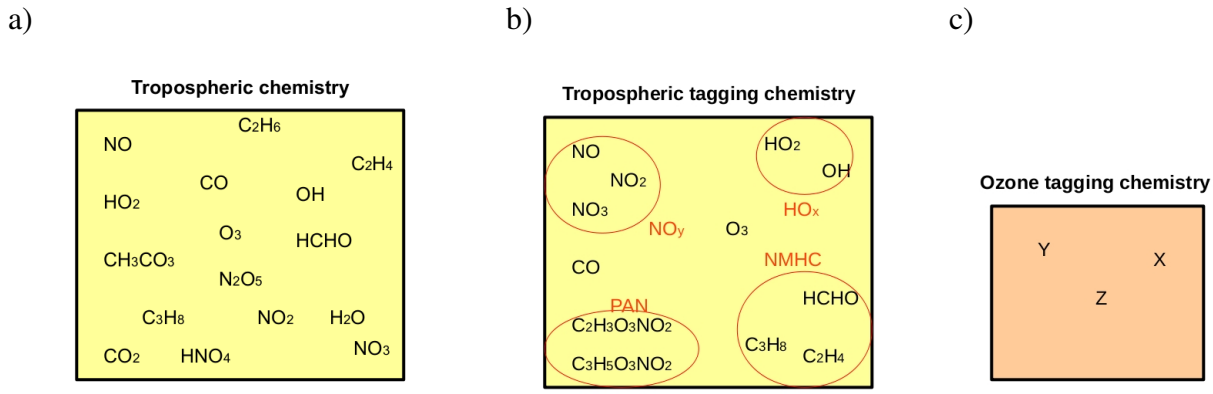

Figure 4.1: Chemical compounds which are relevant for tropospheric chemistry a) and how they are represented in the tagging scheme. Some chemical species are combined into families (red). b) Ozone tagging chemical scheme based on the academic families-species X, Y and Z.

In the following, two academic chemical systems are introduced which only consist of three chemical species X, Y and Z. Examples are given in order to motivate the relation between X, Y, Z and the chemical families and species, NMHC-HO_x, NO_y and O_3, respectively.

Ozone production

- **Example 1: NMHC + NO_y**

$$CH_3O_2 + NO \xrightarrow{O_2} HCHO + HO_2 + NO_2 \tag{4.1}$$

$$NO_2 + h\nu \rightarrow NO + O \tag{4.2}$$

$$O + O_2 + M \rightarrow O_3 + M \tag{4.3}$$

Summing the above chemical reactions that leads to the following, where Air refers to O_2:

$$CH_3O_2 + (NO + NO_2) \xrightarrow{+Air} HCHO + HO_2 + (NO + NO_2) + O_3 \tag{4.4}$$

and by using chemical families (Note that the NMHC and HO_x are defined as X):

$$NMHC + NO_y \xrightarrow{+Air} (NMHC - HO_x) + NO_y + O_3 \tag{4.5}$$

- **Example 2: HO_x + NO_y**
  The sum of ozone production which is described via the chemical equations 2.36 to 2.38 is written as:

$$HO_x + NO_y \xrightarrow{+Air} HO_x + NO_y + O_3 \tag{4.6}$$

Now, the chemical equations 4.5 and 4.6 motivate the reaction:

$$X + Y \xrightarrow{+Air} Z + X + Y \tag{4.7}$$

Ozone loss

$$NO + O_3 \rightarrow NO_2 + O_2 \tag{4.8}$$

$$NO_2 + O_3 \rightarrow NO_3 + O_2 \tag{4.9}$$

Similarly, summing the above chemical equations:

$$(NO + NO_2) + O_3 \rightarrow (NO + NO_2) + O_2 \tag{4.10}$$

and by using chemical families:

$$NO_y + O_3 \rightarrow NO_y + O_2 \tag{4.11}$$

Which motivate the reaction:

$$Y + Z \rightarrow Y + Air \tag{4.12}$$

Similarly, via the chemical equations 2.9, 2.18 (same with NMHC):

$$HO_x + O_3 \rightarrow HO_x + O_2 \tag{4.13}$$

which leads to:

$$X + Z \rightarrow X + Air \tag{4.14}$$

The tropospheric chemistry is not linear, for this reason two different non-linear systems have been chosen in order to implement and compare the perturbation and the tagging method (for more detailed description see Grewe et al. (2010)). In particular, the equations (A.1) to (A.3) and (B.1) to (B.3) describe the first and the second chemical systems, respectively. The $\tilde{Z}$ refers to the second chemical system and it has also similarities to ozone chemistry.

First chemical system:

$$\begin{aligned} X + Y &\longrightarrow Z + X + Y && (A.1)\\ X + Z &\longrightarrow X && (A.2)\\ Y + Z &\longrightarrow Y && (A.3) \end{aligned}$$

Second chemical system:

$$\begin{aligned} X + Y &\longrightarrow \tilde{Z} + X + Y && (B.1)\\ X + \tilde{Z} &\longrightarrow X && (B.2)\\ Y + Y + \tilde{Z} &\longrightarrow Y + Y && (B.3) \end{aligned}$$

The second chemical system differs in the degree of linearity compared to the first one (the reaction (B.3) has the largest degree of non-linearity because the depletion of $\tilde{Z}$ is quadratic in Y). As it will be shown, the more non-linear a chemical system, the larger the difference of solutions of both methods turns out to be.

The differential equations, which describe the above pseudo chemical species X, Y, Z are given in the following equations (4.15) - (4.18) (the assumption that X and Y are emitted linearly),

where E_x and E_y stand for the emissions of the species X and Y respectively. The lifetimes τ_x and τ_y are taken as a constant for the species X and Y for simplicity reasons. The production term for the species Z and $\tilde{Z}$ are the same because it depends on the same combination X and Y and is defined as P_{xy}. The depletion of Z and $\tilde{Z}$ by the reaction with species X is D_x. Finally, the loss terms D_{y1} and D_{y2} are referred to the first and second system corresponding to the destruction of Z by reaction with Y, respectively.

$$\frac{dX}{dt} = E_x - \tau_x^{-1} X \tag{4.15}$$

$$\frac{dY}{dt} = E_y - \tau_y^{-1} Y \tag{4.16}$$

$$\frac{dZ}{dt} = P_{xy} XY - D_x XZ - D_{y1} YZ \tag{4.17}$$

$$\frac{d\tilde{Z}}{dt} = P_{xy} XY - D_x X\tilde{Z} - D_{y2} Y Y \tilde{Z} \tag{4.18}$$

In the following sections, the theoretical background of the perturbation and the tagging method, are presented. In the last section, the comparison of their implementation on both chemical schemes gives the answer to the following question:

Can both methods quantify with accuracy the contribution of the pseudo chemical species Z, $\tilde{Z}$, Y and X respectively, as the equations (4.15) to (4.18) show?

4.2 The perturbation method

In order to estimate the contribution of a specific chemical source the perturbation method has been used (e.g. (Fuglestvedt et al., 2008; Wang et al., 2009; Hoor et al., 2009)). This method is based on the difference between two simulations: the base case, which includes all emissions and the perturbation case where emissions are perturbed. In principle, this method is using the tangent approximation, which is sketched in Fig. 4.2.

Figure 4.2 shows examplarily the Z concentration caused by Y emissions (blue curve). The points $f(e_0)$ and $f(e^c + \alpha e_0)$ represent the Z concentration of the base case and the Z concentration which refers to the perturbation case, respectively (e_0: refers to the emissions of the base case, e_c: refers to a certain emissions). The factor α is the strength of the perturbation, taking values between [-1,1]. The limiting case of $\alpha = -1$ is the case where the emission is set to zero.

Now, the difference between these two points is defined by Δf. Now, the contribution δf can be defined by the change in concentration caused by the change e^c in emissions and can be described from the following equation, where e^c is the emission:

$$\delta f \simeq e^c f'(e_0) \tag{4.19}$$

Assuming that f (blue curve) is differentiable and using the Taylor approximation for quantifying the derivative f' (dashed line) at the point e_0, where $\tilde{f}$ represents the first two factors of the Taylor expansion, it can be written:

$$f(e_0 + \alpha e^c) = \tilde{f}(e_0) + \frac{f^{'}(e_0)}{1!}\alpha e^c + ... \approx f(e_0 + \alpha e^c) \tag{4.20}$$

The contribution δf now can be quantified approximately from the derivative f', Eq. (4.19). The derivative $f'(e_0)$ can be quantified by the perturbation method and it gives the rate of change per emissions of Y to the ozone concentration of the regarded species.

$$f'(e_0) \simeq \frac{f(e_0) - f(e_0 + \alpha e^c)}{(e_0) - (e_0 + \alpha e^c)} = (f(e_0) - f(e_0 + \alpha e^c))\frac{-1}{\alpha e^c} = -\frac{\Delta^\alpha f}{\alpha e^c} \tag{4.21}$$

The deviation of the derivative at the point e_0 (due to the approximation), the green line (see Fig. 4.2) estimates the corresponding error of this approximation. According to the Eq. (4.21) the contribution δf depends on the factor α:

$$\delta^\alpha f = -\frac{\Delta^\alpha f}{\alpha} \tag{4.22}$$

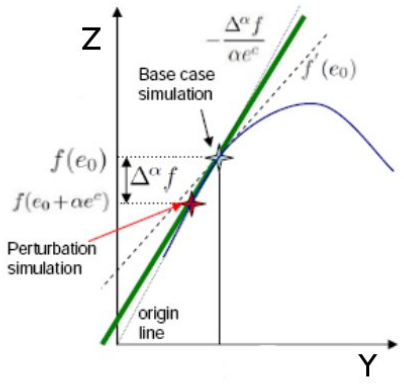

Figure 4.2: Base case $f(e_0)$, where all emissions are included and perturbation case $f(e_0+\alpha e^c)$, for a specific emission category which is changing by the factor α. The perturbation method is based on the tangent approximation $f'(e_0)$ (dashed line). The green line (defined from the two points) is the approximation of the tangent $f'(e_0)$ (Grewe et al., 2010).

As α is getting smaller, these two points converge so that the green and the dashed line tend to coincide. Two errors have been set in order to examine the accuracy of this method (see Appendix A). The error ε_α is related to the factor α and estimates the accuracy in calculating the derivative. The second error, ε_β, calculates whether the total contribution, of all emissions which by definition is 100% deviates from the 100% due to approximation. In case of linear systems both errors, ε_α and ε_β, are equal to zero. A detailed error analysis, for the errors ε_α and ε_β, is given in the Appendix A. Finally, the conclusion from that analysis is that only in specific cases the perturbation method can quantify with accuracy the contributions of the species.

4.3 The tagging method

The tagging method (Grewe et al., 2010) quantifies the contributions of specific emissions categories, (e.g. contribution of road traffic to the ozone concentration etc) following the chemical reaction pathways. The main features of this method are first an entire chemical system is tagged and second that the quantification of the contributions due to the respective emissions is given by following the chemical reaction pathways.

Every individual sector can be separated into *n* categories (the degree of all emissions). Now, the first chemical system is written as follows where the indicators *i* and *j* represents the different chemical sources from which the species X and Y emitted, respectively:

$$X_i + Y_j \longrightarrow \frac{1}{2}Z_i + \frac{1}{2}Z_j + X_i + Y_j \tag{4.23}$$

$$X_i + Z_j \longrightarrow X_i + \frac{1}{2}Z_i - \frac{1}{2}Z_j \tag{4.24}$$

$$Y_i + Z_j \longrightarrow Y_i + \frac{1}{2}Z_i - \frac{1}{2}Z_j \tag{4.25}$$

The X_i, Y_i, Z_i and $\tilde{Z}_i$ are called sub-species and their concentrations are a part of their species X, Y, Z, and $\tilde{Z}$ respectively. Additionally, X and Y are the individual sectors of the emissions E_X and E_Y, respectively

$$\sum_{i=1}^{n} E_{Xi} = E_X \quad \sum_{i=1}^{n} E_{Yi} = E_Y \tag{4.26}$$

The equation (4.23) describes the production of one molecule Z by X_i and Y_j. The Z species is separated now in two different sub-species Z_i and Z_j. The multiplication factor $\frac{1}{2}$ for both of the sub-species means that they are equally important. The equations (4.24) and (4.25) describe the depletion of Z_i and Z_j by the species X_i and Y_i. The $-\frac{1}{2}Z_i$ and $-\frac{1}{2}Z_j$ are the molecules which are going to be depleted by both of these reactions. Mathematically speaking, on the right side of these reactions has to be zero ($-\frac{1}{2}Z_j + \frac{1}{2}Z_i$), separately as a single reaction.

The rate of change, throughout time and for every sub-species, is given from the following equations (4.27) - (4.30), basic from the reactions (4.15) to (4.18). $P_{Z,i}$ and $D_{Z,i}$ are the sum of production and loss terms of ozone, respectively.

$$\frac{dX_i}{dt} = E_{X,i} - \tau_X^{-1} X_i \tag{4.27}$$

$$\frac{dY_i}{dt} = E_{Y,i} - \tau_Y^{-1} Y_i \tag{4.28}$$

$$\frac{dZ_i}{dt} = P_{Z,i}(X_i, Y_i) - D_{Z,i}(X_i, Y_i, Z_i) \tag{4.29}$$

$$\frac{d\tilde{Z}_i}{dt} = P_{Z,i}(X_i, Y_i) - \tilde{D}_{Z,i}(X_i, Y_i, Z_i) \tag{4.30}$$

The following equations (4.31) to (4.34) show the final formulas for $P_{Z,i}(X_i,Y_i)$, $D_{Z,i}(X_i,Y_i,Z_i)$ and $\tilde{D}_{Z,i}(X_i,Y_i,Z_i)$, respectively. For all cases, the considerations to calculate these terms are the same (see also Appendix A): it takes into account all the possible combinations between the precursors X_i and Y_i for the Z production $P_{Z,i}$ (see details in (Grewe et al., 2010)) and all different combination among the species X_i, Y_i and Z_i for giving the Z_i depletion $D_{Z,i}$.

$$P_{Z,i}(X_i, Y_i) = \frac{1}{2} P'_{XY} \left(\frac{X_i}{X} + \frac{Y_i}{Y} \right) \tag{4.31}$$

where

$$P'_{XY} = P_{XY} XY \tag{4.32}$$

$$D_{Z,i}(X_i, Y_i, Z_i) = \frac{1}{2} D_X (X_i Z + X Z_i) + \frac{1}{2} D_Y (Y_i Z + Y Z_i) \tag{4.33}$$

$$\tilde{D}_{Z,i}(X_i, Y_i, \tilde{Z}_i) = \frac{1}{2} D_X (X_i Z + X Z_i) + D_{Y_2} (\frac{1}{3} Y^2 \tilde{Z}_i + \frac{2}{3} Y_i Y \tilde{Z}) \tag{4.34}$$

The quantifications of the sums, for the equations (4.27) to (4.28), and for every *i* are the following:

$$\sum_{i=1}^{n} \frac{dX_i}{dt} = \sum_{i=1}^{n} (E_{X,i} - \tau_X^{-1} X_i) \tag{4.35}$$

because of the constant τ_X and also from the equation (4.26), the above equation is now written:

$$\sum_{i=1}^{n} \frac{dX_i}{dt} = E_X - \tau_X^{-1} \sum_{i=1}^{n} X_i \tag{4.36}$$

because the solutions refer to the steady state calculations, the derivative will be equal to zero

$$\sum_{i=1}^{n} \frac{dX_i}{dt} = 0 \tag{4.37}$$

So the equation (4.36) will be now:

$$\sum_{i=1}^{n} X_i = E_X \tau_X \tag{4.38}$$

Finally, from the equation (4.15) when the solution derives from the steady state calculations, the transformation of the equation (4.38) is the following:

$$\sum_{i=1}^{n} X_i = X \tag{4.39}$$

The same also for the Y precursor. Now, the quantification of the sum, for the species Z (equations (4.29) and for every *i* will be the following (Note that for the species $\tilde{Z}$ the consideration is the same):

$$\sum_{i=1}^{n} \frac{dZ_i}{dt} = \sum_{i=1}^{n} (P_{Z,i}(X_i, Y_i) - D_{Z,i}(X_i, Y_i, Z_i)) \tag{4.40}$$

$$0 = \sum_{i=1}^{n} (P_{Z,i}(X_i, Y_i) - D_{Z,i}(X_i, Y_i, Z_i)) \tag{4.41}$$

Considering the equations (4.31) to (4.33), the equation (4.41) is written now:

$$0 = \frac{1}{2} P_{XY} XY \sum_{i=1}^{n} \left(\frac{X_i}{X} + \frac{Y_i}{Y} \right) - \frac{1}{2} D_X \sum_{i=1}^{n} (X_i Z + X Z_i) - \frac{1}{2} D_Y \sum_{i=1}^{n} (Y_i Z + Y Z_i) \tag{4.42}$$

The sums of production and loss terms have been quantified in the equations (4.43) to (4.45). That becomes evident from the equations (4.15) to (4.18), as they coincide with the right side of the equations.

$$\sum_{i=1}^{n} P_{Z,i}(X_i, Y_i) = P_{XY} XY \tag{4.43}$$

$$\sum_{i=1}^{n} D_{Z,i}(X_i, Y_i, Z_i) = D_X XZ + D_{Y_1} YZ \tag{4.44}$$

$$\sum_{i=1}^{n} \tilde{D}_{Z,i}(X_i, Y_i, Z_i) = D_X X\tilde{Z} + D_{Y_2} Y Y \tilde{Z} \tag{4.45}$$

Conclusively, it has to emphasise that the species X, Y, Z and $\tilde{Z}$ can be given from the following equations:

$$\sum_{i=1}^{n} X_i = X \tag{4.46}$$

$$\sum_{i=1}^{n} Y_i = Y \tag{4.47}$$

$$\sum_{i=1}^{n} Z_i = Z \tag{4.48}$$

$$\sum_{i=1}^{n} \tilde{Z}_i = \tilde{Z} \tag{4.49}$$

Firstly, it can be concluded that the tagging method is convergent, which means that for any different initial conditions, which are giving different solutions (e.g. $A(X_i^1, Y_i^1, Z_i^1)$ and $B(X_i^2, Y_i^2, Z_i^2)$), the respective solutions converge to zero. Second, the tagging method is always fulfilled the equations (4.46) to (4.48).

In the following section, the comparison of the respective solutions from both methods is investigated.

4.4 Comparison between perturbation and tagging method

In this section, the solutions obtained using the perturbation and tagging method, are compared. The solutions of these two chemical systems will be in the equilibrium (where $\dot{X} = \dot{Y} = \dot{Z} = \dot{\tilde{Z}} = 0$). The reason is that it has to verify the solutions of these two methods, against to the respective solutions, of the chemical system (equations from (4.15) to (4.18)).

Perturbation Method In order to find the solutions for the species: X, Y, Z, $\tilde{Z}$, the Eq. (4.22) is applied to the equations (4.15) to (4.18). The respective solutions, $\delta_i^\alpha X$, $\delta_i^\alpha Y$, $\delta_i^\alpha Z$, $\delta_i^\alpha \tilde{Z}$, are shown the Appendix, Table A.2

Tagging Method The respective solutions for tagging method, X_i^{eq}, Y_i^{eq}, Z_i^{eq}, $\tilde{Z}_i^{eq}$, are shown in the the Appendix, Table A.1.

As the two tables A.1 and A.2 show (see Appendix A), both methods give the same concentration results for the species X and Y in equilibrium area. For the first chemical system (see section 4.1), when α is getting smaller (converge to zero), there is agreement between the perturbation and the tagging solution, for species Z^{eq}. For the second chemical system the given solutions do not converge even when α is close to zero, Eq. (4.50). (See Appendix A, for the description of the different parameters).

$$\delta_i^\alpha \tilde{Z} \xrightarrow{\alpha \to 0} \frac{a_i}{c + b_i} - \frac{\tilde{b}_i - \frac{2}{3} D_{y_2} Y_i^{eq} Y^{eq}}{\tilde{c} + \tilde{h}} \tilde{Z}^{eq} \neq \tilde{Z}_i^{eq} \tag{4.50}$$

Conclusively, as it has already been mentioned, a crucial point for every method which quantifies the contribution of regarding chemical species, is that equations (4.46)-(4.49) have always to be satisfied. Comparison is made for both methods with the results given in the Appendix, Tables A.2 and A.1 of the sum of the total contribution of all sub-species. In general, the perturbation method is not able to consistently decompose a given concentration into contributions from individual sources for certain non-linear systems (Grewe et al., 2010), as equations (4.51) to (4.55) show. In contrast, it has to be emphasised that the tagging method always fulfilled the respective equations (see section 4.3).

$$\sum_{i=1}^{n} X_i^{eq} = \sum_{i=1}^{n} \delta_i^\alpha X = X^{eq} \tag{4.51}$$

$$\sum_{i=1}^{n} Y_i^{eq} = \sum_{i=1}^{n} \delta_i^\alpha Y = Y^{eq} \tag{4.52}$$

$$\sum_{i=1}^{n} Z_i^{eq} = Z^{eq} \tag{4.53}$$

$$\sum_{i=1}^{n} \delta_i^{\alpha} Z \neq Z^{eq} \tag{4.54}$$

$$\sum_{i=1}^{n} \delta_i^{\alpha} \tilde{Z} \neq \tilde{Z}^{eq} \tag{4.55}$$

In the following chapter, the configuration characteristics of the tagging sub-model into the EMAC atmospheric chemistry model are presented.

Chapter 5

TAGGING sub-model

In the TAGGING sub-model the tagging method (see section 4.3) is applied to tropospheric chemistry. In principle, in this study and for the first time the tropospheric ozone concentration is quantified by tagging the competitive species and families NO_y, CO, and NMHCs. The impact on tropospheric ozone concentration due to emission sectors (see Appendix C) depends on the region and season. In order to investigate the importance on the impacts on tropospheric ozone, ten emission sectors have been chosen. The origin of the tagged species corresponds to ten different emission sources, natural and anthropogenic and are the following: aviation, shipping, road traffic, industry, biomass burning, soils, lightning, stratosphere, CH_4 and N_2O.

The set of the chemical species are divided in two main categories. The first category is described by the species which have been tagged on the chemical scheme such as O_3, NO_y, PAN, CO, NMHC and HO_x compounds. The second category includes the untagged species such as water vapor. The ten different chemical sectors combined with the six chemical families/species lead to a complex system with a totally sixty parameters.

How does it work?

A simplified structure of the tagging chemical mechanism in the EMAC model is shown in Fig. 5.1. Technically, this structure is separated in three main parts. The starting part begins when data from different emissions sources (coming from observations or other models) are provided to the MECCA chemistry sub-model. The emissions data set are described in Appendix B. The MECCA sub-model calculates (second part) the tendencies of the tracers (=chemical species, e.g. O_{3i} where the indicator *i* refers to the emission sectors such as shipping, aviation etc, see section 4.3). The outputs, tracer tendencies of each species/families i.e. NO_y, NMHC, CO etc, are provided to the tagging sub-model (third part).

Quantifications for tagging O_3 chemistry

The first step of this approach is to extract the main chemical equations which describe the principles of tropospheric ozone chemistry (see Appendix B). For instance, the ozone is produced via the chemical reaction between NO_y and HO_2 as well as NMHC (e.g. see chemical reactions 2.30 and 2.28).

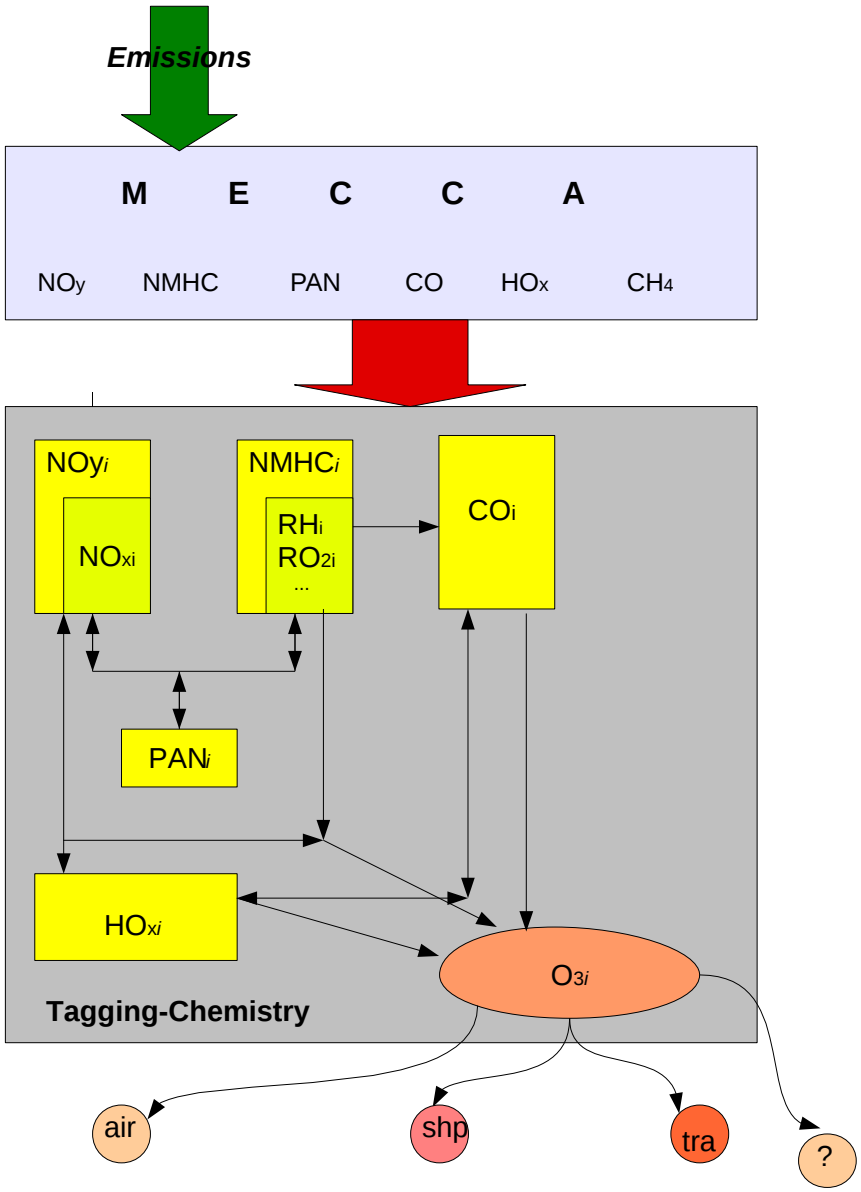

Figure 5.1: Simplified structure of tagging chemistry. Tracers X (e.g. NMHC, CO, NO_y) produce ozone sub-species X_i (e.g. O_{3i}).

On contrary, the ozone is depleted via HO_x, NMHC and NO_y families (e.g. see chemical reactions 2.9, 2.18, 2.23). Note that for the first approximation of this study the HO_x radicals are not tagged to the chemical scheme. Now, the quantification of each production and loss term, P_{O_3} and L_{O_3} respectively, are based on the Eq. (4.42). This gives the following results:

$$P_{O_3} = \frac{1}{2}P'_\alpha \left(\frac{[HO_{2i}]}{[HO_2]} + \frac{[NO_{yi}]}{[NO_y]}\right) + \frac{1}{2}P'_\beta \left(\frac{[NMHC_i]}{[NMHC]} + \frac{[NO_{yi}]}{[NO_y]}\right) \tag{5.1}$$

Since only one chemical species is tagged for each chemical reaction which is described by the NO_y with HO_2, the factor one-half is replaced with one as well as the ratio $[HO_{2i}]/[HO_2]$ is equal to zero, so that:

$$P_{O_3} = P'_\alpha \frac{[NO_{yi}]}{[NO_y]} + \frac{1}{2}P'_\beta \left(\frac{[NMHC_i]}{[NMHC]} + \frac{[NO_{yi}]}{[NO_y]}\right) \tag{5.2}$$

The quantification of ozone loss is following the same consideration as before:

$$\begin{aligned} L_{O_3} = \frac{1}{2}L'_\alpha \left(\frac{[O_{3i}]}{[O_3]} + \frac{[OH_i]}{[OH]}\right) + \frac{1}{2}L'_\beta \left(\frac{[O_{3i}]}{[O_3]} + \frac{[HO_{2i}]}{[HO_2]}\right) + \\ \frac{1}{2}L'_\gamma \left(\frac{[O_{3i}]}{[O_3]} + \frac{[NMHC_i]}{[NMHC]}\right) + \frac{1}{2}L'_\delta \left(\frac{[O_{3i}]}{[O_3]} + \frac{[NO_{yi}]}{[NO_y]}\right) + \\ \frac{1}{2}L'_\epsilon \left(\frac{[O_{3i}]}{[O_3]} + \frac{[X_i]}{[X]}\right) \end{aligned} \tag{5.3}$$

where X contains the rest of the chemical untagged species which are able to deplete ozone (See the included chemical reactions in the Appendix B). Similar to ozone production and for the first approach of this study the HO_x compounds are not tagged, so that (Note that the X chemical species are not tagged in the present study):

$$\begin{aligned} L_{O_3} = L'_\alpha \frac{[O_{3i}]}{[O_3]} + L'_\beta \frac{[O_{3i}]}{[O_3]} + L'_\epsilon \frac{[O_{3i}]}{[O_3]} + \\ \frac{1}{2}L'_\gamma \left(\frac{[O_{3i}]}{[O_3]} + \frac{[NMHC_i]}{[NMHC]}\right) + \frac{1}{2}L'_\delta \left(\frac{[O_{3i}]}{[O_3]} + \frac{[NO_{yi}]}{[NO_y]}\right) \end{aligned} \tag{5.4}$$

where the P'_α, P'_β, L'_α, L'_β, L'_γ, L'_δ, L'_ϵ correspond to the chemical reaction rates of the respective equations. Lastly, the production and loss of the families NO_{yi} and $NMHC_i$ are dependent on PAN_i and CO_i chemistry, see Fig. 5.1 (e.g. chemical reaction 2.26). Furthermore, the quantifications steps for the HO_x tagging chemistry are shown in chapter 7.

Chapter 6

Contribution of natural and anthropogenic emissions to atmospheric concentrations

In this chapter, the results of the tagging method for the species NO_y, NMHC, PAN, CO and O_3 are presented. The tagging method is applied to ten different sectors including anthropogenic and natural categories (see chapter 5). In order to investigate and compare the importance of these sectors for tropospheric ozone abundances, the analysis of the relative contribution (%) is required. Additionally, the distribution of the contribution of the precursors to ozone concentration, such as NO_y, CO and methane, is examined. For a better understanding of the distribution of tropospheric ozone concentration the individual reaction rates with respect to the production and loss terms, are investigated. This investigation will enable the identification of leading reactions as well as the crucial regions where these reactions rates occur. For this reason an analysis for shipping and aviation emitted sectors is presented. Both sectors have similar contribution to tropospheric ozone concentration but their local maxima occur at different altitudes, given their different cruising routes. Also, the overview of the leading individual production and loss reaction channels to ozone concentration is given. At the end, the assessment of the relation between all the precursor concentrations to ozone concentration will show which are the dominant species in which regions, with respect to the chosen specifics sectors. For this analysis the industry and biomass burning were chosen since both are ground emitted sources and their contribution to ozone concentration, in the lower troposphere, exhibits similar local maximum values. Also, the overview among all the emission sectors, with respect to their individual concentration of all the tagged species is given.

Therefore, this chapter is separated into three main sections. The first section reports the distribution of relative contribution of the ten different chemical sectors with respect to NO_y and O_3 concentration. The second section provides the results of two specific chosen sectors, biomass burning (natural) and industry (anthropogenic), in relation to all chemical species. Lastly, the third section presents the investigation of the individual reaction rates for ozone production and loss rates.

6.1 Relative contribution of emission sectors

In this section, the analysis of the relative contribution of the ten different emission sectors to the concentrations of NO_y and O_3 is presented. The relative contribution of any individual emission sector (e.g. aviation contribution to NO_y) is the result of its mixing ratio (mol/mol$_{dryair}$) divided by the total concentration from all the sectors which equals the total simulated concentration.

In this part, the following questions will be answered:

- Which emission sectors dominate the NO_y and ozone concentration in which regions?
- Which sources are most important for global tropospheric ozone mass?

6.1.1 NO_x relative contribution

Figures 6.1 and 6.2 show the zonal mean of the relative contribution (%) of individual emission sectors to the NO_y concentration. Figure 6.1 corresponds to biomass burning, lightning, soils, industry, road traffic and shipping. Figure 6.2 corresponds to air traffic, stratosphere, CH_4 and N_2O.

The highest relative contributions which are simulated in the NH and up to mid-altitudes (referring to a pressure range of 1000 hPa to 380 hPa) are due to anthropogenic emissions sectors. The NO_y concentration from industrial emissions is simulated to have the highest relative contribution, up to 40% in the NH. Its contribution covers the whole NH with a maximum near the surface at mid-latitudes. The second highest relative contribution is coming from road traffic. Its maximum values ($\sim 25\%$) are simulated at the middle northern latitudes, reaching pressure levels up to 850 hP. Shipping exhibits horizontal distribution in both hemispheres and lower altitudes (referring to a pressure range of 1000 hPa to 700 hPa). Its maximal relative contribution, up to 26%, is reached at low altitudes in the NH at mid-latitudes. The maximum NO_y values for air traffic is simulated to be up to 22%, in cruise altitudes (300 hPa). Its vertical distribution covers the NH at mid-latitudes as well as the polar regions.

Lightning exhibits the most dominant distribution of relative contributions, compared to all sectors. Lightning occurs in deep convection which has the maximum occurrence in tropical regions which explains its distribution of contributions. The contribution of lightning to the NO_y concentration reaches values up to 70% and its maximal values are simulated between 200 to 500 hPa. Its distribution covers a large vertical altitude range up to 12 km (200 hPa) and exhibits a symmetry relative to the equator. The maximum contribution of emissions from soils is simulated in the southern tropical regions, reaching up to 20%. The contribution of soil emissions to the NO_y concentration is mainly occurring at low altitudes. Its vertical distribution does not exceed 700 hPa at these latitudes. Its contribution is important mainly in the lower troposphere at southern mid latitudes. The stratospheric NO_y relative contribution, in the troposphere, is simulated at to be maximal in high altitudes (referring to a pressure range of 400 hPa to 200 hPa) and polar regions reaching values up to 22%. The stratospheric contribution exhibits a high significance

compared to all the sectors in these regions. The highest contributions at both hemispheres for the altitudes between 8 to 12 km (pressure range of 400 hPa to 200 hPa), are the results from the stratospheric global circulation, Brewer-Dobson circulation (downweling branches at these regions). Also, the life time of NO_y is increasing with the altitude (see section 2.1.2). These two statements explain why, in these regions, a higher NO_y concentration occur compared to the lower troposphere. The biomass burning contribution has maximum values close to 20% in the tropical regions and reaching altitudes up to roughly 4 km (650 hPa).

Figure 6.2 shows the contribution of NO_y via methane. The loss of methane via oxidation produces NMHC (see chemical reaction 2.33). The NMHC tagged by methane reacts with NO_y (tagged by any sector e.g. shipping) and products PAN (see chemical reaction 2.42). PAN tagged by methane via the reversible chemical reaction 2.26 produces NO_y. Hence, NO_y is produced by this chemical reaction chain and partially is tagged by methane. The maximum NO_y contribution by methane is simulated at higher altitudes around 9 to 12 km (pressure levels between 300 hPa to 200 hPa) in both hemispheres. PAN is transported in long distances in these high altitudes. However, low contribution values are found in the tropics as well as in the NH at lower troposphere since other sectors contribute significantly to the NO_y concentration, in these regions, such as lightning (tropics) and industry (NH).

The N_2O is emitted at the surface and is destroyed in the stratosphere. The NO_y formation, by N_2O photo-oxidation, takes place mainly in the stratosphere ($N_2O + O(^1D) \rightarrow 2NO$) because of the shorter wavelength ($\lambda < 400$ nm) required for this reaction.

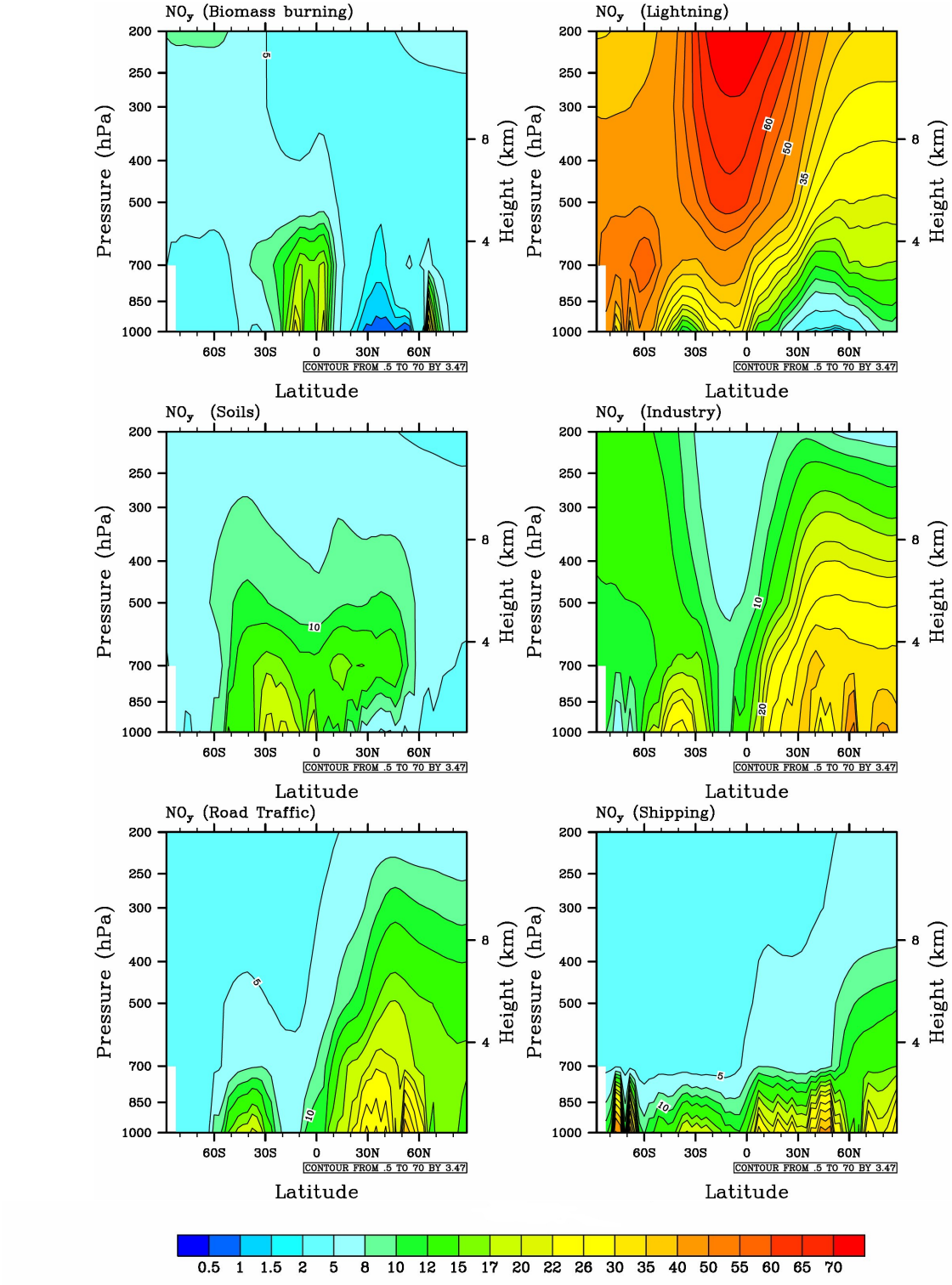

Figure 6.1: Annually relative contribution of emission sectors to the NO_y concentration (%). Zonal mean (pressure levels between 1000 hPa to 200 hPa) for all different emission sectors. From top left: biomass burning, lightning, soils, industry and road traffic, shipping.

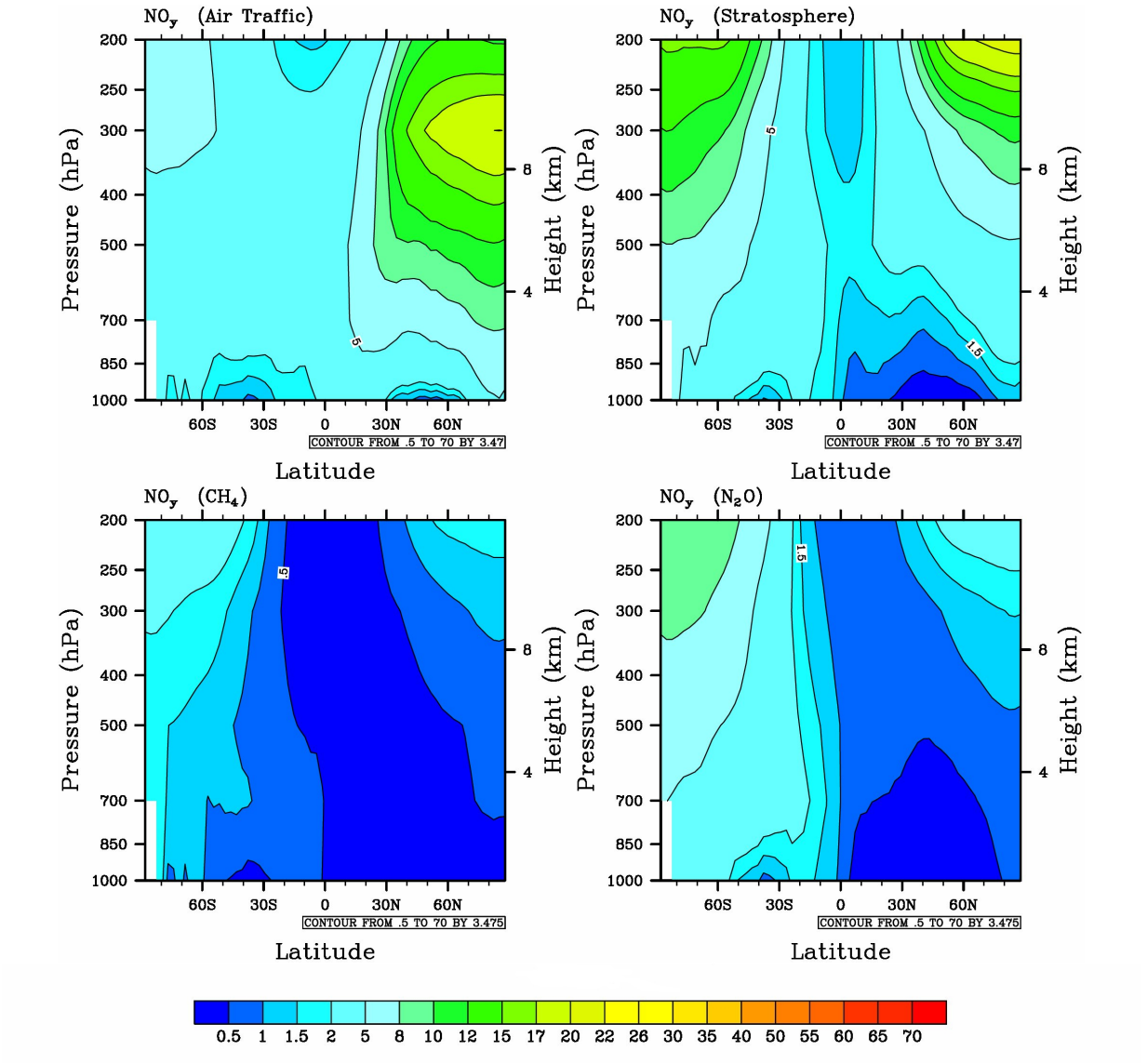

Figure 6.2: Annually relative contribution of emission sectors to the NO_y concentration (%). Zonal mean (pressure levels between 1000 hPa to 200 hPa) for all different emission sectors. From top left: air traffic, stratosphere, CH_4 and N_2O.

6.1.2 O_3 relative contribution

Figures 6.3 and 6.4 show the zonal mean relative contribution (%) of emission sectors to tropospheric ozone. Figure 6.3 corresponds to biomass burning, lightning, soils, industry, road traffic and shipping. Figure 6.4 corresponds to air traffic, stratosphere, CH_4 and N_2O.

Figures 6.3 and 6.4 show that industry has locally the highest relative contribution of emissions to ozone among all of the anthropogenic sectors. Its maximum contribution reaches 27% in the NH at mid-latitudes. The contribution of industry to ozone concentration in the NH is around 15% reaching heights up to the middle troposphere. The relative contributions to ozone from industrial emissions in the SH are relatively high compared to the tropics. This is due to the low total ozone concentration (The Appendix C shows the industrial emissions) in conjunction with low absolute contributions from other sectors in this region.

The maximum contribution of road traffic to ozone concentrations is simulated at around $30°$N and reaches values around 17%. Its vertical distribution has a large broad shape and reaches altitudes much higher than the boundary layer. The maximum contribution of shipping reaches 10%. Its vertical distribution covers mainly the lower troposphere at northern mid-latitudes. The lowest contribution compared to all sectors, is from air traffic. Its contribution is found to be higher in NH and its maximum reaches 7% at cruise altitudes.

In terms of global mean values and among all the sectors, the contribution of lightning is the most important. Its maximum contribution reaches values locally around 60%. The distribution covers the entire tropical troposphere and exhibits symmetry with respect to the equator. High values of the stratospheric contribution in the troposphere are simulated in pressure levels between 200 to 250 hPa in polar regions. This can be explained from the Brewer Dobson circulation (see detailed description in section 2.1.3).

Methane is an important source for HO_2 radicals and hence important for ozone production (see the methane oxidation chain section 2.1.3). Its contribution exhibits a variation between 10 to 20%. In tropical regions at low latitudes, a maximum value of 20% is simulated.

The maximum contribution of biomass burning to the ozone concentration occurs in high pressure levels, close to 850 hPa and close to the equator, reaching values around 20%. Also, compared to all the other natural sectors its maximum values of vertical and horizontal distributions, exhibit in small scale. Lastly, the ozone contribution of soils is simulated to have the lowest values among all natural emission sectors, reaching a maximum of 13%. Its vertical distribution has a broad shape variation in the SH. The contribution of the N_2O to ozone is maximal in the NH at high latitudes.

Finally, it can be concluded that the contribution of the anthropogenic emission sources to NO_y and O_3 concentrations are dominant in the northern hemisphere at low altitudes. Moreover, the natural sources of lightning, stratosphere and CH_4 show a symmetry with respect to the equator. In comparison, soils does not exhibit the same symmetry since more emissions from soils occur in the southern tropical regions due to the larger amount of land mass compared to the northern tropics.

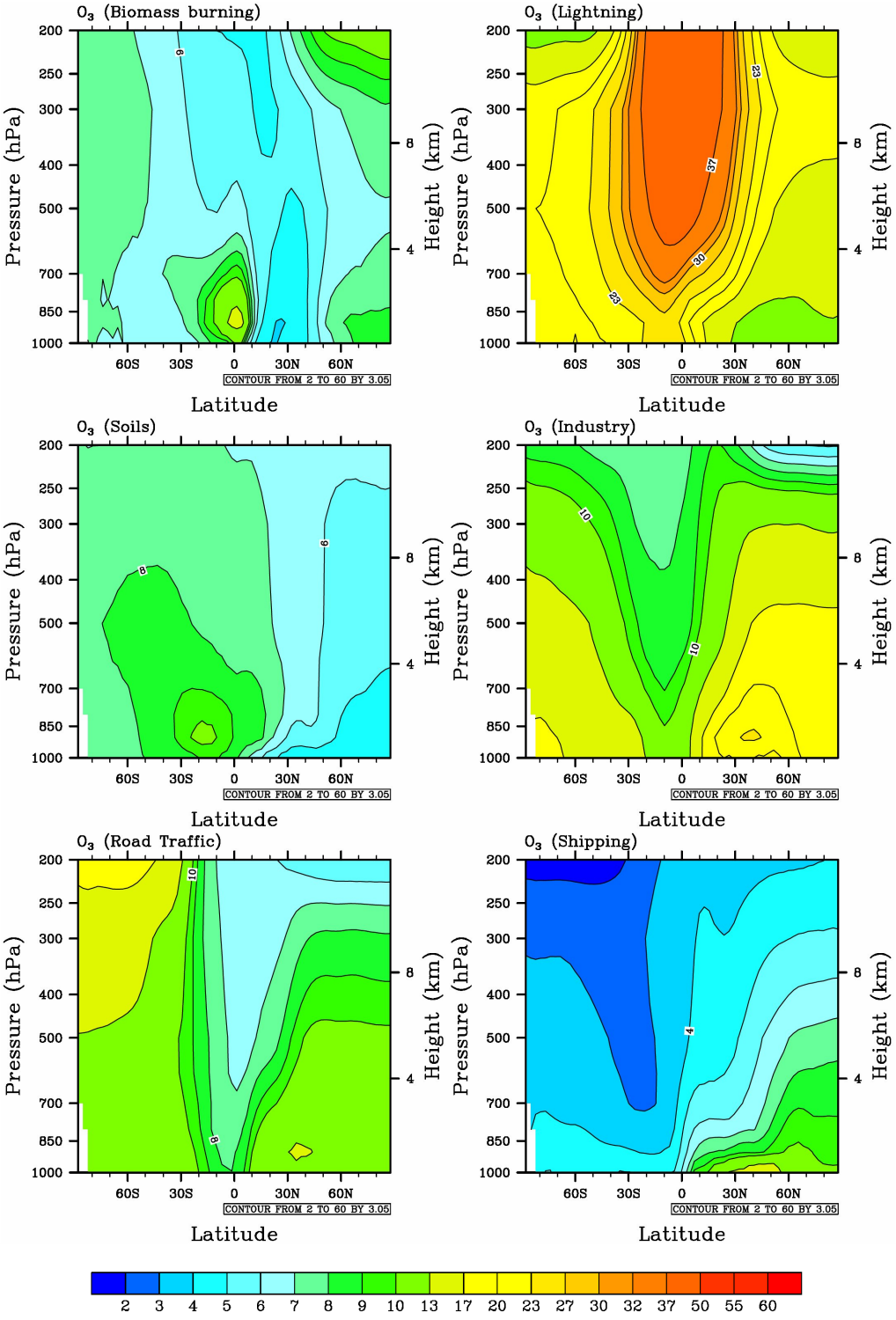

Figure 6.3: Annually relative contribution of emission sectors to the ozone concentrations (%). Zonal mean (pressure levels between 1000 hPa to 200 hPa) for all the different emission sectors. From the top and left: biomass burning, lightning, soils, industry, road traffic and shipping.

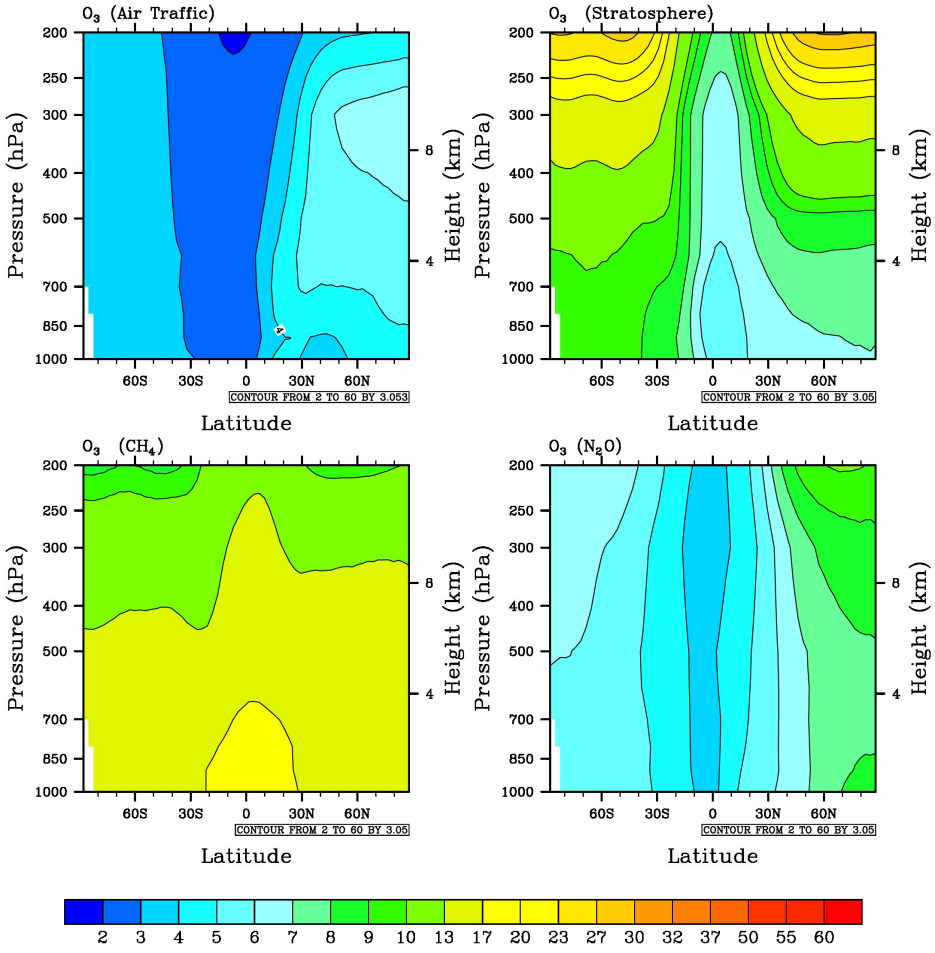

Figure 6.4: Annually relative contribution of emission sectors to the ozone concentrations (%). Zonal mean (pressure levels between 1000 hPa to 200 hPa) for all the different emission sectors. From the top and left: air traffic, stratosphere, CH_4 and N_2O.

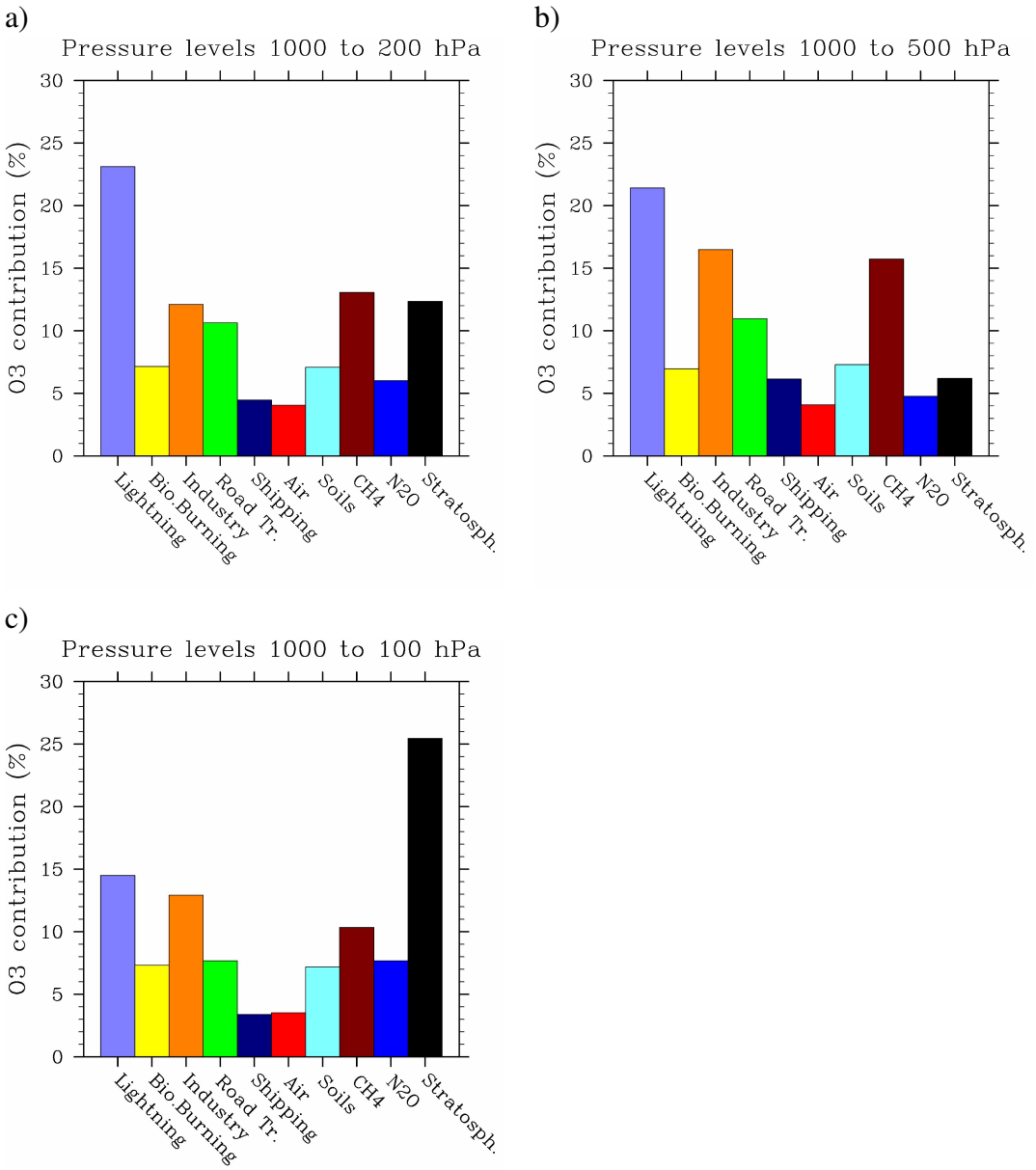

Figure 6.5: Histograms of relative contributions (%) of emission sectors to the global atmospheric burden of ozone mass, for pressure range between **a)** 1000 hPa to 200 hPa **b)** 1000 hPa to 500 hPa and **c)** 1000 hPa to 100 hPa. Violet: lightning, yellow: biomass burning, orange: industry, green: road traffic, navy: shipping, red: aviation, light blue: soils, brown: CH_4, blue: N_2O and black: stratosphere.

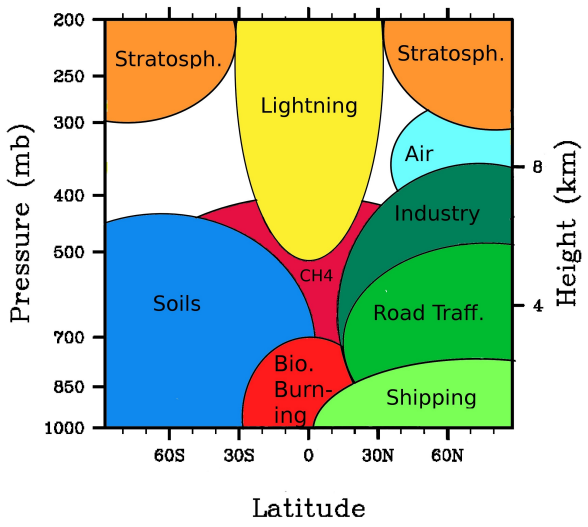

Figure 6.6: Sketch of the regions where the ten individual contributors dominant tropospheric ozone.

The histograms in Fig. 6.5 illustrate the relative contributions of all the ten emission sectors to the ozone mass in the troposphere for different atmospheric pressure layers: first between 1000 hPa to 200 hPa (Fig. 6.5a), second between 1000 hPa to 500 hPa (Fig. 6.5b) and third between 1000 hPa to 100 hPa (Fig. 6.5c). For pressure levels between 1000 to 200 hPa (Fig. 6.5a), the natural sources dominate over the anthropogenic ones. Lightning is simulated to have the highest relative ozone contribution in the troposphere, reaching 23%. However, the stratospheric contribution is the most important sector when lower pressure levels (up to 100 hPa) have been included (Fig. 6.5c). Nonetheless, stratosphere and methane contributions exhibit equal importance (for pressure levels between 1000 to 200 hPa). In the lower troposphere and for pressure levels between 1000 to 500 hPa (Fig. 6.5b), industry and methane are simulated to have the second highest ozone contribution after lightning.

Finally, the total contribution of all anthropogenic sectors to tropospheric ozone concentration reaches almost 40% (Fig 6.5a). Industry is the most important sector, among the man-made ones, reaching 12%. The lowest ozone relative contribution comes from aviation reaching 5%. However, all these results refer to global mean values. In the NH at lower altitudes, the anthropogenic sectors are most important. Figure 6.6 sketches zonal mean the regions where the ten contributors are important to tropospheric ozone. The anthropogenic ones are covering the NH reaching high altitudes. Contrary, the natural ones are important in SH as well as higher tropical regions.

6.2 Chemical impacts of biomass burning and industry

In the previous section the ozone relative contribution of all the emission sectors was presented. Industry, a ground emitting source, is simulated to be the largest tropospheric ozone contributor among of all anthropogenic ones (see Fig. 6.5). In comparison, the natural ground emitting sources, biomass burning and soils exhibit similar contribution to tropospheric ozone mass (see Fig. 6.5) but with different distributions (see Fig. 6.3). Emissions from soils are found to influence the SH over a larger vertical range than other sources, while biomass burning is found to have shorter vertical extent and a more pronounced influence to the tropical regions. However, the maximum value of biomass burning contribution (20%) is two times higher compared to soils (10%) for local zonal mean values. In the lower troposphere biomass burning and industry exhibit similar local maximum values but in different latitudes (tropics and northern mid-latitudes, respectively). For this reason a more comprehensive analysis is given for these two sources, while a conclusion summary is given for all the emission sectors.

In this section, the mixing ratio (mol/mol) of the species (NO_y, O_3, CO, PAN, NMHC) from biomass burning and industry, are presented. It is crucial to investigate the relation between all the precursor concentrations to ozone concentration. The relevant question is the following:

- Which are the dominant species and regions for the tropospheric ozone concentration, with respect to industry and biomass burning?

6.2.1 Biomass burning

In the previous section, the relative contribution was used in order to examine the importance of each individual emission sector, with respect to the same species (e.g. O_3). In this investigation the absolute concentration of each chemical species (NO_y, O_3, CO, PAN, NMHC) for the chosen emission sector is required in order to examine the relation among the species to the specific ozone concentration (e.g. ozone from biomass burning).

Figures 6.7 and 6.8 show the mixing ratios of horizontal and vertical distributions, of the species and families NO_y, O_3, PAN, CO and NMHC in nmol/mol, respectively. Note that the emissions include the primary species: NO_y, NMHC and CO (see Appendix C). The highest CO mixing ratios are simulated in tropical regions at lower altitudes, such as central Africa and S. America. In vertical distribution, its maximum reaches pressure levels up to 850 hPa. The regional maximum mixing ratios in the NH at polar regions (close to 60°N) is a result of high NMHC concentration in this region, such as isoprene (C_5H_8) which is oxidised to CO. The CO emissions (mol/mol/sec) from biomass burning are found to have the lowest values compared to NMHC and NO. However, the CO mixing ratios are found to have the largest values compared to NMHC and NO mixing ratios. This is attributed to higher life time of CO close to months, compared to all the other emitted species at these altitudes.

NO_y emission rates (10^{-10}mol/mol/s) are higher than CO and NMHC (see Appendix C). Instead, the lowest values of mixing ratios are simulated for NO_y concentrations compared to the primary species because of the short life time close to surface (hours). Its maximum values are simulated in Central Africa and South America, regions close to the equator.

High values of NMHC mixing ratios are simulated in Central Africa around 15 nmol/mol, despite to their short life time (hours). The values of the horizontal distribution are maximized over the continents. This is attributed to the high organic compounds which are produced from the combustion of biomass. In vertical distribution, its maximum values are reaching altitudes close to 3 km (pressure levels around 700 hPa) in tropical regions.

The PAN mixing ratios are simulated to have the lowest values compared to all the species. The maximum values reach the 1 nmol/mol. The vertical distribution has a large scale variation because of the long-range transport of PAN. This is attributed to the continuous increase in life time with the increase in altitude, since temperature decreases with altitude and hence thermal decay decreases.

The O_3 biomass burning mixing ratios depend on the concentration of all the other primary species (NO_y and VOCs). It exhibits high levels of mixing ratios, even though its life time is much shorter (days) compared to CO (months). This explains why high values are simulated in Central Africa. However, the highest absolute mixing ratios of biomass burning are found at higher altitudes (about 40 nmol/mol). This is attributed to stratospheric-tropospheric exchange (STE) (see detailed description in section 2.1.3).

It can be summarized that the maximum concentrations with respect to the primary species (NO_y, NMHC and CO) are found in the tropical regions (Central Africa and South America) in the lower troposphere due to their high emission rates of biomass burning in these regions (see Appendix C). Also, the members of the NMHC family play the dominant role for the tropospheric ozone concentration by biomass burning. This is attributed to the highest absolute values of NMHC concentrations compared to NO_y ozone precursor as well as to PAN (see section 6.4).

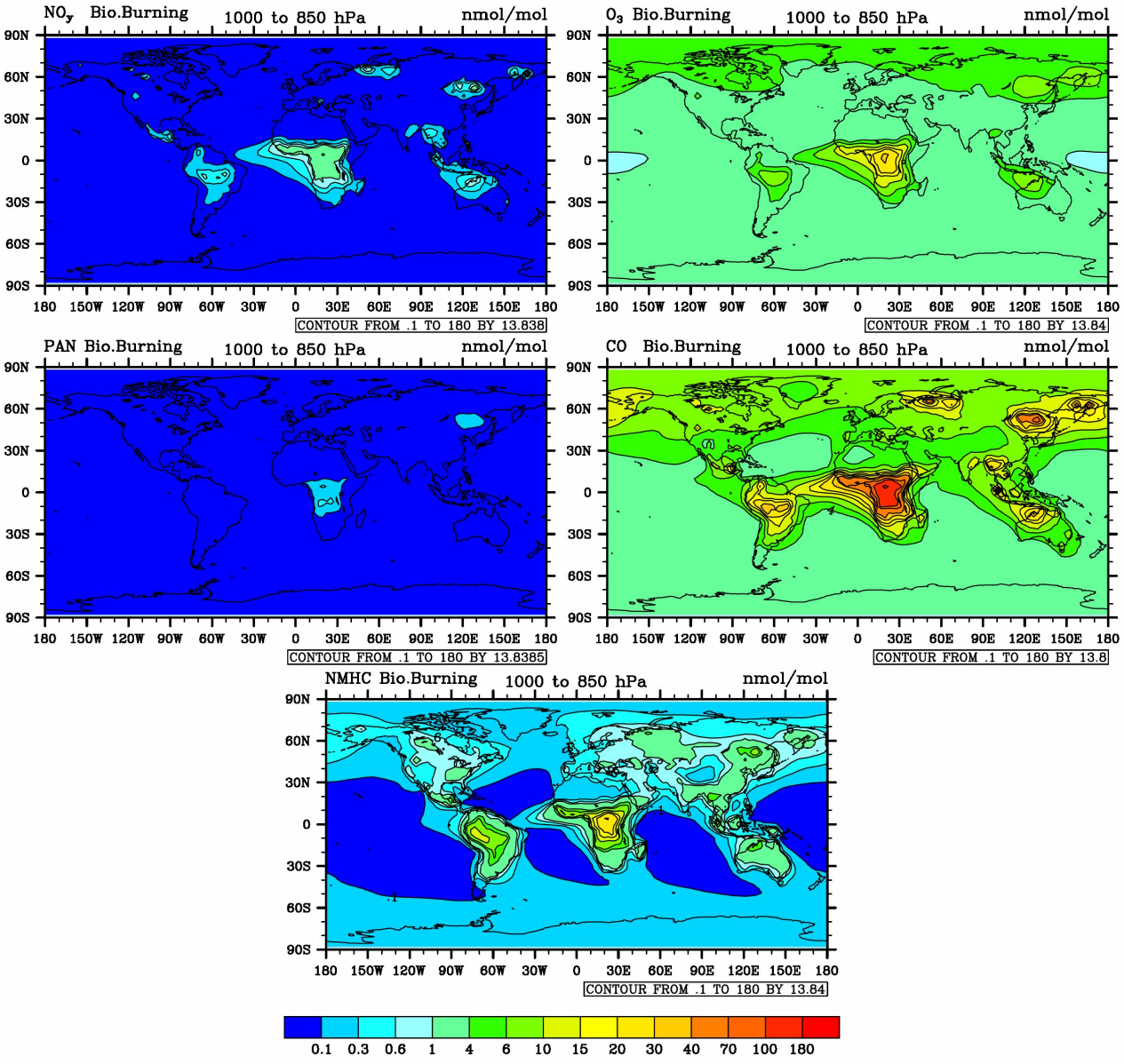

Figure 6.7: Horizontal distribution (pressure levels between 1000 hPa to 850 hPa) of biomass burning. From left to right: NO_y, O_3, PAN, CO and NMHC mixing ratios, nmol/mol.

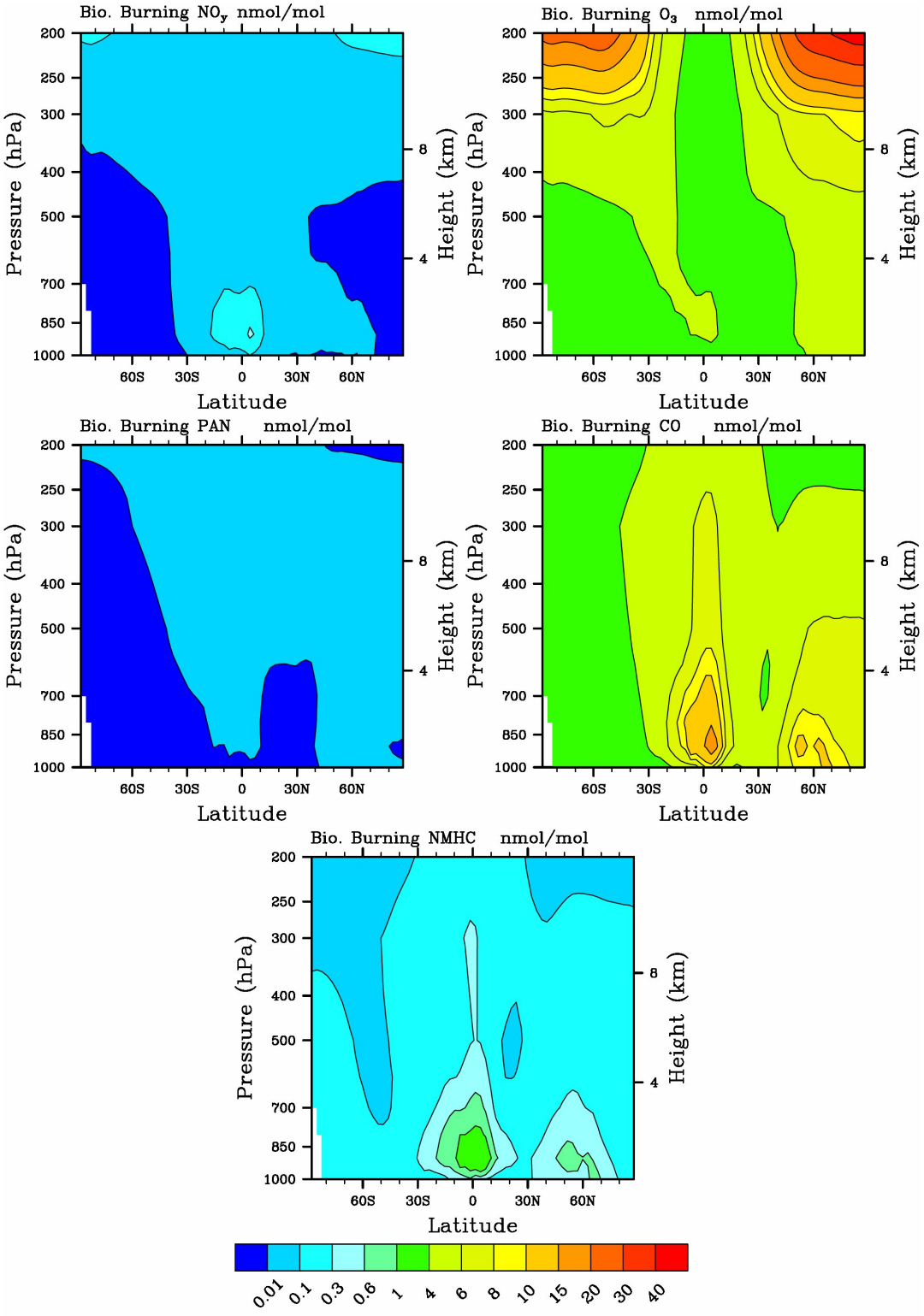

Figure 6.8: From left to right: NO_y, O_3, PAN, CO, NMHC zonal mean (pressure levels between 1000 hPa to 200 hPa) mixing ratios, nmol/mol from biomass burning.

6.2.2 Industry

In this subsection, the mixing ratios of the respective species from industry are presented. Figures 6.9 and 6.10 show the mixing ratios of the horizontal and vertical distribution of the species NO_y, O_3, PAN, CO and NMHC in nmol/mol, respectively. Note that the emissions include the primary species: NO_y, NMHC and CO and are in the order of 10^{-13}mol/mol/s (see Appendix C).

The regions which are most affected by industry are in the NH at lower altitudes (unlike from biomass burning). In particular, high mixing ratios are simulated for CO in Asia, reaching up to 200 nmol/mol. The horizontal and vertical distribution of CO shows a large variation because it is covering the whole NH. High mixing ratios of CO (35 nmol/mol) are simulated in the lower troposphere up to 850 hPa.

The NMHC mixing ratios are simulated to have the second highest values with respect to primary species. Their distribution covers the NH as well as land regions in the southern tropics. Also, its vertical distribution covers mainly the NH reaching high altitudes close to 10 km (300 hPa). High mixing ratios are simulated in Asia reaching 30 nmol/mol. Similarly, the same holds for the CO distribution but with lower concentrations.

The NO_y mixing ratios form industry have the second smallest values compared to all the other species. High values (10 nmol/mol) are simulated over land regions mainly in the NH, such as N.America, Europe and Asia. Its vertical distribution does not show large variations and exhibits high values only in the NH lower troposphere.

PAN is found to have the smallest mixing ratios. The vertical distribution exhibits the maximum values on the NH up to 300 hPa pressure levels. In contrast, its horizontal distribution shows small variations as similar to biomass burning.

The ozone mixing ratios are simulated to have the second highest values after CO (same with biomass burning). Its maximum values are found in Asia and the east coast of USA being around 60 nmol/mol regionally. The vertical distribution has high variation because covers the whole NH and reaches high values in the upper troposphere (200 hPa).

Similar to biomass burning, the regions (North America, Asia and Europe) with the highest concentrations of the primary species (NO_y, NMHC and CO) are the regions in which their highest emission rates occur (see Appendix C). Lastly, for the tropospheric ozone concentration in the NH at the continents the concentrations of NMHC and NO_y are comparable and hence they play an equal role for ozone concentration (see section 6.4).

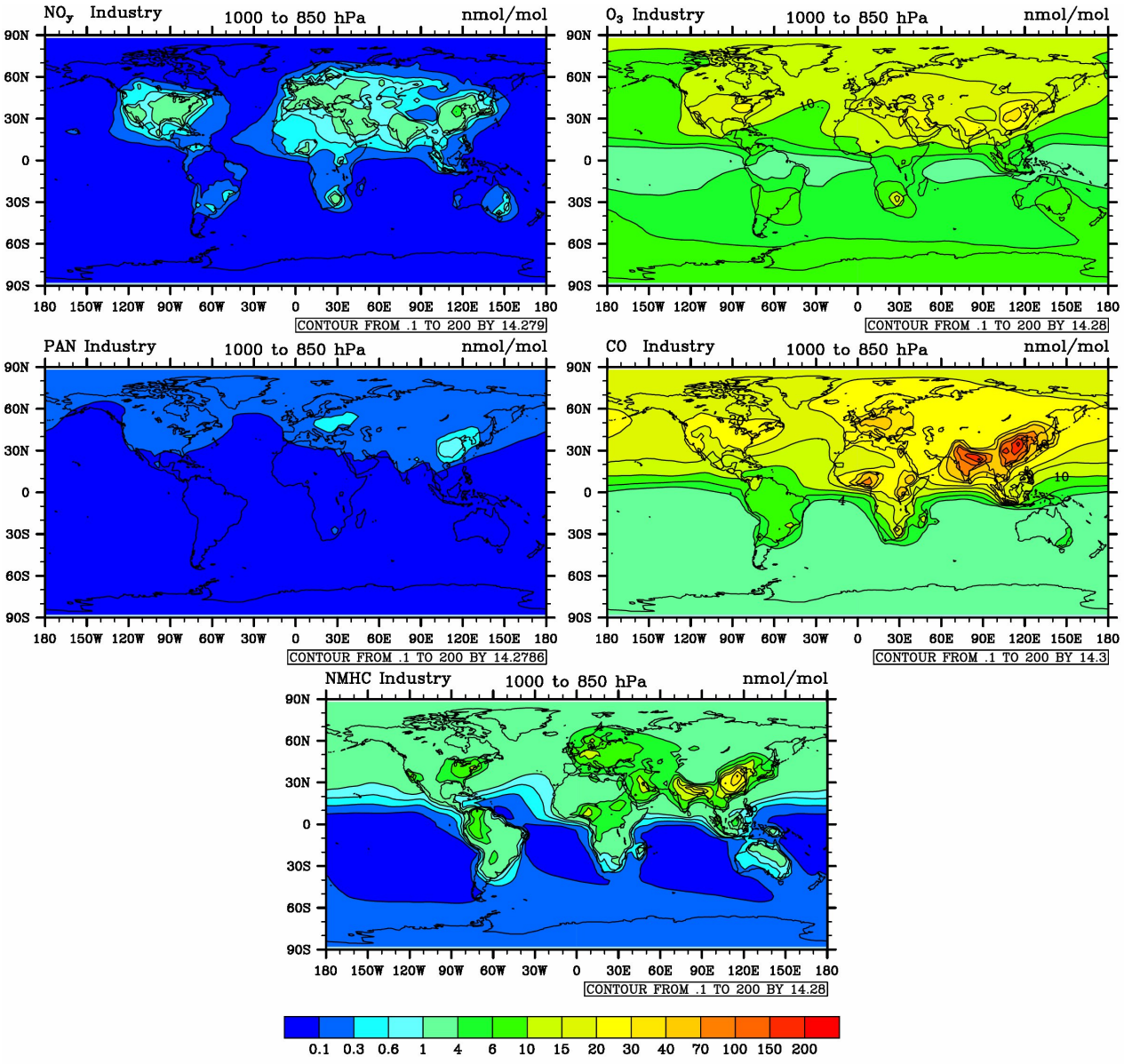

Figure 6.9: Horizontal distribution (pressure levels between 1000 hPa to 850 hPa) of industry. From left to right: NO_y, O_3, PAN, CO and NMHC mixing ratios, nmol/mol.

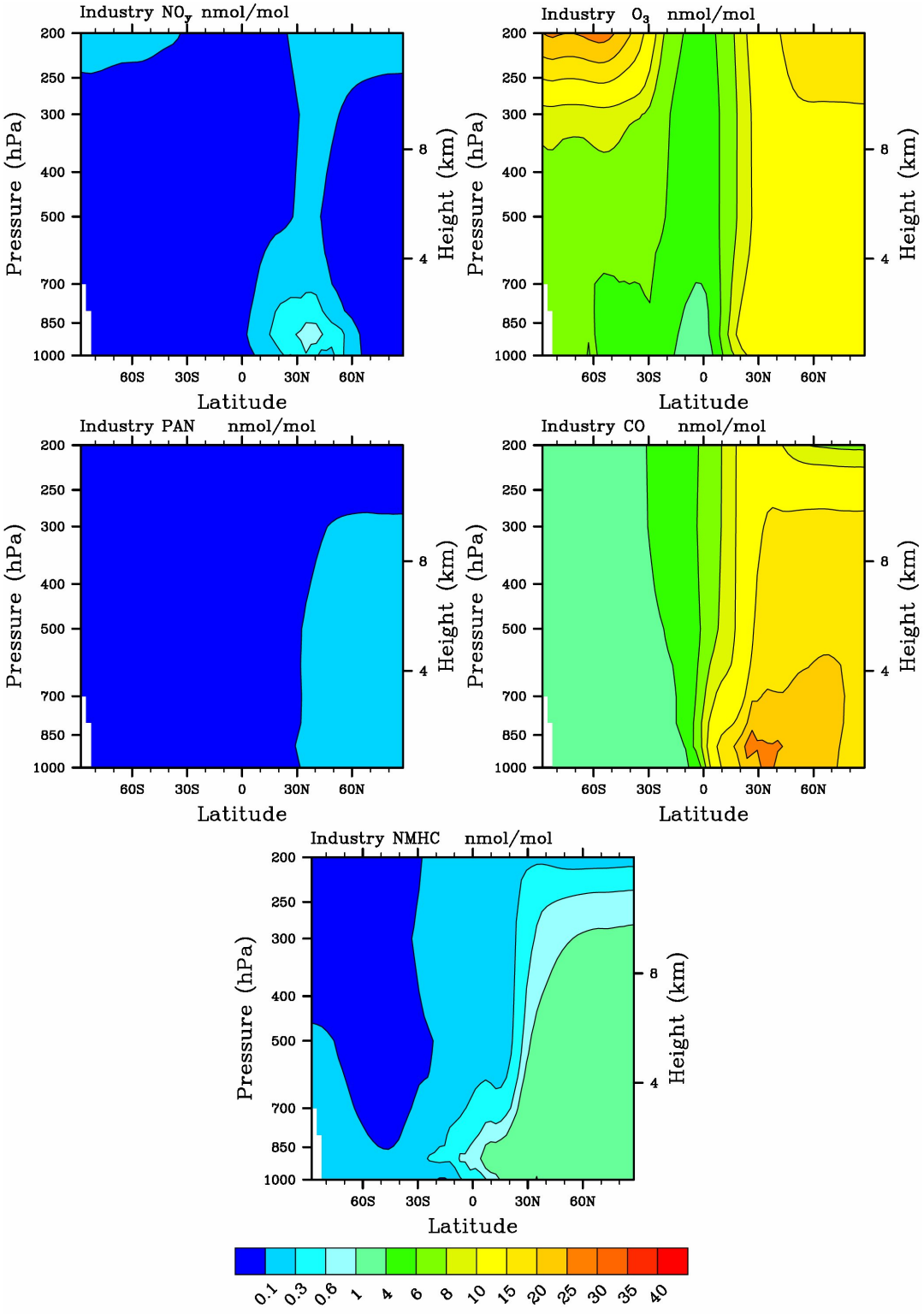

Figure 6.10: From left to right: NO_y, O_3, PAN, CO, NMHC zonal mean (pressure levels between 1000 hPa to 200 hPa) mixing ratios, nmol/mol from industry.

6.3 Global mean values of masses

Figures 6.11 and 6.12 show contribution of individual emission sectors to NO_y, CO, NMHC, PAN and O_3 tropospheric masses (Mt). The masses of NO_y, CO, NMHC depend on their individual emissions as well as on the concentrations of NMHC and PAN. In particular, the formation of CO depends on the concentration of NMHC, chemical reaction 2.14. Additionally, via the reversible chemical reaction 2.26 the production of NO_y and NMHCs depend on the concentration of PAN and vice-versa. The ozone concentration dependent on the concentrations of NO_y in conjunction with NMHC, section 2.1.3. The order among the individual NO_y contributors (such as lightning, soils, shipping etc.) is similar to O_3 one and specially when the masses of NMHC contributions exhibit low values. To the same analogy, the orders between PAN and NO_y exhibit the same similarities (since PAN concentration depends on the NO_y and NMHC ones, chemical reaction 2.42). The low values from lightning in comparison to the other sectors can be attributed to the very low values of NMHC in the same sector. The methane contribution dominates the masses of CO, NMHC and PAN. The starting point begins via the formation of NMHC by CH_4 (chemical reactions 2.15 2.4). Now, the tagged NMHC produce PAN and CO which is tagged by CH_4 (see chemical reactions 2.26 and 2.14 respectively).

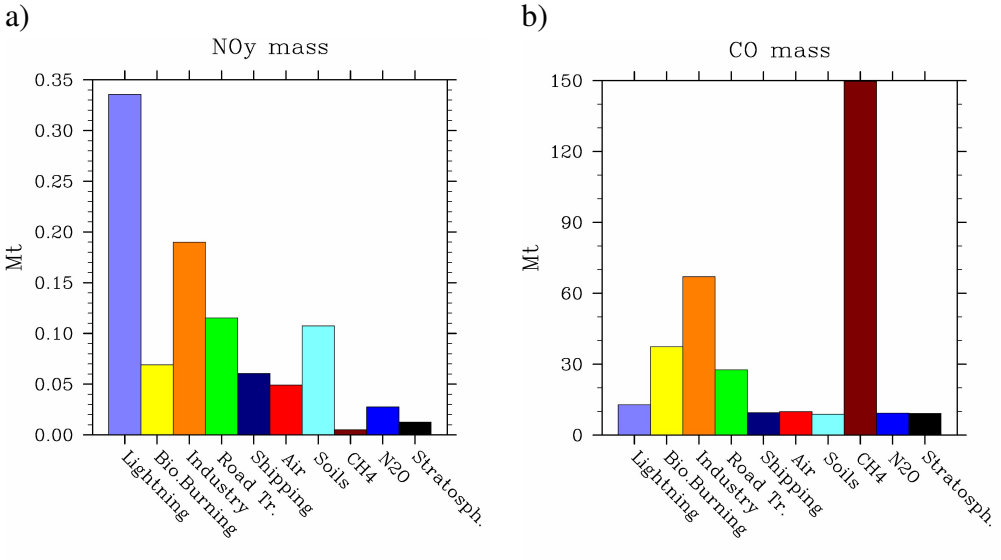

Figure 6.11: Histograms of **a)** NO_y and **b)** CO masses (Mt) for individual emission sectors (pressure levels between 1000 to 200 hPa) for the year 2002. Violet: lightning, yellow: biomass burning, orange: industry, green: road traffic, navy: shipping, red: aviation, light blue: soils, brown: CH_4, blue: N_2O and black: stratosphere.

The stratospheric contribution into the troposphere exhibits low values for NO_y, CO, NMHC and PAN compared to the other emission sectors. This is attributed to the corresponding pressure levels in conjunction with the fact that no stratospheric emissions occur. However, the maximum values of stratospheric ozone are caused to the general circulation (Brewer-Dobson circulation)

as well as to stratospheric-tropospheric exchange (STE) (see Fig. 6.5 and section 2.1.3). Ozone is produced in the stratosphere via photolysis, it is moved to the lower altitudes via the Brewer-Dobson circulation and it finally reaches the troposphere due to stratospheric-tropospheric exchange. The total ozone mass produced by anthropogenic emission sectors is simulated around $138\ Mt$, while the lightning sector is around $115\ Mt$. Lastly, the highest values are simulated for CO and O_3, which possess the highest longest life times (months, days) compared to the other species.

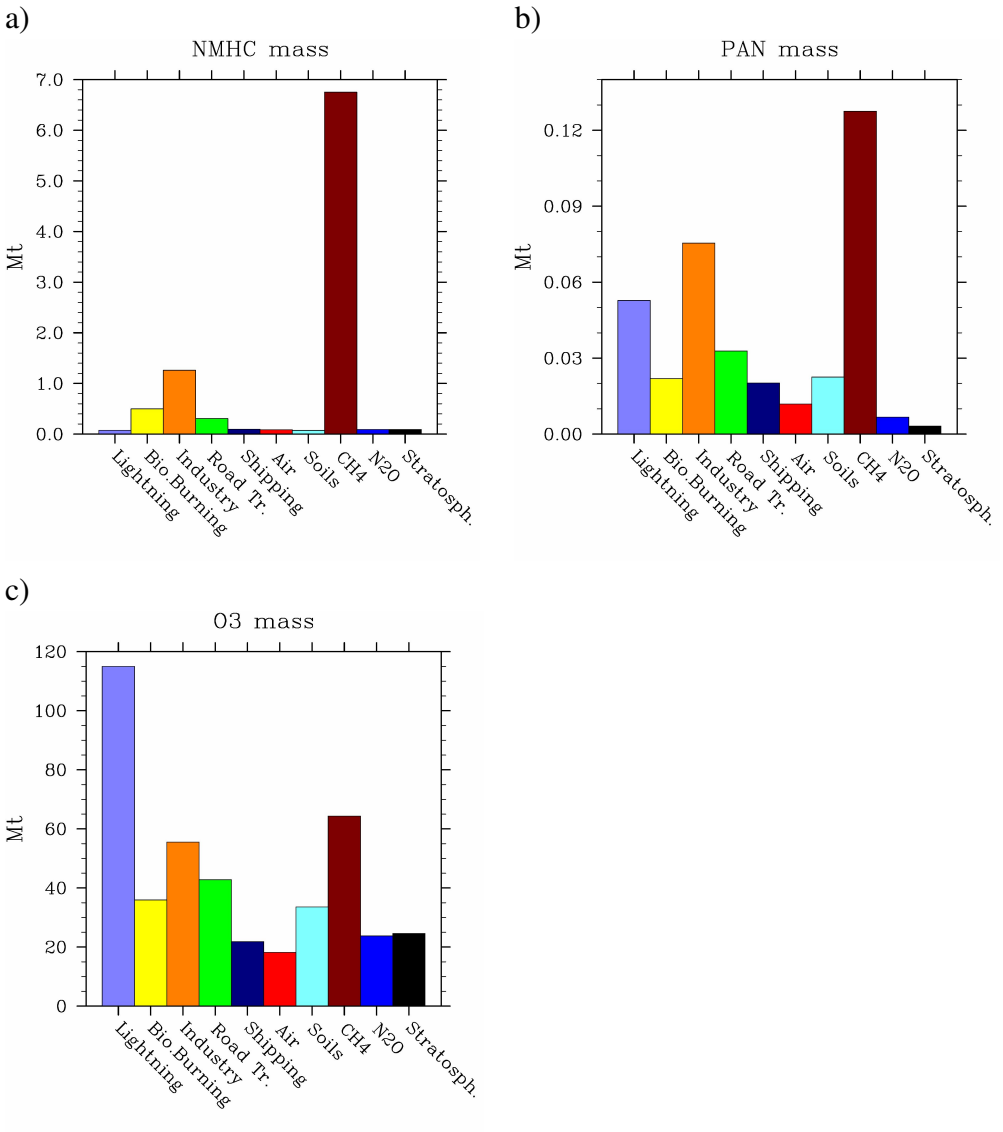

Figure 6.12: Histograms of **a)** NMHC, **b)** PAN and **c)** O_3 masses (Mt) for individual emission sectors (pressure levels between 1000 to 200 hPa) for the year 2002. Violet: lightning, yellow: biomass burning, orange: industry, green: road traffic, navy: shipping, red: aviation, light blue: soils, brown: CH_4, blue: N_2O and black: stratosphere.

6.4 Impacts of individual reaction rates for ozone

The tropospheric ozone concentration is calculated via the sum of the chemical production equations minus the sum of the chemical loss equations (see chapter 5). In order to investigate which of these reactions (production and loss) is the most important for tropospheric ozone distribution, the separation to individual reaction channels is required. Table 6.1 shows the chemical reactions of production and loss rates for ozone. In this section, the study of the impacts of these individual reaction channels (production and loss rates) for ozone is presented.

The analysis is focusing on the contributions of anthropogenic emissions mainly for aviation and shipping sectors. The relative contributions of shipping and aviation emitting sectors to the global atmospheric burden of ozone, Fig. 6.5a, are equally important (4%). However, their annual ozone concentration is referring to the different cruising altitudes (see Fig. 6.6). The conjunction of these two statements gives the reason why these emitting sectors have been selected. Also, the overview among all the emission sectors to the respective reaction channel, is given.

Figure 6.13 shows the mixing ratios of ozone by shipping and aviation sectors. Maximum ozone concentrations with respect to ships (pressure levels between 1000 hPa to 850 hPa) are found in the North Atlantic ocean close to 10 nmol/mol. Also, with respect to aviation sector (pressure levels between 450 hPa to 200 hPa) maximum ozone concentrations are simulated in USA, Europe and Asia.

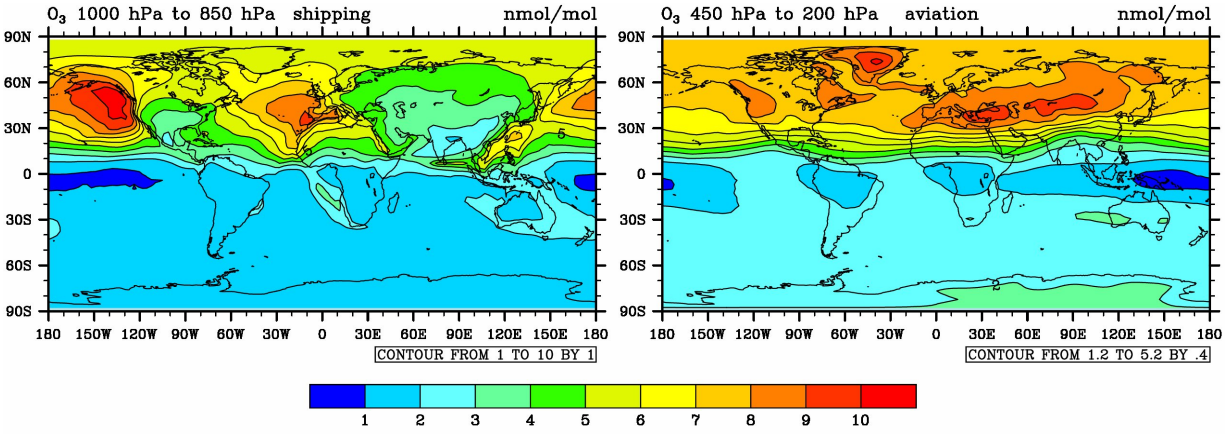

Figure 6.13: Mixing ratios nmol/mol of ozone with respect to shipping (left) and aviation (right) sectors (shipping: pressure levels between 1000 hPa to 850 hPa, aviation: pressure levels between 450 hPa to 200 hPa).

In this section the relevant questions are the following:

- Which chemical reaction is most important for the tropospheric ozone concentration?
- Pertaining to shipping and aviation, which are the most affected regions?

The first step of this analysis is the comparison between the shipping and aviation emitting sectors with respect to two different arbitrary grid points (GP) A_1 and A_2, respectively (see Table 6.1). In particular, the two arbitrary grid points are A_1(120E, 20N, Z41) and A_2(80E, 45N, Z21), where Z41 and Z21 corresponds to 1017 hPa and 300 hPa respectively. A_1 and A_2, refer to the locations in which shipping and aviation sectors have high ozone contributions (see Fig. 6.3 and 6.4).

In order to estimate the importance of each individual reaction, the total contribution of each reaction channel is calculated at each specific grid point, with respect to the total production and loss rates from all the emissions sectors. The Table 6.1 shows the percentages of all individual reactions rates corresponding to shipping and aviation sectors. The ozone production channel $P_{shp}(A)$ by shipping is found to have almost half (43.2%) of the total production contribution P(A) (80.6%) at the specific location compared to all the emission sectors. In comparison, the ozone production $P_{air}(A)$ by aviation (32.3%), in the same reaction channel P(A) but at the grid point A_2, reaches the one third of the total P(A). However, the ozone production rates of the channel $P_{air}(B)$ (15.7%) by aviation is around two times lower compared to $P_{air}(A)$ (32.3%).

The loss reaction channels by aviation $L_{air}(A)$ (14.8%) and $L_{air}(B)$ (11.3%) play an important role for ozone loss, where the total ozone loss by aviation $L^{tot}_{air}O_3$ is up to 34.24% at this specific location. This leads to the conclusion that HO_x chemistry is responsible for almost two times higher ozone loss rates, at the respective location. The leading reaction channel of ozone loss by shipping is the $L_{shp}(E)$ reaching values up to 15.6%. However, the loss reaction channels $L_{shp}(A)$ and $L_{shp}(B)$ exhibit also high numbers: 10.4% and 13.9%, respectively. The total ozone loss contribution by the sum of these reaction channels which corresponds to HO_x chemistry $(L_{shp}(A) + L_{shp}(B))$ is around more than half 24.3% to the total loss rates $L^{tot}_{shp}O_3$, 43.6% by shipping at this location.

	Reactions	ref	A_1 Shipping (%)	A_2 Aviation (%)
Production	$HO_2 + NO_y^{tag}$	P(A)	43.2	32.3
	$NMHC^{tag}$ + NO_y^{tag}	P(B)	37.4	15.7
$P^{tot}O_3$			80.6	48
Loss	$O_3^{tag} + OH$	L(A)	10.4	14.8
	$O_3^{tag} + HO_2$	L(B)	13.9	11.3
	$O_3^{tag} + NO_y^{tag}$	L(C)	3.8	0.7
	$O_3^{tag} + NMHC^{tag}$	L(D)	0.3	0.04
	$O_3^{tag} + X$	L(E)	15.6	10.4
$L^{tot}O_3$			43.6	37.2

Table 6.1: The reaction channels of production and loss rates of ozone. The species and families which have been tagged are: O_3, NO_y, NMHC. The rest of the species have been calculated via background chemistry. Chosen sectors: shipping and aviation with respect to two arbitrary grid points A_1 and A_2, respectively.

6.4.1 Ozone production rates

The ozone production is distinguished in two main chemical reaction channels (see Table 6.1), P(A) and P(B), respectively. The reaction channel P(A) represents the chemical reactions between the tagged NO_y and HO_x species (see chemical reaction 2.30) and P(B) represents the chemical reaction between NO_y and members of the NMHC families.

Shipping

Figure 6.14 shows the horizontal distribution for the ozone production rates (fmol/mol/s) by the two different reaction channels P(A) and P(B). Both plots show similar distributions. For both channels the shipping routes are visible. In the lower troposphere, the production rate contribution of the channel P(A) is almost double compared to P(B) (see Fig. 6.15). This is a result of different reaction rate constants between the two reaction channels. The reaction channel P(A) exhibits higher values for tropospheric ozone production because of the contained radicals. In addition, the maximum values from both reaction channels occurred mainly in the tropical mid-latitudes of the NH (see Fig. 6.14). For the tropical regions, this can be explained by the higher photolysis rates. For the middle troposphere (heights above 4 km), Fig. 6.15, the ozone production is low compared to the lower troposphere. This is attributed to the lower concentrations of the chemical species and families of P(A)and P(B) at these altitudes.

Aviation

Figure 6.16 shows the horizontal distribution, of the ozone production rates (fmol/mol/s), by the two different reaction channels P(A) and P(B). The maximum ozone production at cruise altitudes are found in the NH at mid-latitudes. Central Europe, Asia and USA are found to have the maximum ozone productions rates of 3 fmol/mol/s. Figure 6.15 shows the vertical distributions for both reaction channels. For both reaction channels the maximum values occur in the free troposphere at NH at cruise altitudes, between 9 to 10 km. The longer life time in higher altitudes of NO_y (days to weeks), as compared to the proximity of the surface (hours), is an additional reason to the greater production of ozone up in theses altitudes. Moreover, in the northern tropical regions at lower altitudes (up to 700 hPa), high production rates are found for both reaction channels.

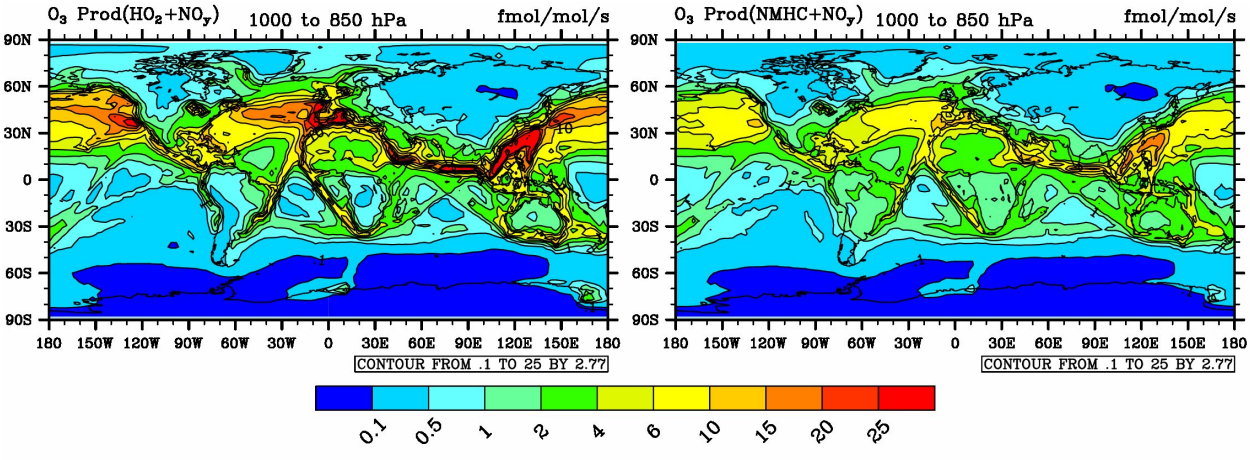

Figure 6.14: Shipping horizontal distributions (pressure levels between 1000 hPa to 850 hPa) of ozone production rates (fmol/mol/s) with respect to two different reaction channels: P(A) (left) and P(B) (right).

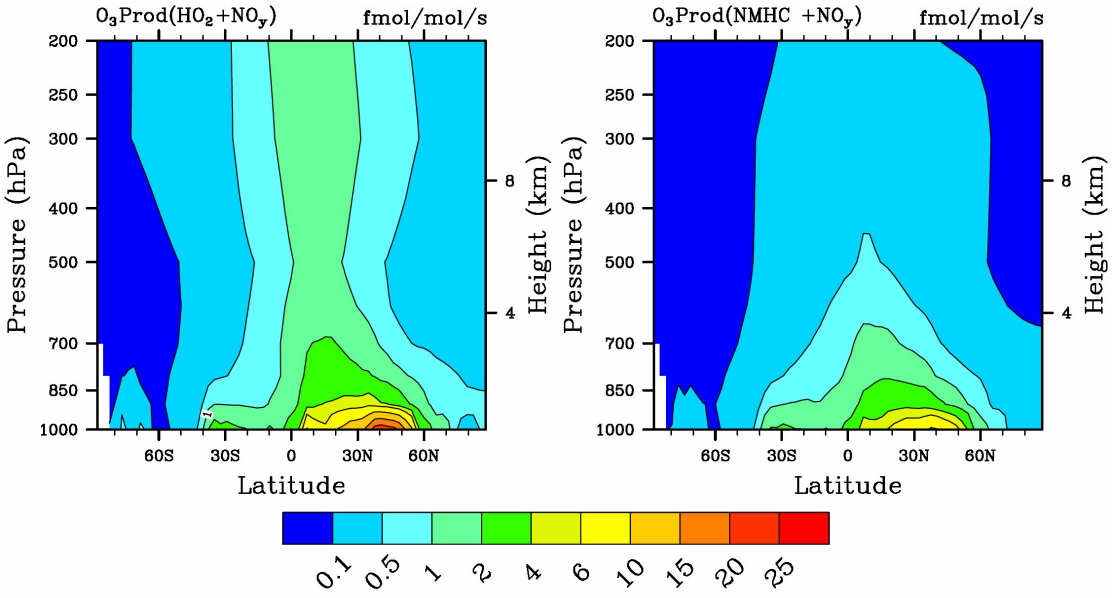

Figure 6.15: Shipping zonal mean distributions (pressure levels between 1000 hPa to 200 hPa) of ozone production rates (fmol/mol/s) with respect to two different reaction channels: P(A) (left) and P(B) (right).

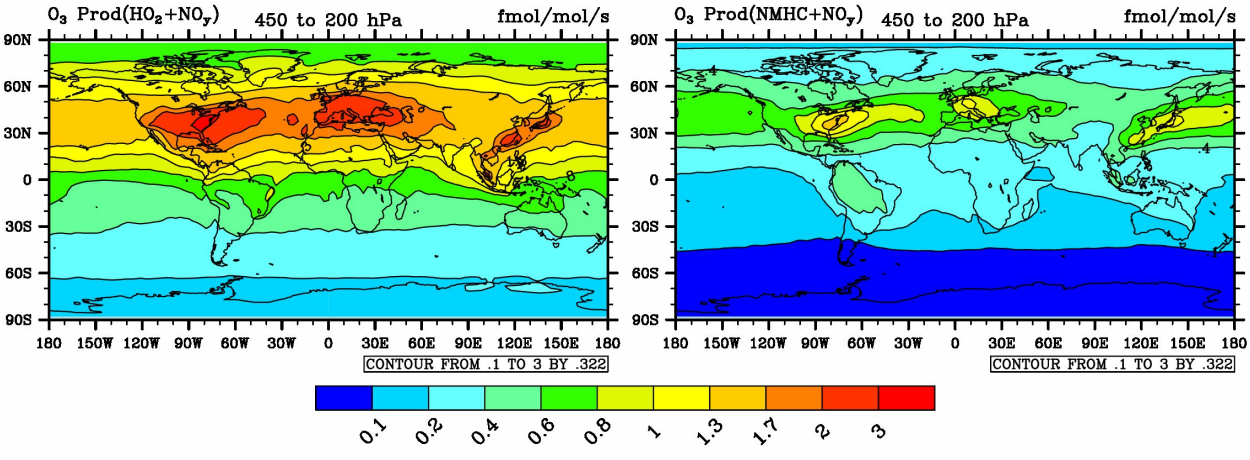

Figure 6.16: Aviation horizontal distributions (pressure levels between 450 hPa to 200 hPa) of ozone production rates (fmol/mol/s) with respect to two different reaction channels: P(A) (left) and P(B) (right).

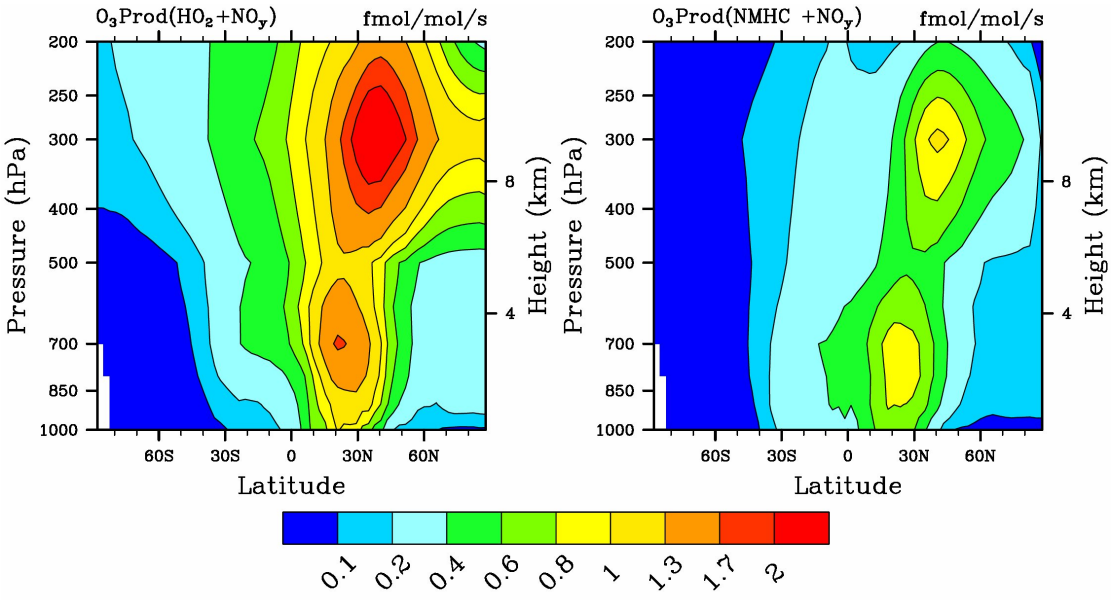

Figure 6.17: Aviation zonal means distributions (pressure levels between 1000 hPa to 200 hPa) of ozone production rates (fmol/mol/s) with respect to two different reaction channels: P(A) (left) and P(B) (right).

6.4.2 Ozone loss rates

The ozone loss is distinguished in five main chemical reaction channels: L(A), L(B), L(C), L(D) and L(E) respectively (see Table 6.1). The consideration is the same as in section 6.4.1 for the production channels. The first two reaction channels L(A) and L(B) represent the ozone loss rates by the untagged OH and HO_2 radicals, respectively. The third L(C) and the forth L(D) reaction channels represent the ozone loss rates from species which belong to NO_y and NMHC families, respectively. Lastly, the fifth reaction channel contains the rest of the chemical untagged species which are able to deplete ozone (see the included chemical reactions in the Appendix B). This means that in this reaction channel only the ozone is tagged and the rest of the species are calculated via MECCA chemistry as for HO_x.

Shipping

The horizontal and vertical distributions for ozone loss rates (10^{-1}fmol/mol/s) by the five different reaction channels are shown in the figures 6.18 and 6.19. In general, the regions with the highest ozone loss rates are the regions where the highest concentrations of the regarding reacted species occur (see Appendix B).

The reaction channels L(A) and L(B) which correspond to OH and HO_2 (see chemical reactions 2.9 and 2.18) to deplete the ozone respectively, show similar horizontal and vertical distributions. The maximum values are simulated in the lower troposphere at northern mit-latitudes (0.5fmol/mol/s). However, the HO_2 radicals are simulated to have higher ozone loss rates compared to OH. This is attributed to high NO_y concentration (see section 2.1.1) in the NH as well as explains the wide horizontal and vertical distributions in northern polar regions. The OH radicals are produced via photolysis (see chemical reactions 2.1 and 2.2) so that in the higher tropical regions high OH concentrations occur (see Fig. 2.2). This explains why the vertical distribution of the reaction channel L(A) has higher values compared to L(B) reaching pressure levels close to 200 hPa. Nevertheless, the highest loss values are simulated in the NH at tropical regions and mid-latitudes (vertical scale).

The horizontal distribution of loss rates L(C) is mainly important in the NH at mid-latitudes. This is explained by the high NO_y concentration of ships in these regions (see Appendix B). The shipping routes across the oceans are visible with high ozone loss rates close to Europe, Asia and USA. Zonal mean of ozone loss rates by NO_y are important in the lower troposphere, which can be attributed to the short life time of NO_y in these altitudes.

The reaction channel L(D) gives the lowest values of shipping ozone loss. The ozone loss rates which are simulated over the tropical continents (S. America, central Africa, Fig 6.18) can be attributed to high mixing ratios of NMHC which are simulated in these regions (see Appendix B.2). However, the short life time, at these low altitudes, leads to an additional cause for low ozone loss. All in all, the highest rates in the horizontal and vertical distributions come from the reaction channel L(E) because of the photolysis reactions (via $O(^1D)$) are contained. The maximum values are simulated in the northern tropical regions. The horizontal distribution exhibits large variation over the oceans. Moreover, its vertical distribution exhibits symmetry with respect to the equator, for pressure levels above to 700 hPa.

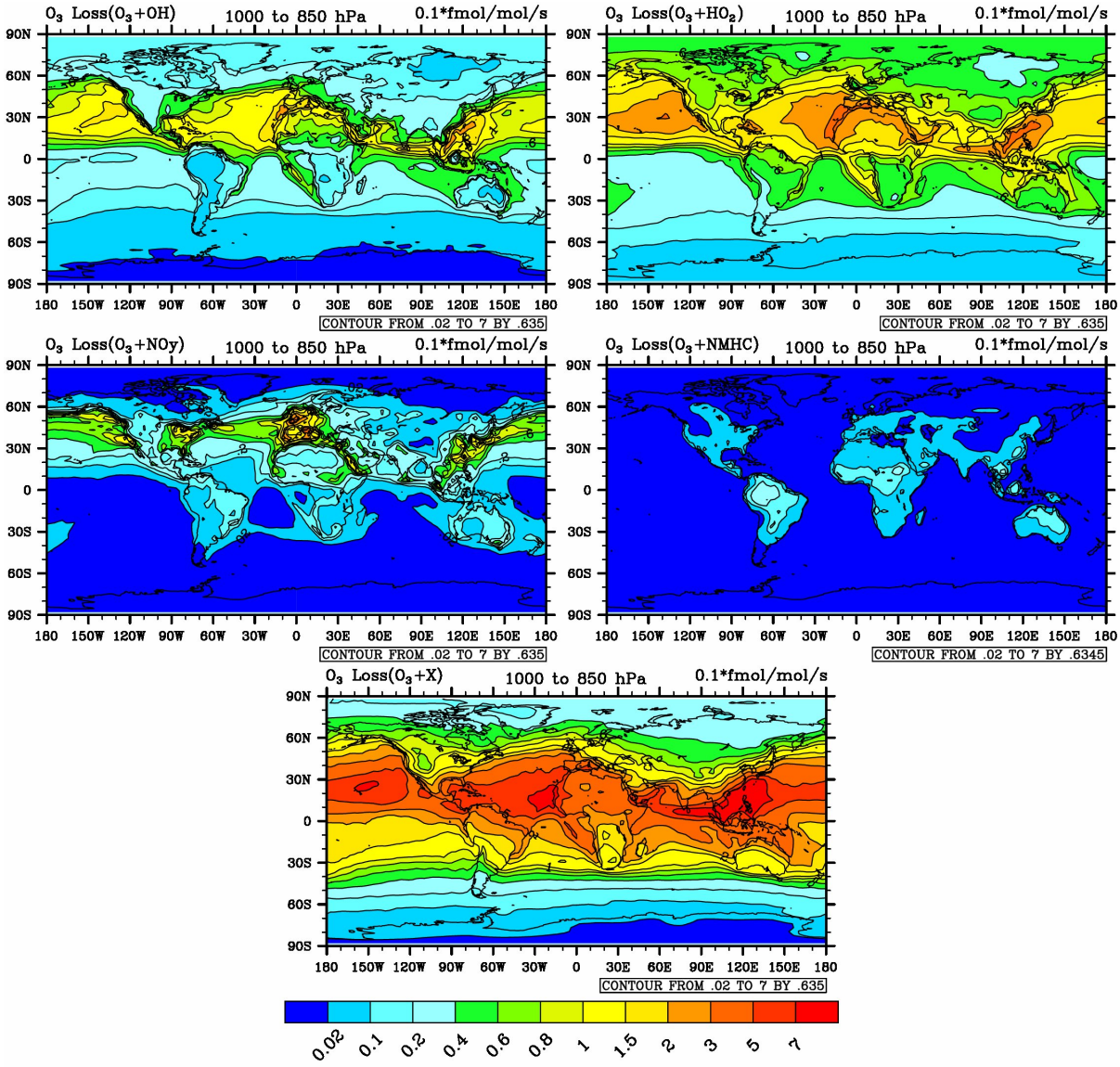

Figure 6.18: Horizontal distributions (pressure levels between 1000 hPa to 850 hPa) of shipping ozone loss rates, 10^{-1}fmol/mol/s, for five different reaction channels: L(A), L(B), L(C), L(D) and L(E).

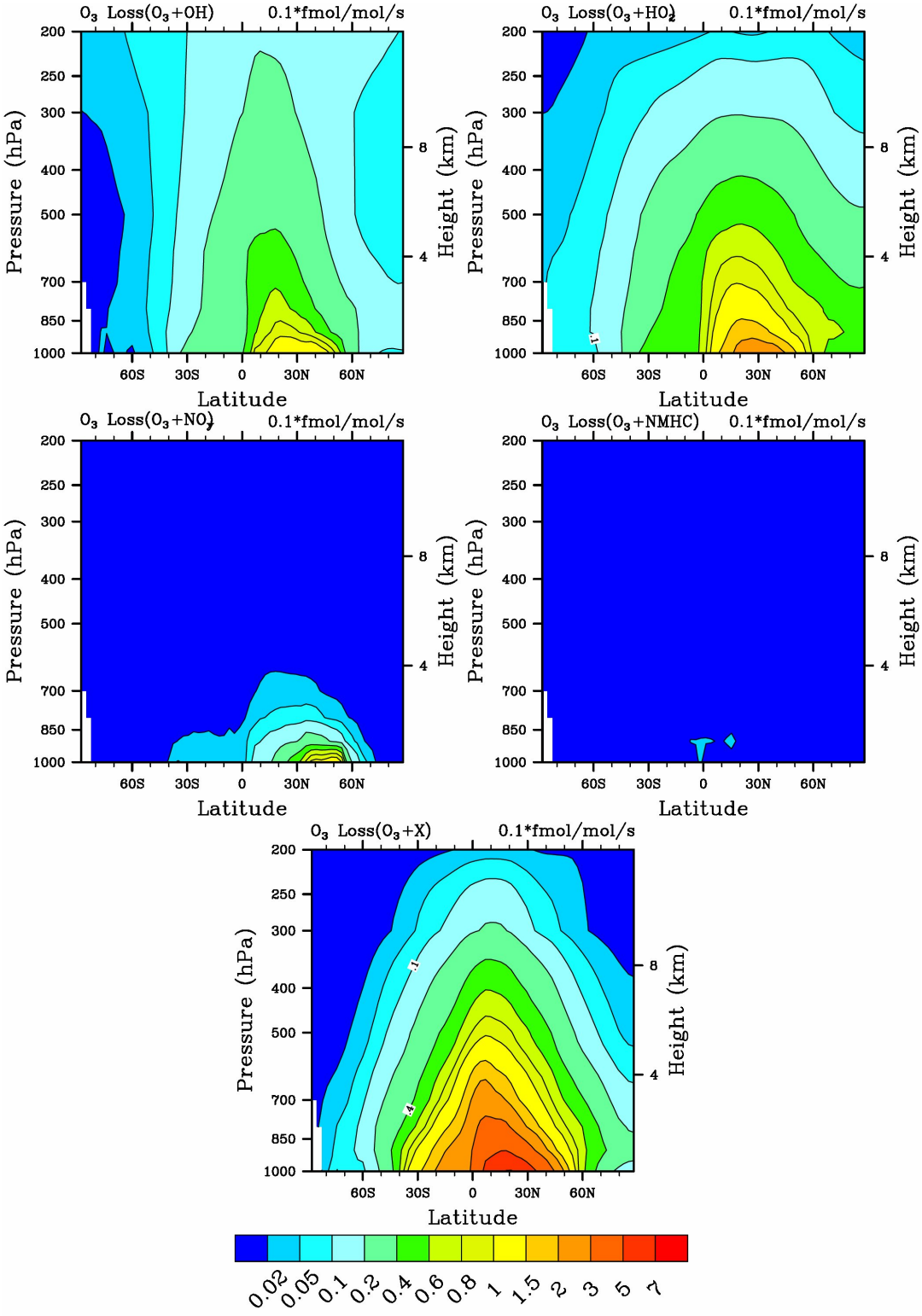

Figure 6.19: Zonal mean distributions (pressure levels between 1000 hPa to 200 hPa) of shipping ozone loss rates, 10^{-1}fmol/mol/s, for five different reaction channels: L(A), L(B), L(C), L(D) and L(E).

Aviation

Figures 6.21 and 6.22 show the horizontal and vertical distributions of ozone loss rates (10^{-1}fmol/mol/s) by the five different reaction channels, respectively. The reaction channels L(A) and L(B) show similar horizontal distributions. Higher values are found in northern tropical regions and mid-latitudes. The local maxima are found in east USA for both reaction channels as well as in Asia. Zonal mean values of L(B) are simulated to be higher compared to L(A). The maximum values of L(B) are around 0.3fmol/mol/s in NH low troposphere at mid-latitudes (two times higher) compared to L(A) in the same regions.

The reaction channel L(E) is simulated to have the highest ozone loss rates. In particular, in cruising altitudes the maximum values are found in the northern tropical regions as well as at the mid-latitudes is around $3.5 \cdot 10^{-1}$fmol/mol/s. The contribution of aviation to ozone loss (zonal mean) is maximized in the northern low troposphere at tropical regions reaching values around $24 \cdot 10^{-1}$fmol/mol/s. This is explained by the following: the L(E) reaction channel represents the ozone loss from aviation via the species which have not been tagged but are calculated via background. The high ozone production rates of aviation which are found in the lower northern troposphere (see Fig. 6.17) in conjunction with the high absolute concentrations of the untagged species X (L(E) reaction channel) in tropical regions leads to high ozone loss rates in these altitudes.

The reaction channels L(C) and L(D) have the lowest loss rates (similar to shipping). The vertical variation of the reaction channel L(C) is larger than L(D), mainly because of the higher life time of NO_y which occurs in higher altitudes (days-weeks). Also, the life time of NO_y is higher compared to NMHC. However, the ozone loss values, for both channels, are the smallest compared to all the other reaction channels.

Figures 6.23a and 6.23b illustrate the histograms, for the individual reaction rates for global mean values, for shipping and aviation emission sectors. The ozone production channel P(A), for both sectors, is around 35% higher compared to P(B). Nevertheless, the loss reaction channel L(C) has the greatest contribution compared to all the others channels (shipping: 49%, aviation: 44%). However, the total ozone loss rates from HO_x radicals are reaching similar numbers (shipping: 47%, aviation: 54%).

Figure 6.23d illustrates the histograms including all the ten emission sectors. The total P(A) production channel, from all the emission sectors, is around 48% higher compared to P(B). This leads to 13% higher ozone production rates from the total P(A) compared to the average value of shipping and aviation emission sectors (43%). The contribution of HO_x chemistry to ozone loss (reaction channels L(A) and L(B)) is around 47% and is similar to the average loss values of shipping and aviation sectors (shipping: 47%, aviation: 54%).

Figure 6.20 illustrates the reaction channels P(A) (blue bars) of each emission sector. The yellow bar represents the reaction channel P_{CH_4}(B) from methane. Its contribution is around 95%. This is attributed to high methane contribution for the tagged NMHC. However, the average percentages for the P(A) for all the bars (except methane) is around 60%.

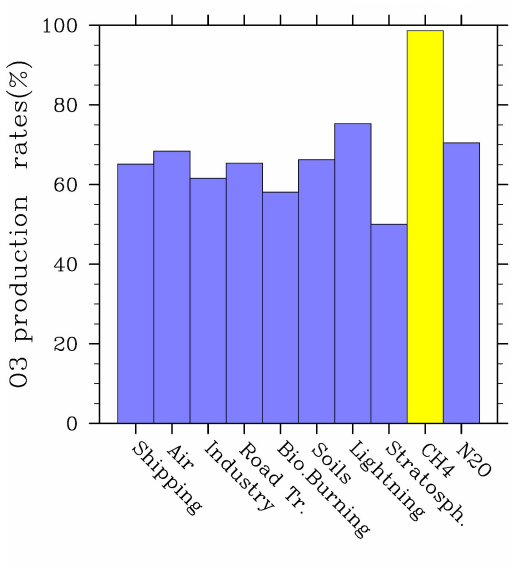

Figure 6.20: Ozone production channel P(A) corresponding to the OH radical contribution (purple). The reaction channel P(B) corresponds to ozone production by NMHC (yellow).

To summarize the above investigation, it is concluded the following:

- The most important channel for ozone production is P(A). The ozone production rates by shipping emissions are larger compared to the aviation at respective cruise altitudes (aviation cruising levels between 450 to 200 hPa, shipping around 1000 hPa). The maximum production rates of shipping (24 fmol/mol/s) are about eight times higher, than the maxima of aviation (3 fmol/mol/s). This is a result of higher mixing ratios at the lower altitudes of the species HO_2 and NO_y.

- The ozone loss rates exhibit particular interest. At the respective cruise levels (see horizontal distribution, shipping: pressure levels between 1000 hPa to 850 hPa and aviation: pressure levels between 450 hPa to 200 hPa) the maximum loss rates of shipping (0.7 fmol/mol/s) are about two times higher compared to aviation (0.5 fmol/mol/s). The leading reaction channel for ozone loss rates is the L(E) for both emission sectors and exhibits the same vertical symmetry (zonal mean). However, in the NH at lower altitudes, aviation is found to have maximum values (2.4 fmol/mol/s) three times higher compared to shipping (0.7 fmol/mol/s) for the same loss reaction channel L(E). This is a result of higher ozone mixing ratios from aviation compared to shipping, at this altitudes.

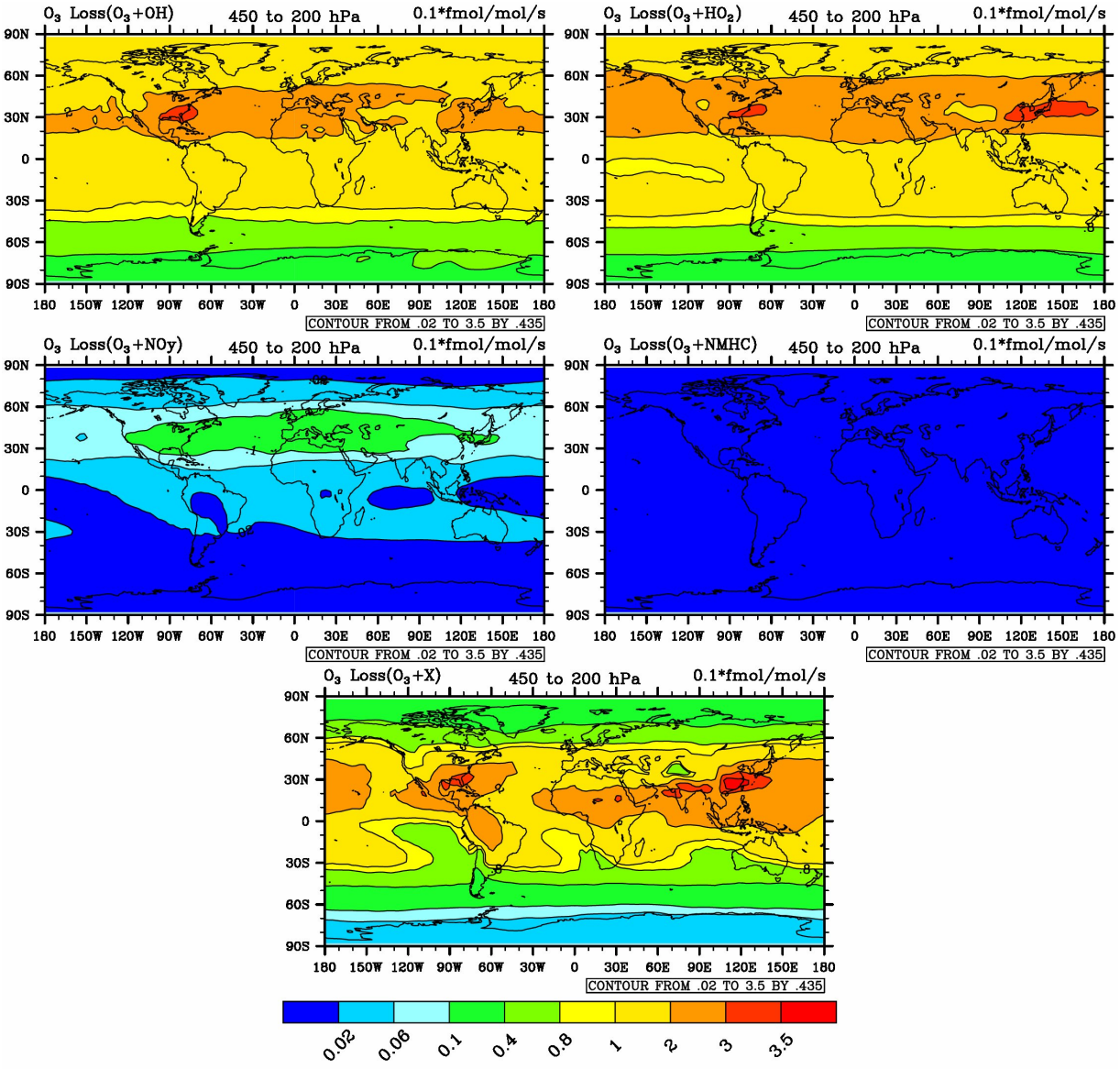

Figure 6.21: Horizontal distributions (pressure levels between 450 hPa to 200 hPa) of aviation ozone loss rates, 10^{-1}fmol/mol/s, for five different reaction channels: L(A), L(B), L(C), L(D) and L(E).

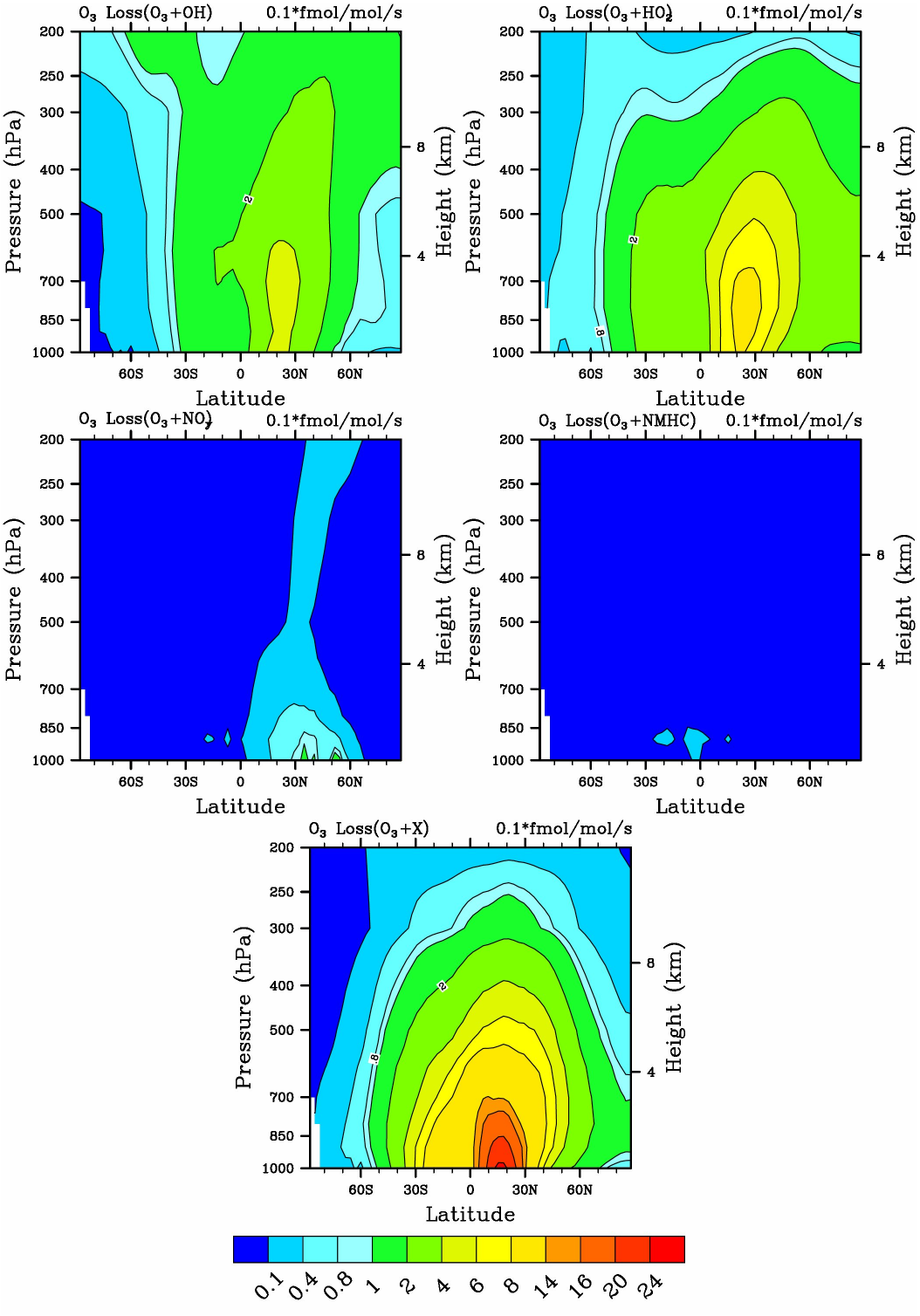

Figure 6.22: Zonal mean distribution (pressure levels between 1000 hPa to 200 hPa) of aviation ozone loss rates, 10^{-1}fmol/mol/s, for five different reaction channels: L(A), L(B), L(C), L(D) and L(E).

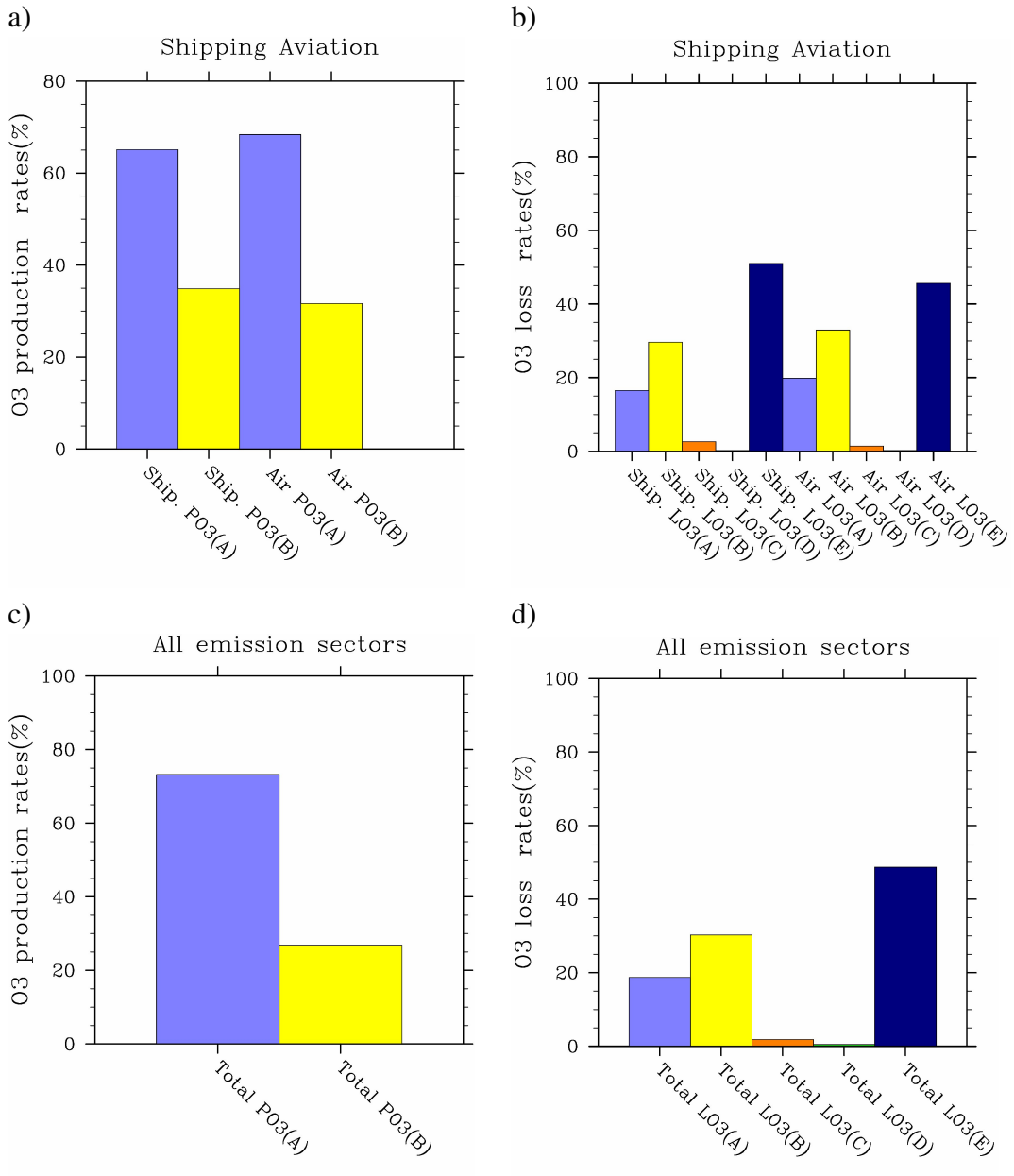

Figure 6.23: Histograms of individual reaction channels to tropospheric ozone in global mean values (%). **a)** Production and **b)** loss reaction channels, for shipping and aviation emission sectors. **c)** Production and **d)** loss reaction channels, including all emission sectors.

6.5 Discussions

In this chapter the analysis and comparison of the impacts of natural and anthropogenic emissions to the tropospheric concentrations was presented. For the first time the tropospheric ozone concentration is quantified by the contributions of NO_y, CO and NMHC families/species. Also, the contribution of methane to NO_y concentration was taken into account for the first time.

In the first section of this chapter the analysis of the relative contribution of NO_y and tropospheric O_3, with respect to emission sources, was presented. This gave the opportunity to compare the distributions and contributions of the emitting sources into the troposphere of the respective species and families. The NO_y emissions with respect to different emitting sources such as aviation, are significant influencing the contribution of NO_y in the troposphere. In comparison, the contribution of O_3 in the troposphere is depending on the emissions of NO_y, NMHC and CO (see chapter 5). For pressure levels up to 200 hPa and for global mean values, the highest tropospheric ozone contribution (23%) is found to be from lightning. Its distribution covers the tropical troposphere reaching maximum local values of around 37%. The distribution of contribution of the anthropogenic emission sectors are found to cover the whole NH. For global mean values their total contribution reaches almost 40%.

In the second section the analysis of the chemical impacts in the troposphere with respect to the primary species/families NO_y, NMHC and CO to tropospheric ozone and PAN concentrations, due to all the ten emission sectors, was presented. Now, the concentrations of the primary species due to their interaction lead to the concentration of the secondary species/families such as tropospheric ozone and PAN. In addition, it has to be emphasised that the concentration amount of the chemical species also strongly depends on their life time. For instance, the NO_y emissions of biomass burning exhibit the higher values (10^{-10} mol/mol/s) than CO (10^{-12} mol/mol/s). However, for global mean values the masses of CO and NO_y are found to be around 40 Mt and 0.07 Mt, respectively. CO and tropospheric ozone exhibit the highest masses (Mt). Their average values are around 40 Mt and 60 Mt, respectively. Lastly, for global mean values, the total ozone mass due to natural sources is 100 Mt higher than the anthropogenic sources.

In the last section the investigation of the distribution of the tropospheric ozone contribution was presented. This came to fruition by examining the individual production and loss reaction rates of ozone. The parameters which play the most crucial role in this section firstly, are the differences among the reaction rate constants of the respective reaction channels and secondly the mixing ratios of the respectively tagged species. The outstanding message of this investigation is that the tropospheric ozone production channel P(A) (members of NO_y family reacting with HO_2 radicals) is found to be around 60% higher than average compared to P(B) reaction channel (members of NO_y family reacting with members of NMHC family) for all the emission sectors (expect methane). This is attributed to the stronger reactivity due to HO_2 radicals in the P(A) production channel.

For the tropospheric ozone loss rates the highest rates occur for the sectors with the respectively highest production rates. For instance, the maximum loss rates for shipping are about two times higher compared to aviation with respect to the different cruising levels (shipping: pressure levels between 1000 hPa to 850 hPa and aviation: pressure levels between 450 hPa to 200 hPa). The

loss reaction channel L(E) (tropospheric ozone loss due to the untagged species such as H_2O etc., rest of the chemical species which do not belong to the NMHC, NO_y and HO_2 families) is found to have the highest ozone loss rates because of the highest reaction rate constants. The loss reaction channels L(C) and L(D) (ozone loss rates due to NO_y and NMHC respectively) exhibit the lowest values, lower than 5%. This is attributed to the relatively lower reaction rate constants in these channels compared to L(E) as well as L(A) and L(B) (loss ozone reaction channels with respect to HO_x radicals).

Chapter 7

The tagging implementation in HO_x chemistry

A complete tagging scheme which describes the contributions of the emission sectors to the concentration of the chemical species is too complex to be applied in a general circulation model (GCM) in one step. For this reason the present study is separated in two different wise-steps. The first step is included the analysis of the tagged species NMHC, PAN, CO, NO_y to the tropospheric ozone (tagged) concentration (see chapters 5 and 6). The second step includes additionally the tagged HO_x species to the previous chemical scheme (first step).

The HO_x species has low abundance in the troposphere but influences the tropospheric chemical composition because of their high reactivity (see chapter 2). The main initial photochemical reaction for OH radical production is the photolysis of ozone, which leads to the reaction between the excited oxygen and water vapor (see chemical reaction 2.1). Additionally, the highest concentrations are simulated to be around mid-day, when the highest solar energy occurs. The HO_x radicals dominate the oxidative capacity of the atmosphere because they react with trace gases (e.g chemical reactions 2.15 2.18) and therefore eliminate them from the atmosphere. In comparison, the reaction between nitrogen oxides and HO_x radicals produce ozone ($HO_2^{tag} + NO_y^{tag} \rightarrow O_3^{tag}$, see Table 6.1). At the end, as has been shown in section 2.1.1, the HO_x chemistry is influenced by the different concentration levels of NO_y (see Fig. 2.1).

For the first time, a chemical scheme which describes the main principles of tropospheric HO_x chemistry is tagged and implemented in a global chemistry-climate model. The distribution of contributions for OH and HO_2 radicals, which is derived from Eq. (4.31) to Eq. (4.34), with respect to all emission sectors, are analyzed. The main chemical reactions which describe the HO_x chemistry (see Appendix B) are selected in order to set up the first tagged HO_x chemistry scheme. However, adding more chemical reactions to this specific chemical scheme is a key aspect in order to better describe the tropospheric HO_x chemistry.

In the previous chapter, the analysis of the tagging implementation to the included species NO_y, NMHC, PAN, CO and O_3 was presented as the first order of this investigation. In this chapter, the description of this implementation of HO_x tagging chemistry is presented, as it has been the second and higher step of this investigation. The analysis of two specific anthropogenic emission

sources (shipping and aviation) is shown in the second section of this chapter. Their analysis and comparison is focused on mixing ratio distributions, since their relative contributions to the global atmospheric burden of ozone mass are equally important (see section 6.1.2), but exhibit in different pressure levels. Lastly, a short summary of the HO_x tagging application to the REACT4C project with respect to methane loss from OH is presented.

7.1 The tagging HO_x chemistry

In this section, the implementation of the tagging method to HO_x chemistry, is presented. In chapter 2.1.1, two basic statements are made about HO_x chemistry: first, the HO_x family influences the tropospheric ozone chemistry (see Fig. 2.1) and second, there is a strong interaction between these two molecules, OH and HO_2. Therefore, the quantification of HO_x contribution is taken into consideration as a system OH-HO_2 and not as an independent term. Also, the lifetime of both species is very short, around few seconds.

The equations which have been chosen in order to describe the HO_2 and OH chemistry, are shown in Appendix B and are taken from the chemistry text books: Seinfeld and Pandis (2006) and Jacob (2004). Implementing the tagging method means to consider the differential equations which describe the evolution of the concentrations of tagging sub-species (HO_{2i} and OH_i), by following the reaction path ways. The differential equations for HO_{2i} and OH_i which are derived from the Eq. (4.29) (see section 4.3) are described from the following equations:

$$\frac{dHO_{2i}}{dt} = P_{HO_{2i}}(O_3, NO_y, HO_x, ...) - L_{HO_{2i}}(O_3, HO_x, NO_y, ...) \tag{7.1}$$

$$\frac{dOH_i}{dt} = P'_{OH_i}(O_3, NO_y, HO_x...) - L'_{OH_i}(O_3, HO_x, ...) \tag{7.2}$$

Where P (as well as P') and L (as well as L') represent the production and loss terms of HO_{2i} (and OH respectively). In particular, the most important reaction for the HO_2 production depends on ozone and hydroxyl, whether for OH production the reaction between water vapor and excited oxygen atom is the leading one (Fig. 2.1). These chemical schemes which refer to the terms (P, P', L and L') are shown in Appendix B. The above differential equations (7.1) and (7.2) with respect to steady state calculations (since the time step of the model is much larger than chemical reaction time) (see Eq. (4.37)) are:

$$0 = P_{HO_{2i}}(O_3, NO_y, HO_x, ...) - L_{HO_{2i}}(O_3, HO_x, NO_y, ...) \tag{7.3}$$

$$0 = P'_{OH_i}(O_3, NO_y, HO_x...) - L'_{OH_i}(O_3, HO_x, ...) \tag{7.4}$$

The calculations of each production and loss term is based on Eq. (4.42). This gives the following results (note that the ratio of the excited oxygen atom $\frac{[O(^1D)_i]}{[O(^1D)]}$ is equal to ozone one $\frac{[O_{3i}]}{[O_3]}$):

$$\begin{aligned} P'_{OH_i} =& P'_1 \frac{[O_{3i}]}{[O_3]} + \frac{1}{2} P'_3 \left(\frac{[HO_{2i}]}{[HO_2]} + \frac{[O_{3i}]}{[O_3]} \right) + \\ & \frac{1}{2} P'_4 \left(\frac{[HO_{2i}]}{[HO_2]} + \frac{[NO_{yi}]}{[NO_y]} \right) \end{aligned} \tag{7.5}$$

$$\begin{aligned} L'_{OH_i} =& \frac{1}{2} D'_1 \left(\frac{[OH_i]}{[OH]} + \frac{[O_{3i}]}{[O_3]} \right) + \frac{1}{2} D'_2 \left(\frac{[OH_i]}{[OH]} + \frac{[NMHC_i]}{[NMHC]} \right) + \\ & \frac{1}{2} D'_4 \left(\frac{[OH_i]}{[OH]} + \frac{[CO_i]}{[CO]} \right) + \frac{1}{2} D'_5 \left(\frac{[OH_i]}{[OH]} + \frac{[HO_{2i}]}{[HO_2]} \right) + \\ & \frac{1}{2} D'_6 \left(\frac{[OH_i]}{[OH]} + \frac{[CH_{4i}]}{[CH_4]} \right) + \frac{1}{2} D'_7 \left(\frac{[OH_i]}{[OH]} + \frac{[NO_{yi}]}{[NO_y]} \right) \end{aligned} \tag{7.6}$$

$$\begin{aligned} P_{HO_{2i}} =& \frac{1}{2} P_1 \left(\frac{[OH_i]}{[OH]} + \frac{[CO_i]}{[CO]} \right) + \frac{1}{2} P_3 \left(\frac{[OH_i]}{[OH]} + \frac{[O_{3i}]}{[O_3]} \right) + \\ & \frac{1}{2} P_4 \left(\frac{[NMHC_i]}{[NMHC]} + \frac{[NO_{yi}]}{[NO_y]} \right) \end{aligned} \tag{7.7}$$

$$\begin{aligned} L_{HO_{2i}} =& \frac{1}{2} D_1 \left(\frac{[HO_{2i}]}{[HO_2]} + \frac{[O_{3i}]}{[O_3]} \right) + \frac{1}{2} D_2 \left(\frac{[HO_{2i}]}{[HO_2]} + \frac{[NO_{yi}]}{[NO_y]} \right) + \\ & \frac{1}{2} D_3 \left(\frac{[HO_{2i}]}{[HO_2]} + \frac{[NMHC_i]}{[NMHC]} \right) + D_4 \frac{[HO_{2i}]}{[HO_2]} + \frac{1}{2} D_5 \left(\frac{[HO_{2i}]}{[HO_2]} + \frac{[OH_i]}{[OH]} \right) \end{aligned} \tag{7.8}$$

Now the differential equations (7.3) and (7.4) can be written:

$$0 = \left(A_i + \mathbf{P} \frac{[OH_i]}{[OH]} \right) - \left(B_i + \mathbf{D} \frac{[HO_{2i}]}{[HO_2]} \right) \tag{7.9}$$

$$0 = \left(\Gamma_i + \mathbf{P'} \frac{[HO_{2i}]}{[HO_2]} \right) - \left(\Delta_i + \mathbf{D'} \frac{[OH_i]}{[OH]} \right) \tag{7.10}$$

where the first and the second brackets, Eq. (7.9) describe the production and loss of HO_{2i}. Similar, the production and loss of OH are described from the first and the second brackets respectively in Eq. (7.10). Solving the above system Eq. (7.9) and (7.10) with respect to OH and HO_2:

$$[HO_{2i}] = [HO_2]\frac{[\mathbf{D'}(B_i - A_i) + \mathbf{P}(\Delta_i - \Gamma_i)]}{\mathbf{PP'} - \mathbf{DD'}} \tag{7.11}$$

$$[OH_i] = [OH]\frac{[\mathbf{D}(\Delta_i - \Gamma_i) + \mathbf{P'}(B_i - A_i)]}{\mathbf{PP'} - \mathbf{DD'}} \tag{7.12}$$

The above equations (7.11) and (7.12) describe the concentrations of the tagged species HO_{2i} and OH_i as a function of their total concentrations multiplied with the respective ratios. Both equations exhibit the same symmetry with respect to their individual terms such as Δ_i, Γ_i, **P'** and **D** etc. In particular, both ratios are expressed by the same denominator. The terms **P** and **P'** express the net production (P-L) of HO_2 and OH due to OH and HO_2, respectively (see Table 7.1). Specifically, the product **PP'** determines the net production HO_x chemistry which is created from the production and loss of OH and HO_2. Moreover, the **DD'** represents the total loss of HO_x (**D**: total HO_2 loss, **D'**: total OH loss). The functions A_i, B_i, Δ_i and Γ_i correspond to the tagged species. In particular, the A_i determines the HO_2 production due to non-HO_x chemistry, such as CO, NMHC etc. The B_i determines the HO_2 loss also due to non-HO_x chemistry. Similarly, the functions Γ_i and Δ_i express the production and loss of OH due to non-HO_x chemical compounds. Therefore, the equations $B_i - A_i$ and $\Delta_i - \Gamma_i$ determine the net of HO_2 and OH respectively via the non-HO_x chemistry.

Furthermore, the chemical mechanism of these equations (7.11) and (7.12) can be described from the following example: In case of increase of the ozone contributions by for instance road traffic emissions, the denominators of both ratios as well as the functions **P**, **P'**, **D** and **D'** will be constant due to this change. However, the equations A_i, B_i and Δ_i (see Table 7.1) will reach higher values multiplied by the terms P_3, D_2 and D_1', respectively. However, the equation Γ_i will also reach higher values yet by the term $P_3' + 2P_1'$. These changes will contribute to the decrease of both numerators since the Γ_i equation has an overall minus. Finally, the concentrations of both tagged radicals HO_{2i} and OH_i will also decrease. This can be proven also through the chemical reactions (2.18) and (2.9), where the increase of O_3 leads to HO_x loss.

Now, the previous equations (7.11) and (7.12) can be written:

$$HO_{2i} = HO_2 \cdot \omega_i \qquad OH_i = OH \cdot \varphi_i \tag{7.13}$$

where

$$\omega_i = \frac{[\mathbf{D'}(B_i - A_i) + \mathbf{P}(\Delta_i - \Gamma_i)]}{\mathbf{PP'} - \mathbf{DD'}} \qquad \varphi_i = \frac{[\mathbf{D}(\Delta_i - \Gamma_i) + \mathbf{P'}(B_i - A_i)]}{\mathbf{PP'} - \mathbf{DD'}} \tag{7.14}$$

the factors φ_i and ω_i replaced the respective ratios. Furthermore, both equations (7.13) have to satisfy the Eq. (7.15) (see Eq. (4.26)) so that the sum of φ_i and ω_i be equal to one.

$$\sum_{i=1}^{n} HO_{2i} = HO_2 \qquad \sum_{i=1}^{n} OH_i = OH_i \tag{7.15}$$

In this first approach the sums of the φ_i and ω_i are close to one. In other words, the total concentration of the regarding emission sectors underestimate the total concentrations of OH and HO_2 respectively. Since the HO_x chemistry is characterised by high reactivity as well as by the very short life time of the including radicals, additional chemical reactions may lead to a better chemical description of this family, in terms of distributions of the concentrations and hence the equations (7.15) be fulfilled.

Symbols	Equations	Physical meaning
A_i =	$P_1 \frac{[CO]_i}{[CO]} + P_3 \frac{[O_3]_i}{[O_3]} + P_4 \left(\frac{[NMHC]_i}{[NMHC]} + \frac{[NO_y]_i}{[NO_y]} \right)$	HO_{2i} production due to non-HO_x reaction partners
B_i =	$D_1 \frac{[O_3]_i}{[O_3]} + D_2 \frac{[NO_y]_i}{[NO_y]} + D_3 \frac{[NMHC]_i}{[NMHC]}$	HO_{2i} loss due to non-HO_x reaction partners
Γ_i =	$(2P'_1 + P'_3) \frac{[O_3]_i}{[O_3]} + P'_4 \frac{[NO_y]_i}{[NO_y]}$	OH_i production due to non-HO_x reaction partners
Δ_i =	$D'_1 \frac{[O_3]_i}{[O_3]} + D'_2 \frac{[MNHC]_i}{[MNHC]} + D'_4 \frac{[CO]_i}{[CO]} + D'_6 \frac{[CH_4]_i}{[CH_4]} + D'_7 \frac{[NO_y]_i}{[NO_y]}$	OH_i loss due to non-HO_x reaction partners
P =	$P_1 + P_3$ - D_5	Net production (P-L) of HO_2 due to OH
P' =	$P'_3 + P'_4$ - D'_5	Net production (P-L) of OH due to HO_2
D =	$D_1 + D_2 + D_3 + 2D_4 + D_5$	Total HO_2 loss
D' =	$D'_1 + D'_2 + D'_4 + D'_5 + D'_6 + D'_7$	Total OH loss

Table 7.1: References to the respective symbols.

7.2 The tagging HO_x chemistry to different emission sectors

A second simulation which included the tagged species NO_y, NMHC, PAN, CO, O_3 and HO_x has been made in order to investigate the impact of HO_x chemistry to tropospheric composition. In this section, the first results of tagging HO_x chemistry are presented. The selected emission sectors are referring to aviation and shipping. In the previous chapter (see section 6.4) the analysis of the same emission sectors of the impacts of the individual reactions rates showed the regions with the highest sensitivity to ozone production and loss. Additionally, the shipping sector is found to have higher ozone contribution compared to aviation for global and local mean values (see Fig. 6.15, 6.17 and Table 6.1). However, the analysis of both sectors showed that the HO_x chemistry is important for ozone production and loss (regarding reaction channels P(A), L(A) and L(B)).

In this section, the absolute concentrations (mol/mol) of the emitted sectors aviation and shipping to the regarding species OH and HO_2, is presented.

7.2.1 Shipping

Figures 7.1 and 7.2 illustrate the vertical and horizontal distribution of mixing ratios, for the species HO_2 and OH, respectively. In vertical scale, maximum mixing ratios, 3 fmol/mol, for OH are simulated in the northern tropical and mid-latitudes regions reaching pressure levels close to 860 hPa. Its vertical distribution exhibits larger variation compared to HO_2 and reaches altitudes close to 4 km (630 hPa). The maximum values (4 fmol/mol), in horizontal distribution (pressure levels between 1000 to 850 hPa), are simulated over Atlantic and Pacific Ocean in the NH (tropics and mid-latitudes).

The maximum values of HO_2 (1.3 fmol/mol) are around two times smaller compared to OH (3 fmol/mol). However, its maxima are found in the same regions as OH. Its vertical distribution does not exhibit a large variation and its maxima reach pressure levels close to 850 hPa. Also, its horizontal distribution shows similar pattern with OH. Its maximum values are found to cover the northern tropical and mid-latitudes. However, the OH mixing ratios are higher than HO_2 (same with the aviation) in these regions because of higher ozone production occurred from shipping (see Fig. 6.14 and 6.15). The HO_2 is produced mainly from OH depletion in conjunction with the fact that O_3 produces OH. This leads to lower HO_2 mixing ratios as well as to shorter HO_2 vertical distribution compared to OH (similar for aviation).

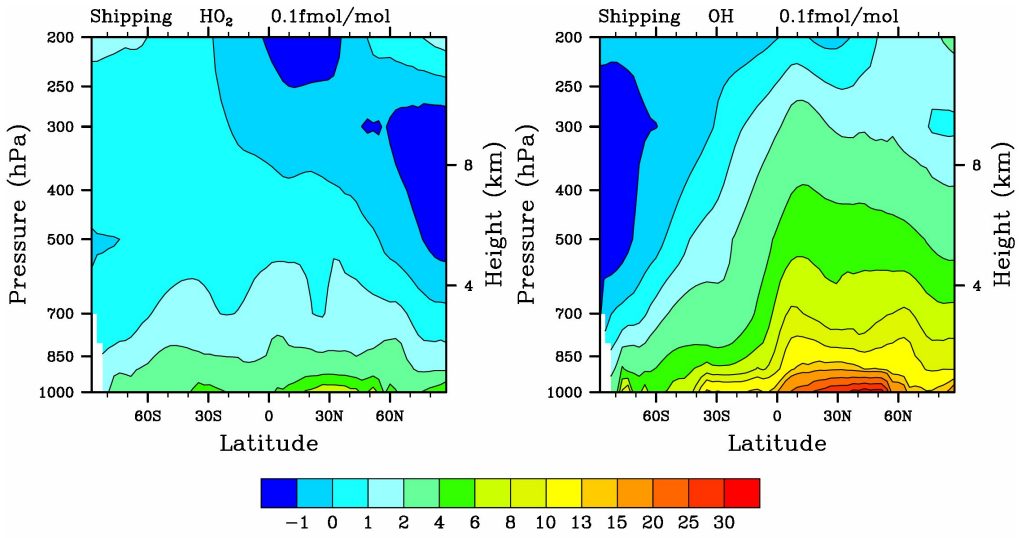

Figure 7.1: Zonal mean (pressure levels between 1000 hPa to 200 hPa) mixing ratios of shipping, 10^{-1} fmol/mol, for the species HO_2 (left) and OH (right).

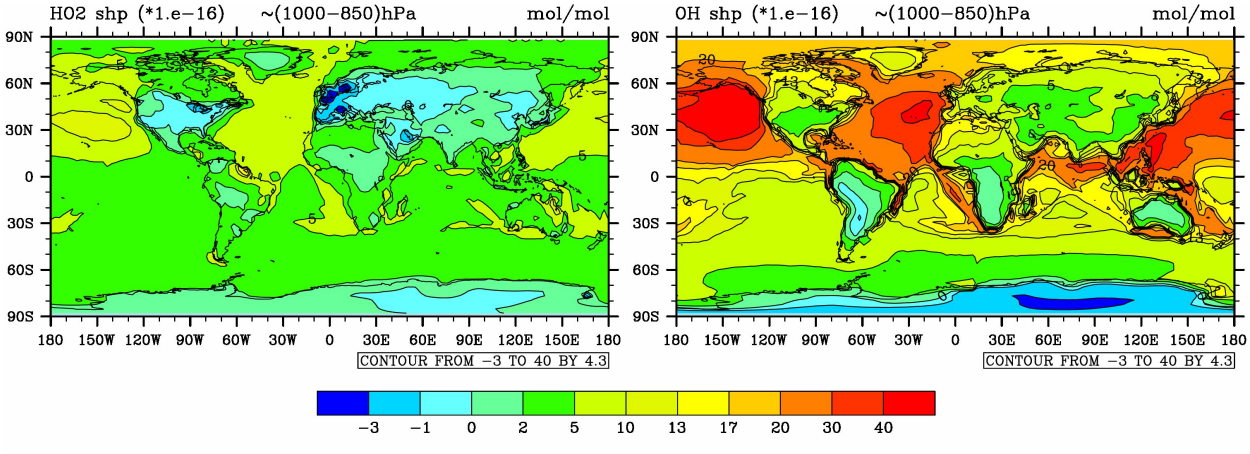

Figure 7.2: Horizontal distribution (pressure levels between 1000 hPa to 850 hPa) of shipping, 10^{-1} fmol/mol for the species HO_2 (left) and OH (right).

7.2.2 Aviation

Figures 7.3 and 7.4 illustrate the vertical and horizontal distribution of mixing ratios, for the species HO_2 and OH, respectively. In vertical scale, maximum OH mixing ratios, 0.8 fmol/mol, are simulated in the low northern tropical regions, reaching pressure levels around 870 hPa. Also, it exhibits large vertical variation for values up to 0.6 fmol/mol for pressure levels close to 450 hPa in the NH. In the SH at mid-latitudes and polar regions, the OH mixing ratios exhibit small values because of less flight cruising in conjunction to the very short life time of OH (seconds). In horizontal scale (pressure levels between 450 to 200 hPa), the cruising lines are visible and cover the pathways between Europe and N. America. The local maxima are simulated in central Europe and USA (across the costs).

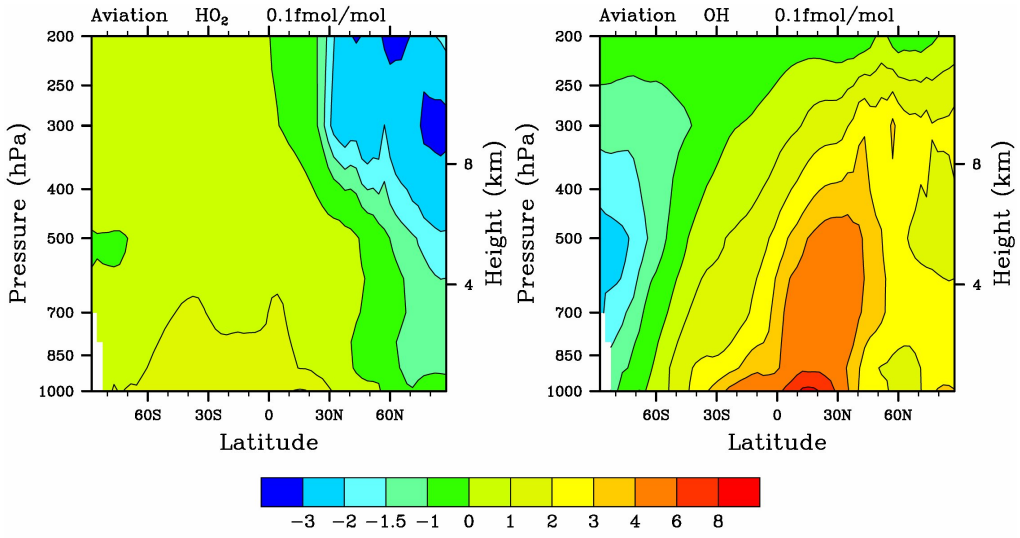

Figure 7.3: Zonal mean (pressure levels between 1000 hPa to 200 hPa) mixing ratios of aviation, 10^{-1} fmol/mol, for the species HO_2 (left) and OH (right).

The maximum HO_2 mixing ratios are simulated in the SH where also its vertical distribution exhibits large scale variation. In horizontal scale, the maximum mixing ratios are simulated covering the whole SH as well as in central Europe and USA (across the costs). In the NH both distributions show negative values as has been found for OH distribution in the SH (see Fig. 7.4). The negative values represent the depletion of the regarding species and are simulated in regions in which the other radical exhibits very small values. This is attributed to the internal relation between OH and HO_2 radicals. In particular, as the chemical scheme shows, the depletion of OH radical (via O_3, CO, NMHC etc) leads to HO_2 production and vice-versa (see chemical reactions 2.18 and 2.19). However, the highest mixing ratios are simulated for OH compared to HO_2. This can be attributed to the HO_x chemical cycle which starts with the production of OH and furthermore leads to HO_2 production (see Fig. 2.1).

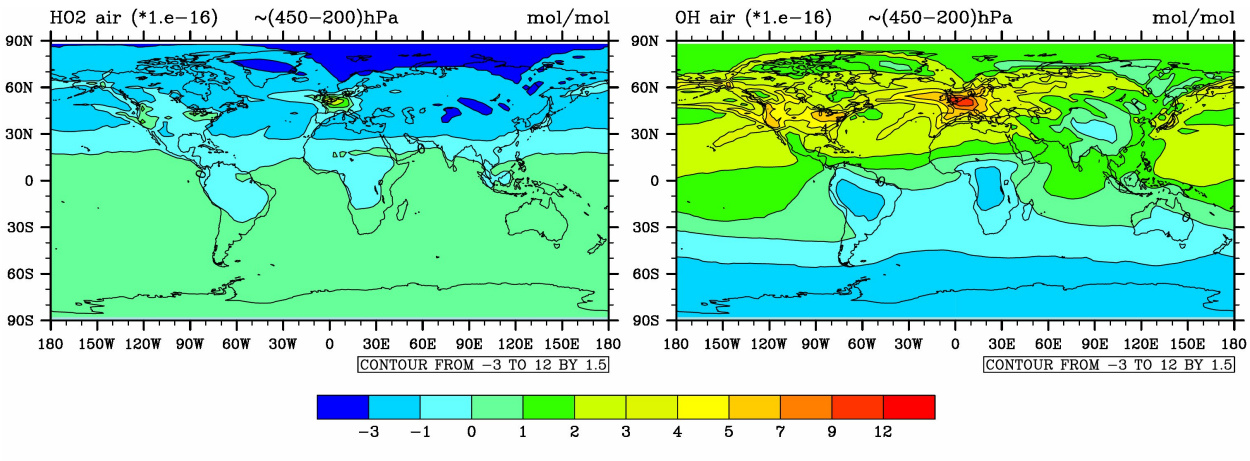

Figure 7.4: Horizontal distribution (pressure levels between 450 hPa to 200 hPa) of aviation, 10^{-1} fmol/mol for the species HO_2 (left) and OH (right).

Application for the aviation in the REACT4C project

The project REACT4C (Reducing Emissions from Aviation by Changing Trajectories for the benefit of Climate) (Matthes, 2012; Matthes et al., 2012) has as its main object the exploration of the optimal cruising routes of aircraft for reduce the emission as well as their fuel consumption. In order to investigate the impact of air traffic emissions on the climate, a measure which is so-called climate cost function is used. Climate cost functions are derived from complex climate-chemistry simulations which provide a measure of the atmospheric sensitivity to emissions in terms of climate impact (e.g. using average temperature response as a metric). The importance of the impacts of aircraft emissions to the atmospheric composition is related to these parameters since different grid points exhibit different chemical compositions. The focus on changes in ozone, methane and water vapor in conjunction to their radiative forcing link to the climate cost functions.

The HO_x tagging chemistry was applied to the AIRTRAC (V1.0) sub-model, within the chemistry climate model EMAC (see chapter 3), in order to calculate the depletion of methane by air traffic emissions (Grewe et al., 2014). Figure 7.5 shows the evolution of the contribution due to different chemical species (O_3, NO_x, H_2O and CH_4) to the atmospheric burden (Kg). In order to calculate the chemical evolutions, the tagging method, section 7.1, were used. In this study the chemical ratios of the related species H_2O, CO, RH, and CH_4 are not taken into consideration (see Table 7.1), since the contributions by aircraft emissions are very small. In particular, the methane depletion is dependent on the NO_x and O_3 concentrations. The increase of NO_x emissions by aviation leads to OH production via the chemical reaction 2.30 as well as to the O_3 production via the chemical reaction 2.30. The production of OH now (via the NO_y and O_3 contributions) leads to a decrease of CH_4 via the chemical reaction 2.4.

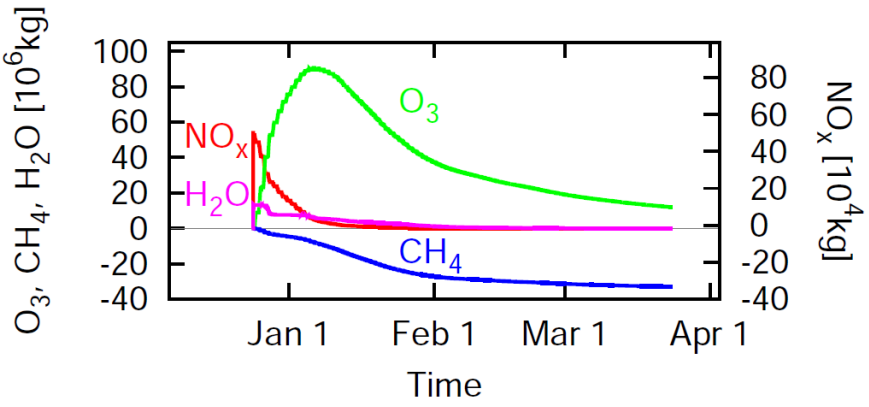

Figure 7.5: Contributions from NO_x and H_2O emissions in a certain time region to NO_x (red), ozone (green), methane (blue) and water vapor (magenta) global atmospheric masses [kg] (Grewe et al., 2014).

The comparison of the results were made with other studies, such as Stevenson et al. (2006) since observation data of aircraft emissions at flight altitude which are related to climate impact are not available. Stevenson et al. (2006) made the inter-comparison of different models due to ozone burden and methane lifetime and showed that the models simulate with consistently these sensitivities.

7.3 Discussions

In this chapter the tagging implementation in HO_x chemistry was presented. For the first time a tagged chemical scheme which describes the main principles of HO_x chemistry was developed and implemented via a climate chemistry model (CCM). This new HO_x tagged chemical scheme was attached in the previous tagged scheme (see chapter 5) with the included NO_y, PAN, CO, NMHC and O_3 tagged chemical compounds. The HO_x chemistry exhibits a strong difference compared to the other tagged chemical families (such as NO_y, NMHC) because firstly of the strong interaction between the molecules OH and HO_2 and secondly of their short life time (seconds).

The analysis was focused on the mixing ratios distribution of shipping and aviation emitting sectors. The maximum values of mixing ratios are found, for both emitting sectors, in the regions with the respective highest emissions rates. In particular, the maximum values of mixing ratios of HO_x family for shipping are found in the NH at mid latitudes. In comparison, the maximum values of mixing ratios for aviation are found also in the NH but reaching higher altitudes around 6 km (400 hPa). The OH mixing ratios are depending on the O_3 mixing ratios (see Fig. 2.1) since they are produced via the chemical reaction 2.1. For instance, this can be observed from the Fig. 7.2 and 6.13 for the shipping sector since the maximum values of the distributions of the tropospheric ozone and OH mixing ratios coincide.

Generally, it can be concluded that:

- The patterns of shipping and aviation emitting sectors show maximum values of mixing ratios, at the respective cruising regions. Also, the cruising lines are visible in the respective horizontal distributions.
- In the NH where the human activities play a dominant role for tropospheric ozone production (see Fig. 6.6) the OH values of mixing ratios are positive and higher than HO_2. This is because the photolysis ($h\nu$) of ozone which occurred form these sources, leads to OH production. Furthermore, the production of HO_2 is controlled from OH.

All in all, this is the first new study so as to describe the impacts of HO_x chemistry in the troposphere by emitting sectors. For future simulations more chemical reactions can be added (such as the photolysis of hydrogen peroxide, H_2O_2) to the existing HO_x tagging chemical scheme in order to better describe this complex chemical scheme. Finally, the comparison of HO_x distribution by aviation and shipping emission sectors have been made with Hoor et al. (2009) (see detailed description in chapter 8). The main important message is that both investigations are in agreement with respect to distributions by shipping and aviation emitting sectors.

Chapter 8

Final discussions

In order to estimate the contribution of different emission sources to the total concentration of species, several studies have been published (Grewe, 2007; Fuglestvedt et al., 2008; Wang et al., 2009; Hoor et al., 2009; Gromov et al., 2010; Horowitz and Jacob, 1999; Butler et al., 2011; Emmons et al., 2012; Dentener et al., 2003; Lamarque et al., 2010). As has been described in chapter 4, these approaches can be separated in two main categories. The first category is based on the perturbation method while the second one is based on the tagging methodologies. The tagging methodologies have different designs but have the tagged species in common. The contributions of the regarding emission categories can be quantified with respect to tagging methods by following the chemical reaction pathways due to the origin in the emission categories. For instance, Gromov et al. (2010) introduced a new tagging technique taking into consideration isotopes [1] with respect to a kinetic chemistry scheme. The isotopic composition is calculated via the ratio of the rare isotope to the abundant one. In comparison, the molecular concentrations are calculated based on the reaction kinetics of the particular chemical system. However, in the present study the contribution of the emitting sectors is based on the concentration of tagged chemical species. On the contrary, the perturbation method is based on the difference between two simulations the base case (all emissions) and the perturbation case which refers to the emissions of the respective category (see analytical description in section 4.2). Although, several studies (e.g (Grewe et al., 2010, 2012; Emmons et al., 2012; Wang et al., 2009)) have made comparisons between the perturbation and a certain tagging method. Grewe et al. (2012) investigated the NO_x contribution of road traffic emissions to ozone concentration. Their results show that the perturbation method underestimates by a factor of five the regarded contribution unlikely with the tagging method. Therefore, the main outcome of these investigations, which have focused on the tropospheric ozone contribution, related to the contribution of its precursors, has shown that the perturbation method does not provide a reliable estimate since it underestimates the total ozone contribution.

Horowitz and Jacob (1999) used a global three dimensional model of tropospheric chemistry to investigate how the emissions of the fossil fuel combustions influence the global distribution of NO_x and its reservoir NO_y, with respect to different world regions. In particular, they tagged

[1] Isotopes: same atoms with different number of neutrons but with the same atomic number

the NO_x and NO_y families in order to examine their relative contribution due to their concentrations. Their study was focused on Northern Hemisphere summer season from June to August. They found out that the 40% of the NO_x concentration in the lower and middle troposphere is attributed to fossil fuel combustion emissions. Also, the PAN contribution due to the NO_x contribution, is found to be important over the oceans due to its long path ways reaching values up to 80%. For instance, Horowitz and Jacob (1999) showed that, over the North Atlantic Ocean, half of the NO_x concentration is attributed to the United States fossil fuel contribution. Similarly, in the western North Pacific Ocean also the half of the NO_x concentration is attributed to the emissions from China. In the present study the sum of the emission sectors of industry and road traffic (land fossil fuel emissions) due to NO_y contribution is found to be around 60% in the lower Northern Hemisphere. This contribution difference can be attributed to the different input emission data set due to the increase of fossil fuel emissions throughout the years. Also, in the present study the model simulations correspond to a longer time period since winter seasons have been included (tow years model simulations). Both studies are in agreement with respect to the importance of the relative contribution of fossil fuel emissions in the same regions (lower Northern troposphere).

Grewe (2007) investigated the variability of tropospheric ozone by focusing on the impact of climate. He used the climate-chemistry model E39/C and his simulations covered the time period from 1960 to 1999. In principle, he examined how the contributions of nitric oxides emissions due to several sectors influence the concentration of tropospheric ozone. Grewe points out that lightning emissions of NO_x contributed up to 70% for NO_y and 40% for O_3 in the tropics and Southern Hemisphere. In the present study the NO_y and O_3 contribution by lightning for the same regions are simulated up to 60% and 37% respectively. The contribution differences are around 6.5% for both chemical compounds and are attributed firstly, to the additional contributors for tropospheric ozone concentration such as NMHC in the present study. Secondly, in the present study more tagging emission sectors have been included such as the CH_4 contribution, which may reduce the individual percentages of the respective emission sectors compared to Grewe (2007). Thirdly, the duration difference between the present study (three years) in comparison to Grewe (2007) (nine years) as well as to the different input data set may also contribute to this difference. For the Northern Hemisphere low troposphere, Grewe (2007) showed that industry and land transportation are the dominant sources for the ozone concentration up to 30% and 25% respectively. Both studies are well correlated not only due to the importance of sectors in conjunction with specific regions (tropics etc) but also due to the respective contribution values of O_3 and NO_y.

Hoor et al. (2009) implemented the perturbation method in six different models in order to investigate the impact of traffic emissions on ozone and OH. The emission sources have included aviation, shipping and land transportation. It was found that the most important contribution to ozone is simulated by shipping emissions. In particular, in the lower troposphere at NH, the $50,6\% \pm 10,9\%$ of the total traffic ozone contribution, is attributed to ships. The road traffic exhibits $36,7\% \pm 9,3\%$ and lastly the aviation is simulated close to $12,7\% \pm 2,9\%$ of the total ozone contribution. However, the maximum values 70% from aviation in the upper northern troposphere is attributed to the longer lifetime of NO_x and its reservoir PAN. In this investigation

the relative contributions among these three emitting sectors is well correlated with Hoor et al. (2009) since the shipping, road traffic and aviation contributions are close to 50%, 40% and 10%, respectively, in the lower troposphere at NH. However, in this study and for global mean values the road traffic ozone contribution is found around two times higher compared to shipping one.

However, both studies are in agreement with respect to HO_x chemistry distribution by aviation and shipping sectors. The horizontal distributions show maximum contributions in the northern hemisphere at mid-latitudes, by aircraft. Although, in the present study, the OH maximum contribution is simulated in central Europe in comparison to the northern Atlantic region between 30°W and 90°W, which is simulated by Hoor et al. (2009). With respect to shipping emissions, when the simulations by perturbation method correspond to summer season both methods show the maximum OH concentrations in the northern Atlantic and pacific oceans, close to 3 fmol/mol.

Emmons et al. (2012) implemented the tagging method in order to estimate the tropospheric ozone contribution by different emission sources, using the Model for Ozone and Related chemical Tracers (MOZART-4). They added artificial tracers (similar to the present study) without affecting the standard chemical scheme by tagging the NO_x emissions related to the sources. The emission sources are categorized into the anthropogenic surface sources, aviation, lightning, soil, biomass burning and stratosphere. The analysis showed that the surface anthropogenic emissions lead to the largest ozone contribution in the NH for both winter and summer seasons since in the SH the ozone contribution is much less. Also, the lightning contribution to ozone is dominant in the tropics. The aviation contribution which occurs in the upper troposphere is found to affect mainly the NH. Biomass burning is found to have a small ozone contribution compared to other sources but with a large seasonal variation in the tropics which maximized during summer. Similarly, the soil contribution is maximized during summer at mid-latitudes of both hemispheres. Lastly, the stratospheric contribution to tropospheric ozone is found to affect the tropopause regions reaching the 100 ppbv. All, these results with respect to individual distributions of ozone contribution are in agreement with this present study.

8.1 Uncertainties

The uncertainties of the present study are categorized in the three different factors: the input emissions, the model, which is used, and lastly, the tagging method. The emissions of different chemical compounds, such as CO, NMHC etc are imported via the sub-models OFFLEM or ONLEM (see detailed description Appendix C). The OFFLEM emissions are based on different datasets such as by Van der Werf et al. (2010) for biomass burning, by Lamarque et al. (2010) for industry and shipping, by Borken et al. (2007) for road traffic and by Lee et al. (2005) for aviation. In general, the uncertainties related to the offlem emissions are strongly dependent from

the different pollutants, regions and sectors. In principle, Van der Werf et al. (2010) estimate that the emission uncertainties due to biomass burning for global annual carbon sums are close to 20% even though these estimations are more reliable than their previous studies. Lamarque et al. (2010) point out that the uncertainties in regional emissions can be expected to be as large as a factor of two. Also, Borken et al. (2007) separate the uncertainties with respect to different road fuel consumption and showed that the global uncertainties are about 10% for gasoline and about 20% for diesel fuel. Although, for the countries which belong to the Organization for Economic Co-operation and Development (OECD) and therefore account for two thirds of the global road fuel consumption, the uncertainty is at the order of 5%.

In the model, the uncertainties are referring to the estimation of the rate coefficients of the respective chemical reactions. Also, the uncertainties due to the convection parameterisation for long-lived species such as CO and O_3, are less than 25% (Tost et al., 2010). However, for short-lived species the uncertainties reach up to $\pm$ 100 % (Tost et al., 2010). Lastly, it has to be emphasized, that since the tagging method is a mathematical approach, the uncertainties are associated with it are limited. In conclusion, the propagation of the uncertainties due to the emissions is the key aspect for the uncertainties in the results of this study.

Chapter 9

Summary and conclusion

The impact of different emission sectors to the atmospheric composition has been investigated by numerous studies (e.g. (Dameris et al., 1998; Grooß et al., 1998; Grewe et al., 2002a,b; Granier and Brasseur, 2003; Matthes et al., 2007; Grewe, 2007; Matthes et al., 2007; Hoor et al., 2009; Myhre et al., 2010; Koffi et al., 2010; Dahlmann et al., 2011)) by using different methodologies. Their results show that the tropospheric chemical composition due to anthropogenic activities has changed by increasing the concentrations of green house gases. Additionally, the NH exhibits the highest changes caused by man-made emissions. In order to understand how a specific emission sector can influence the chemical composition on the atmosphere, several theoretical methods have been published (e.g. (Fuglestvedt et al., 2008; Wang et al., 2009; Hoor et al., 2009; Gromov et al., 2010; Emmons et al., 2012; Horowitz and Jacob, 1999; Butler et al., 2011)).

In this thesis the summary of the perturbation and tagging methods were presented as well as having their differences highlighted. The tagging method (Grewe et al., 2010) was explicitly used in this investigation. The main feature of this method is that an entire chemical system can be tagged by following the reaction pathways of the particular chemical scheme as well as that the non-linearity of the chemical systems is taken into consideration. This method is applied to the global atmospheric chemistry-climate model, EMAC. The development focused on the tropospheric O_3 and HO_x chemistry whose important chemical equations have been taken into consideration. For the first time, the tropospheric ozone concentration is examined by taken into consideration the competitive species and families NO_y, CO, and NMHCs. Also, a chemical tagged scheme, which describes the main principles of the tropospheric HO_x chemistry has been developed and constitutes the only existing implementation in a global chemistry-climate model. Finally, the ten different chemical emission categories which constitute the total chemical contribution of each species, are: aviation, shipping, road traffic, industry, biomass burning, soils, lightning, stratosphere, CH_4 and N_2O. The combination of the chemical species and sectors leads to a complex system of seventy parameters.

The goals of this study are firstly, to investigate and compare the importance of the emission sectors for tropospheric ozone abundances by the analysis of their relative contributions. Secondly, the assessment of the relation between all the precursor concentrations to ozone concentration which showed the dominant species and regions. The last goal is, the analysis and comparison

of the ozone distribution by distinguishing its individual production and loss reaction rates.

The answers to the questions which were addressed in the begging of this investigation, (see section 1.2) are the following:

1. How can the contributions from different emissions sources to concentrations of trace gases be quantified?

   Implementing the tagging method means to consider the differential equations which describe the evolution of the concentrations of the tagged species by following the reaction path ways of a certain non-linear chemical scheme. In particular, the primary competed species (NO_y, CO, NMHC) are tagged based on the origin of the emission categories in order to quantify their contributions to the concentrations of the secondary tagged species (O_3, PAN, HO_x). In this study the origin of the emissions are categorized to the natural (lightning, biomass burning, soils, stratosphere, N_2O) and anthropogenic (industry, land transportation, ships, aviation) ones.

2. How important are the contributions from anthropogenic emission sources versus the natural ones and which are the main contributors for tropospheric ozone concentration?

   For the first time, the comparison of the contributions of the competitive species and families NO_y, CO, and NMHCs, to the ozone concentration was determined and shows a major contribution of methane to ozone in the tropics and industry emissions to NH mid-latitudes ozone concentrations. In particular, the natural sources are dominant in the SH compared to NH where the anthropogenic contributions are leading to ozone concentration. The total contribution from the anthropogenic sources to ozone mass is simulated close to 38%. In the tropical regions at higher altitudes (above to 4 km) lightning exhibit the highest contribution compared to all the other sectors. In the lower tropical regions biomass burning and methane are found to affect the tropical regions reaching global mean values around 19%. Lastly, the total ozone mass produced by anthropogenic emission sectors is simulated around $138\ Mt$ while the lightning sector is close to $115\ Mt$.

   Finally, this investigation focused on the individual contributions to ozone concentration at different altitudes. In particular, for the pressure levels until to 200 hPa, the sum of the individual natural ozone contributions is found around three times higher compared to anthropogenic ones. However, including pressure up to 100 hPa, the stratospheric contribution reaches the highest values close to 25% of atmospheric ozone burden. Lastly, in the lower troposphere (1000 hPa to 500 hPa) the sum of anthropogenic contributions is reaching around 40% with industry having the highest contribution of 17% compared to all the anthropogenic sectors.

3. What is the importance of individual production and loss rates to the ozone concentration?

In order to investigate the distribution of the tropospheric ozone contribution, its individual production and loss rates were examined. The ozone production is separated in two main reaction channels. The first reaction channel, P(A), determines the reactions between members of NO_y family with the HO_2 radical. The second reaction channel, P(B), corresponds to the reaction between members of NO_y family with members of NMHC family. Furthermore, the ozone loss rates are separated in five different reaction channels L(A), L(B), L(C), L(D) and L(E). The first two reaction channels L(A) and L(B) represent the ozone loss rates by the untagged OH and HO_2 radicals respectively. The third L(C) and the forth L(D) reaction channels represent the ozone loss rates from species which belong to NO_y and NMHC tagged families, respectively. Lastly, the fifth reaction channel contains the rest of the chemical species (untagged species) which are able to deplete the ozone (e.g. $H_2O + O(^1D)$).

The first step of this investigation included the analysis and comparison between two anthropogenic specific emission sectors: shipping and aviation. These two emission sectors are selected because, firstly they are found to be equally important with respect to the global atmospheric burden of ozone mass (4%), and secondly their maximum annual ozone concentrations are referring to the different pressure levels, given the difference in their cruising altitudes (shipping between: 1000 to 850 hPa and aviation between: 450 to 250 hPa). The conjunction between these two statements gave the opportunity to investigate the strength of the individual reaction channels firstly, with respect to two arbitrary grid points A_1 and A_2 and secondly, in terms of the different altitudes. Lastly, the third step, included the comparison among all the ten emission sectors in global mean values.

The analysis for the ozone production by the reaction channel P(A) is found to be around 35% higher compared to P(B) for both aviation and shipping emission sectors. This is in agreement with the total average percentage of all the emission sectors which are found to be around 60% of the total ozone production. However, the dominant reaction channel of ozone production by methane corresponds to P(B) whose contribution reaches around 95%. Nevertheless, the sum of P(A) production channels, from all the emission sectors, is around 48% higher compared to P(B). This is attributed of different reaction rates constant between the reaction channels, since the reaction channel P(A) has stronger reactivity because of the HO_2 radical. In the tropical regions higher photolysis rates occur which contribute to P(A) reaction channel.

For ozone loss rates, the maximum values of ships are about two times higher compared to aviation, at the respective cruise pressure levels. The leading reaction channel for ozone loss rates is the L(E) for both emission sources. However, the sum of the ozone loss rates by the untagged HO_x radicals (L(A)+L(B)) exhibits similar values compared to L(E) (by shipping: 47% and by aviation: 54%). This is in agreement with the total average by all the emission sectors since the sum of reaction channels L(C) and L(D), which correspond to NO_y and NMHC tagged families respectively, exhibit values lower than 5%.

4. How the individual transport emitting sources influence the HO_x chemistry?

   For the first time a HO_x tagging chemical scheme was developed and implemented via a climate chemistry model (CCM). In this case, the additional tagged species which were included to the previous chemical scheme are the OH and HO_2 radicals. Since these radicals consist of a chemical family and their chemical dependency between them is strong, the quantification of their contribution to the troposphere must be taken into consideration as a system and not independently. The first results with respect to the distribution of their contribution, by ships and aviation sectors, are reasonable and also in agreement with other studies such as (Hoor et al., 2009), which also quantifies the mean values of OH, by using the perturbation method. In particular, both studies show maximum contributions in the northern hemisphere at mid-latitudes, by aircraft. According to contribution of shipping to OH the maximum concentrations are simulated in the northern Atlantic and pacific oceans. Finally, it has to be emphasized that the application of HO_x tagging chemistry has already been used in REACT4C project (Reducing Emissions from Aviation by Changing Trajectories for the benefit of Climate).

For the first time, the extensive analysis of the contribution and distribution of non-linearly competing species and families (NO_y, CO, NMHC), to the tropospheric ozone concentration has been accomplished. This has come to fruition by applying the tagging method to a complex non-linear chemical scheme which constitutes a part of TAGGING sub-model which belongs to the global atmospheric chemistry-climate model, EMAC. The results of distribution of contributions of all emitted sectors in conjunction to all the different species and families are well presented and the main messages are in agreement with other studies. Also, more analysis can be done in order to better describe the contributions of HO_x sectors in the troposphere by adding more chemical reactions (such as the photolysis of hydrogen peroxide, H_2O_2) to the new existing HO_x tagging chemical scheme.

For future applications more simulations can be conducted in order to estimate future scenarios, due to climate change, with respect to different emission sectors. Also, different input emission data sets, in comparison to this present study, can be used in the model, in order to a better estimate the uncertainties in it. Finally, new chemical tagging schemes can be added, which describe the principles of stratospheric chemistry, in order to investigate the chemical influences to stratosphere by the anthropogenic emission sectors.

Appendix A

Tagging and perturbation method

Calculations steps for production and loss with respect to tagging method

The following equations show the calculation steps for $\mathrm{P}_{Z,i}(\mathrm{X}_i,\mathrm{Y}_i)$, $\mathrm{D}_{Z,i}(\mathrm{X}_i,\mathrm{Y}_i,\mathrm{Z}_i)$ and $\tilde{D}_{Z,i}(\mathrm{X}_i,\mathrm{Y}_i,\mathrm{Z}_i)$, respectively.

- $$P_{Z,i}(X_i, Y_i) = P_{XY}(X_iY_i + \sum_{i\neq j}\frac{1}{2}X_iY_j + \sum_{i\neq j}\frac{1}{2}X_jY_i) \tag{A.1}$$

$$= P_{XY}(X_iY_i + \frac{1}{2}X_i(Y - Y_i) + \frac{1}{2}Y_i(X - X_i))$$

$$= \frac{1}{2}P_{XY}(X_iY + XY_i)$$

- $$D_{Z,i}(X_i, Y_i, Z_i) = D_X(X_iZ_i + \sum_{i\neq j}\frac{1}{2}X_iZ_j + \sum_{i\neq j}\frac{1}{2}X_jZ_i) \tag{A.2}$$

$$+D_Y(Y_iZ_i + \sum_{i\neq j}\frac{1}{2}Y_iZ_j + \sum_{i\neq j}\frac{1}{2}Y_jZ_i) =$$

$$= D_X(X_iZ_i + \frac{1}{2}X_i(Z - Z_i) + \frac{1}{2}Z_i(X - X_i))$$

$$= D_Y(Y_iZ_i + \frac{1}{2}Y_i(Z - Z_i) + \frac{1}{2}Z_i(Y - Y_i)) =$$

$$= \frac{1}{2}D_X(X_iZ + XZ_i) + \frac{1}{2}D_Y(Y_iZ + YZ_i)) \tag{A.3}$$

Analysis of two chemical systems

The general solutions for the two chemical systems (corresponding solutions: $X^{eq}, Y^{eq}, Z^{eq}, \tilde{Z}^{eq}$), when the derivative is zero (steady-state solution, $\dot{X} = \dot{Y} = \dot{Z} = \dot{\tilde{Z}} = 0$), are:

$$X^{eq} = E_x \tau_x \tag{A.4}$$

$$Y^{eq} = E_y \tau_y \tag{A.5}$$

$$Z^{eq} = \frac{P_{xy} X^{eq} Y^{eq}}{D_x X^{eq} + D_{y_1} Y^{eq}} \tag{A.6}$$

$$\tilde{Z}^{eq} = \frac{P_{xy} X^{eq} Y^{eq}}{D_x X^{eq} + D_{y_2} Y^{eq} Y^{eq}} \tag{A.7}$$

Figure A.1 shows the equilibrium concentrations for the species Z^{eq} (isopleth lines - system 1) and $\tilde{Z}^{eq}$ (isopleth lines - system 2), for both systems according to solutions eq. A.6 (system 1) and eq. A.7 (system 2), as a function of the precursors X and Y. This figure illustrates similar ozone characteristics as it showed on the figure 2.5. In general, when both concentrations of X and Y are increased, the concentrations of species Z^{eq} and $\tilde{Z}^{eq}$, for the first and second chemical systems are also increased. Also, both chemical reaction systems manifest the same characteristics in the area under the blue line. In particular, it means that for the same combination changes for the precursors X and Y, the concentrations of Z^{eq} and $\tilde{Z}^{eq}$ would be the same for both systems. Another feature is that (vertical black line) the second system needs a richer environment of Y precursor so that the concentration of $\tilde{Z}^{eq}$ reaches equal concentration as the Z^{eq} (e.g. 175 ppbv to 200 ppbv).

Figure A.2 a) depicts the equilibrium concentrations for Z^{eq} (origin - red line) and $\tilde{Z}^{eq}$ (origin - blue line) for constant concentration of the precursor X (X = 20 ppbv). In the very early beginning, the rate of change of concentrations of Z^{eq} and $\tilde{Z}^{eq}$ are almost equal, $\dot{Z}^{eq} \simeq \dot{\tilde{Z}}^{eq}$, when Y is approximately until 12 ppbv. Also, an other aspect is that when the Y is between 15 ppbv and 46 ppbv, the concentration of $\tilde{Z}^{eq}$ is almost doubled compared to Z^{eq}. This is because the second chemical system (origin - blue line) needs a double amount of the Y concentration, in case it will deplete the same Z^{eq} molecules as the first (origin - red line), (see equations (A.3) and (B.3)). The second issue refers when the ratio between X and Y is constant ($\frac{X}{Y} = 10$), (solid lines). In this case, the first chemical system (solid - red line) has linear increase of Z^{eq} production as opposed to the second system (solid - blue line), which has a saturation effect.

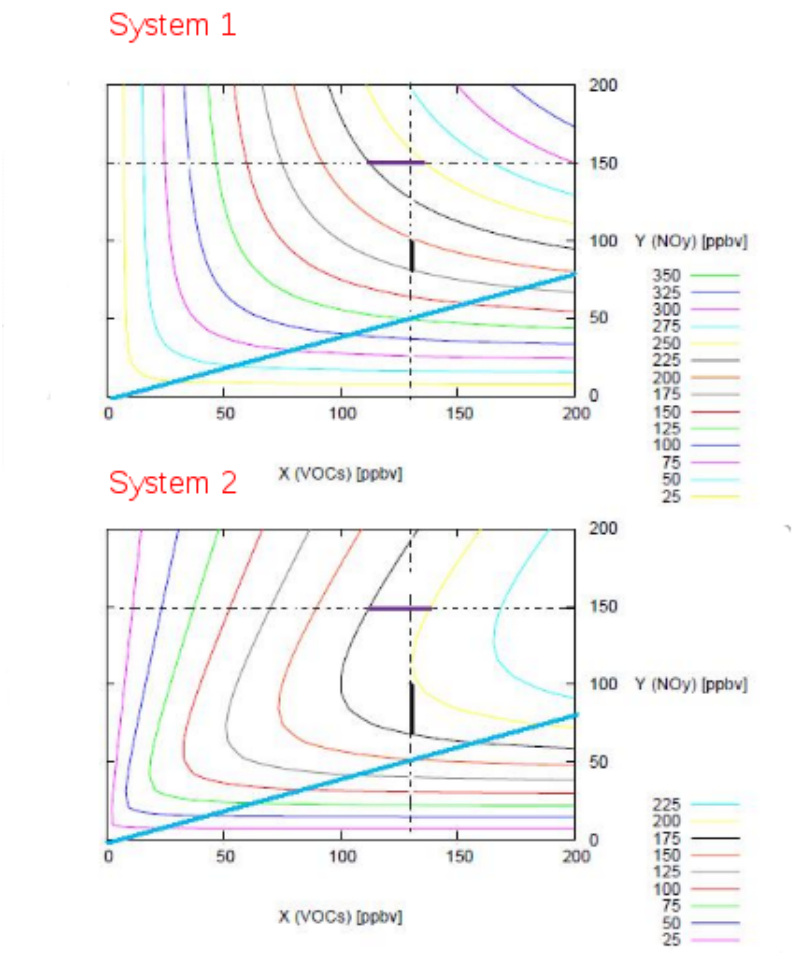

Figure A.1: Equilibrium concentrations for both systems Z(top) and $\tilde{Z}$ (bottom) as function of the pressures X and Y. The isopleth lines show typical ozone characteristics, as the figure 1.4 show (Grewe et al., 2010).

a) b)

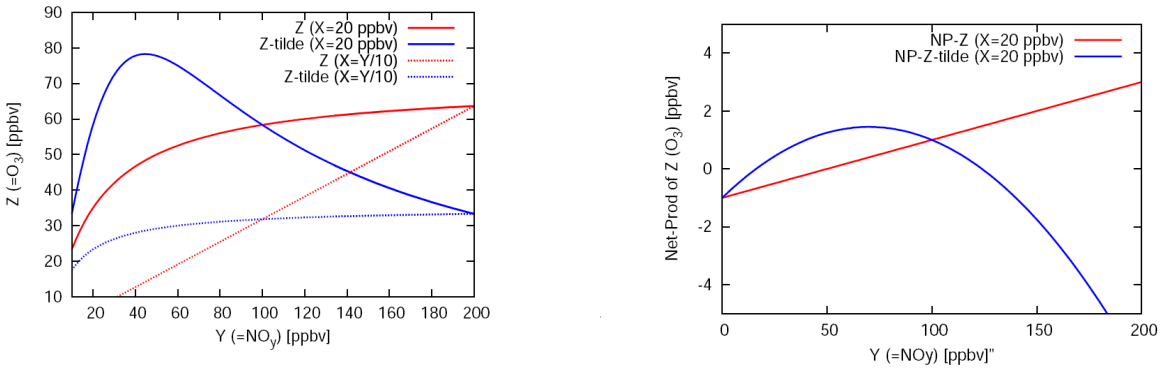

Figure A.2: **a)** (i) origin lines: Equilibrium concentrations of Z^{eq} and $\tilde{Z}^{eq}$ for constant X, 20 ppbv, as a function of Y.(ii) solid lines: Equilibrium concentrations of Z^{eq} and $\tilde{Z}^{eq}$ for constant ratio between X and Y. X/Y = 1/10 **b)** Net production rates (ppbv/sec) for production of species Z and $\tilde{Z}$ when X and Z ($=\tilde{Z}$) are constant between 20 ppbv and 40 ppbv respectively (Grewe et al., 2010).

Figure A.2 b) shows the net production rates (ppbv/sec) for both systems, when X has constant concentration 40 ppbv and Z (red line) has concentration equal to $\tilde{Z}$ (blue line) and is 20 ppbv. The first chemical system (red line) has linear characteristics through the increase of the Y concentration. The second reaction system (blue line) shows strong $\tilde{Z}$ production approximately until when Y is around 60 ppbv. When the concentration of Y is between 60 ppbv to 90 ppbv approximately, the net amount of $\tilde{Z}$ remains constant and for higher Y concentrations, the $\tilde{Z}$ is strongly decreasing.

Error analysis for perturbation method

Figure A.3, shows the error ε_α, depend on the factor α. As long as the factor α is getting smaller, the more accurate the perturbation method becomes. So, the first criterion is the accuracy of the determination of the contribution which depends from α. The sum of individual contributions has to be equal with the contribution of the total emission

The second error, ε_β, describes the part of the ozone contribution which will not be determined. The perturbation method underestimates the concentration of ozone. As Figure 4.2 shows, if the ratio $-\frac{\Delta^\alpha f}{\alpha}$ (green line) is going through the point e.g. $O_3(x_1)$, the ozone contribution will not be quantified form this method. It will be equal two the contribution which corresponds $O_3(x_1)$. The error ε_β describes the part of the ozone concentration which will not be quantified from the perturbation method.

a) b)

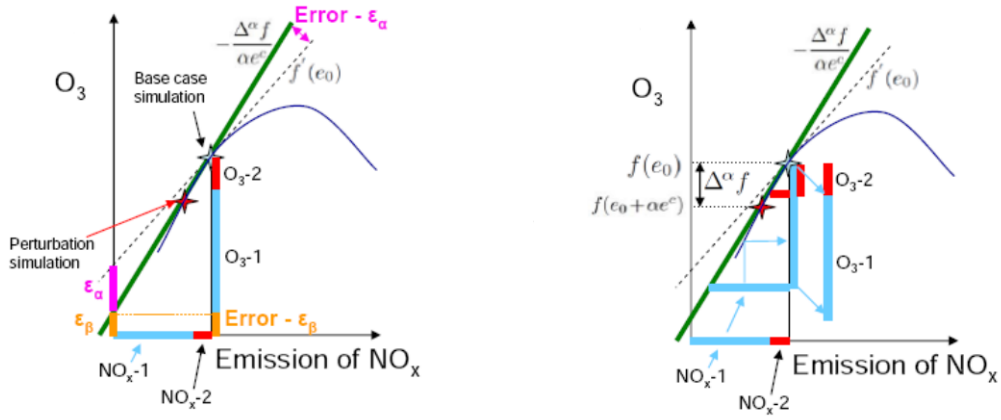

Figure A.3: a) Error analysis for the perturbation approach. The error ε_α describes the discrepancy between $f'(e_0)$ and $-\frac{\Delta^\alpha f}{\alpha}$ and ε_β the part of ozone concentration will not be determined. b) Two different emission categories, NO_x^1 and NO_x^2, and the corresponding ozone concentration O_3^2 and O_3^2, respectively (Grewe et al., 2010).

Solutions of the tagging and perturbation method

Tagging method

Species	Steady-state solution
$X_i^{eq} =$	$E_{x,i}\tau_x$
$Y_i^{eq} =$	$E_{y,i}\tau_y$
$Z_i^{eq} =$	$\frac{a_i}{c} - \frac{b_i}{c} Z^{eq}$ $a_i = P_{xy}\tau_x\tau_y(E_{x,i}E_y + E_x E_{y,i})$ $= P_{xy}(X_i^{eq}Y^{eq} + X^{eq}Y_i^{eq})$ $b_i = D_x\tau_x E_{x,i} + D_{y_1}E_{y,i}\tau_y$ $= D_x X_i^{eq} + D_{y_1}Y_i^{eq}$ $c = D_x\tau_x E_x + D_{y_1}E_y\tau_y$ $= D_x X^{eq} + D_{y_1}Y^{eq}$
$\tilde{Z}_i^{eq} =$	$\frac{a_i}{\tilde{c}} - \frac{\tilde{b}_i}{\tilde{c}} \tilde{Z}^{eq}$ $\tilde{b}_i = D_x X_i^{eq} + \frac{3}{4} D_{y_2} Y_i^{eq} Y^{eq}$ $\tilde{c}_i = D_x X_i^{eq} + \frac{2}{3} D_{y_2} (Y^{eq})^2$

Table A.1: Steady-state solutions ($\dot{X}_i = \dot{Y}_i = \dot{Z}_i = \dot{\tilde{Z}}_i = 0$) for both chemical systems using the tagging method.

Perturbation method

Species	Steady-state solution
$\delta_i^\alpha X =$	$E_{x,i}\tau_x$
$\delta_i^\alpha Y =$	$E_{y,i}\tau_y$
$\delta_i^\alpha Z =$	$\frac{a_i}{c+\alpha b_i} + \frac{\alpha P_{xy}\tau_x\tau_y E_{x,i}E_{y,i}}{c+\alpha b_i} - \frac{b_i P_{xy}\tau_x\tau_y E_x E_y}{c+(c+\alpha b)}$ $a_i = P_{xy}\tau_x\tau_y(E_{x,i}E_y + E_x E_{y,i})$ $= P_{xy}(X_i^{eq}Y^{eq} + X^{eq}Y_i^{eq})$ $b_i = D_x\tau_x E_{x,i} + D_{y_1}E_{y,i}\tau_y$ $= D_x X_i^{eq} + D_{y_1}Y_i^{eq})$ $c = D_x\tau_x E_x + D_{y_1}E_y\tau_y$ $= D_x X^{eq} + D_{y_1}Y^{eq})$ $d_i = P_{xy}\tau_x\tau_y E_{x,i}E_{y,i}$
$\delta_i^\alpha \tilde{Z} =$	$\frac{a_i+\alpha d_i}{\tilde{c}+\tilde{h}} - \frac{\tilde{b}_i-\tilde{g}_i}{\tilde{c}+\tilde{h}+\alpha(\tilde{b}_i-\tilde{g}_i)}\tilde{Z}^{eq}$ $\tilde{b}_i = D_x X_i^{eq} + \frac{3}{4}D_{y_2}Y_i^{eq}Y^{eq}$ $\tilde{c}_i = D_x X_i^{eq} + \frac{2}{3}D_{y_2}(Y^{eq})^2$ $\tilde{g}_i = \frac{2}{3}D_{y_2}Y_i^{eq}Y^{eq} - \alpha D_{y_2}(Y_i^{eq})^2$ $\tilde{h} = \frac{1}{3}D_{y_2}(Y^{eq})^2$

Table A.2: Steady state solutions for both chemical systems using the perturbation method.

Appendix B

Chemistry

List of NOx and NMHC species

Table B.1: List of tracers which belong to NOy and NMHC families

NO_y familiy	**NMHC family**	
N	CH_3OH	MVK
NO	C_3H_8	$MVKO_2$
NO_2	CH_3O_2	MVKOOH
NO_3	HCHO	MEK
N_2O_5	HCOOH	$LMEKO_2$
HONO	C_2H_6	LMEKOOH
HNO_3	CH_3OOH	BIACET
HNO_4	C_2H_4	$LC_4H_9NO_3$
NACA	$C_2H_5O_2$	C_5H_8
MPAN	C_2H_5OOH	ISO_2
$IC_3H_7NO_3$	CH_3CHO	ISOOH
$LC_4H_9NO_3$	CH_3CO_2H	ISON
ISON	CH_3CO_3	$LC_4H_9O_2$
$ClNO_3$	CH_3CO_3H	LC_4H_9OOH
$BrNO_3$	NACA	NC_4H_{10}
	C_3H_8	$IC_3H_7NO_3$
	C_3H_6	MPAN
	$IC_3H_7O_2$	MGLYOX
	IC_3H_7OOH	ACETOL
	$LHOC_3H_6O_2$	HYPERACET
	$LHOC_3H_6OOH$	$CH_3COCH_2O_2$
	CH_3COCH_3	

List of chemical equations

1. **Equations for O_3 chemistry**

A. P(A) production channel : NO_y + HO_2

$NO + HO_2 \longrightarrow NO_2 + OH$

B. P(B) production channel: NO_y + NMHC

$CH_3O_2 + NO \longrightarrow HCHO + NO_2 + HO_2 + ...$

$C_2H_5O_2 + NO \longrightarrow CH_3CHO + HO_2 + NO_2 + ...$

$CH_3CO_3 + NO \longrightarrow CH_3O_2 + NO_2 + ...$

$LHOC_3H_6O_2 + NO \longrightarrow CH_3CHO + HO_2 + NO_2 + LC_4H_9NO_3 + ...$

$CH_3COCH_2O_2 + NO \longrightarrow NO_2 + CH_3CO_3 + HCHO + ...$

$LC_4H_9O_2 + NO \longrightarrow NO_2 + MEK + HO_2 + C_2H_5O_2 + ...$

$MVKO_2 + NO \longrightarrow NO_2 + CH_3CO_3 + MGLYOX + ...$

$LMEKO_2 + NO \longrightarrow CH_3CO_3 + NO_2 + LC_4H_9NO_3 + ...$

$ISO_2 + NO \longrightarrow NO_2 + MVK + HCHO + ...$

A. L(A) loss channel: O_3 + OH

$OH + O_3 \longrightarrow HO_2 + O_2$

B. L(B) loss channel: O_3 + HO_2

$HO_2 + O_3 \longrightarrow OH + O_2$

C. L(C) loss channel: O_3 + NO_y

$NO + O_3 \longrightarrow NO_2 + O_2$

$NO_2 + O_3 \longrightarrow NO_3 + O_2$

$NO_3 + HO_2 \longrightarrow NO_2 + ...$

$CH_3O_2 + NO_3 \longrightarrow NO_2 + ...$

$HCHO + NO_3 \longrightarrow HNO_3 + ...$

$C_2H_5O_2 + NO_3 \longrightarrow NO_2 + ...$

$CH_3CHO + NO_3 \longrightarrow HNO_3 + ...$

$CH_3CO_3 + NO_3 \longrightarrow NO_2 + ...$

$C_5H_8 + NO_3 \longrightarrow ISON + ...$

$N_2O_5 + H_2O \longrightarrow HNO_3 + HNO_3$

D. L(D) loss channel: O_3 + NMHC

MVK + $O_3 \longrightarrow$ HCOOH + MGLYOX + CH_3CO_3 + ...

$C_2H_4 + O_3 \longrightarrow$ HCOOH + ...

$C_3H_6 + O_3 \longrightarrow$ HCHO + ...

$C_5H_8 + O_3 \longrightarrow$ HCOOH + CO + ...

ISOP + $O_3 \longrightarrow$ HCOOH + MVK + ...

E. L(E) loss channel: O_3 + X

$H_2O + O^1D \longrightarrow ... \longrightarrow 2OH$

$N_2O + O^1D \longrightarrow ... \longrightarrow 2NO$

$N_2O + O^1D \longrightarrow ... \longrightarrow N_2 + O_2$

$CH_3Cl + O^1D \longrightarrow ... \longrightarrow OH + Cl$

$CH_3CCl_3 + O^1D \longrightarrow ... \longrightarrow OH + 3Cl$

$CH_3SO_2 + O_3 \longrightarrow ... \longrightarrow CH_3SO_3 + O_2$

2. **Equations for HO_x chemistry**

A. OH production:

$H_2O + O^1D \longrightarrow 2OH$ **(P'1)**$\times 2$

$HO_2 + O_3 \longrightarrow OH + 2O_2$ **(P'3)**

$NO + HO_2 \longrightarrow NO_2 + OH$ **(P'4)**

B.OH loss:

$OH + O_3 \longrightarrow HO_2 + O_2$ **(D'1)**

$OH + NMHC \xrightarrow{O_2} NMHC + H_2O$ **(D'2)**

$OH + CO \xrightarrow{O_2} HO_2 + CO_2$ **(D'4)**

$OH + HO_2 \longrightarrow H_2O + O_2$ **(D'5)**

$OH + NO_2 \longrightarrow HNO_3$ **(D'7)**

C. HO_2 production:

$OH + CO \xrightarrow{O_2} HO_2 + CO_2$ **(P1)**

$OH + O_3 \longrightarrow HO_2 + O_2$ **(P3)**

$NMHC + NO \longrightarrow NMHC + HO_2 + NO_2$ **(P4)**

D. HO_2 loss:

$HO_2 + O_3 \longrightarrow OH + 2O_2$ **(D1)**

$NO + HO_2 \longrightarrow NO_2 + OH$ **(D2)**

$NMHC + HO_2 \longrightarrow NMHC + O_2$ **(D3)**

$HO_2 + HO_2 \longrightarrow H_2O_2 + O_2$ **(D4)**

$OH + HO_2 \longrightarrow H_2O + O_2$ **(D5)**

Annual mixing ratio for shipping and aviation sectors

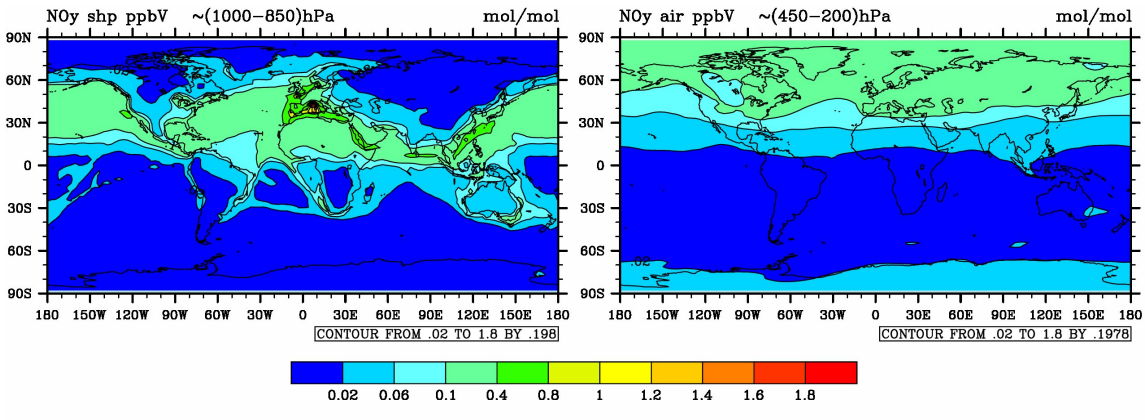

Figure B.1: Annual mixing ratio of NO_y, for shipping and aviation sectorsin ppb(mol/mol).

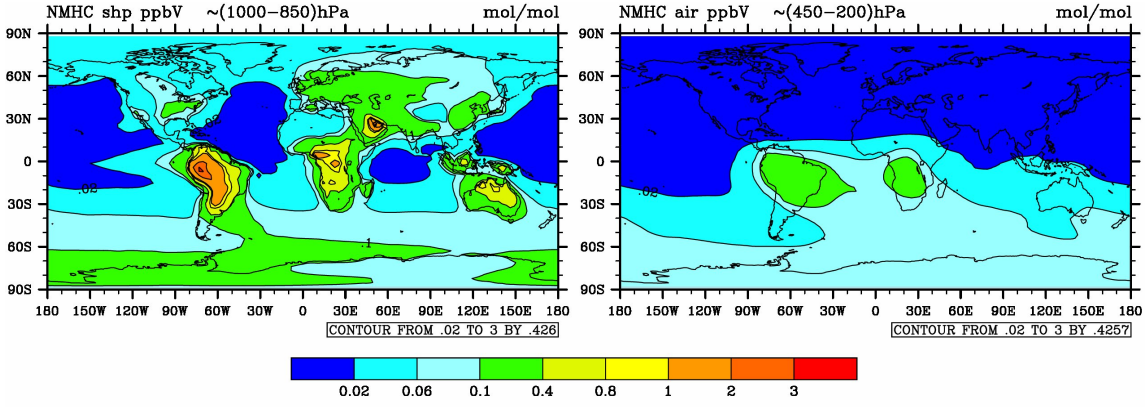

Figure B.2: Annual mixing ratio of NMHC, for shipping and aviation sectors in ppb(mol/mol).

Appendix C

Emissions data set

The input emissions are separated in two categories, the man made emissions which are calculated based on different emissions datasets via OFFLEM sub-model and the emissions coming form natural sources. The emissions from natural sources include: Lightning-soils-methane-nitric dioxide-stratosphere, and are computed via ONLEM sub-model. Onlem emissions calculations implies that, natural conditions according to the different places, such as wind speed, solar cycle etc are taken into consideration at each time step. These categories are strongly dependent on these factors.

- Man-made

Man-made input emissions are calculated via offlem and are based on different datasets (Table C.1). The emissions from industry and shipping are based on IPCC dataset and include emissions from NMHC, CO and NO_x for the 1850-2000 time period (Lamarque et al., 2010). The horizontal resolution is spread into $0.5^\circ \times 0.5^\circ$ grid boxes for latitude and longitude and the inventory covers 40 world regions. High emissions from industry found in the northern hemisphere, with China exhibiting the most relatively important ones compared to US and W.Europe. The emissions from road traffic include NMHC, CO and NO_x species and cover 216 countries and are based on QUANTIFY dataset. The road transportation emitted is of the order of 10^6 tons, including all the species, for the year 2000 (Borken et al., 2007). Emissions in northern America are higher by a factor of two, more than Europe. Emissions from aviation are based on QUANTIFY dataset and include NO_x emissions (Lee et al., 2005). Biomass burning emissions are based on Global Fire Emissions Database, version 3, (GFED, 3.1) over 1997-2009 year period. Fire is one of the most important contributors of trace gases into the atmosphere in last decades by humans. For this time period carbon emissions were $2.0\,\mathrm{PgCyear}^{-1}$. More sensitive are the tropical regions, Africa 52% and South America 15% , because of the deforestation, degradation and peat land fires (Van der Werf et al., 2010). Emissions from NMHC, CO and NO_x are taken into account.

	Sources	Input emissions
On-line	Lightning	-
	Soils	-
	CH_4	-
	N_2O	-
	Stratosphere	-
Off-line	Biomass burning	Van der Werf et al. (2010)
	Industry	IPCC Lamarque et al. (2010)
	Shipping	IPCC Lamarque et al. (2010)
	Road traffic	QUANTIFY Borken et al. (2007)
	Aviation	QUANTIFY Lee et al. (2005)

Table C.1: List of the ten different emission sources and their data set files.

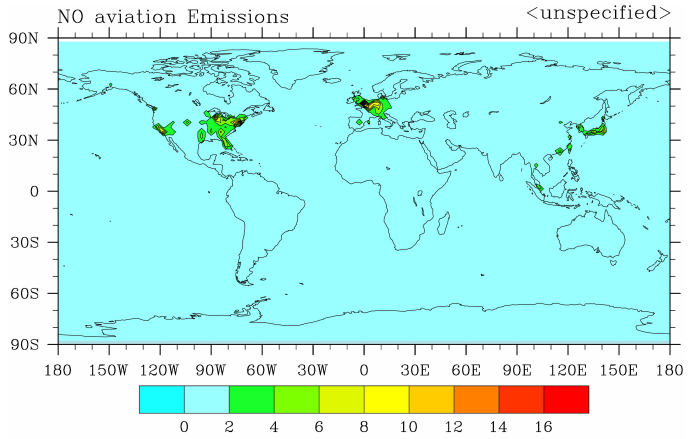

Figure C.1: Air traffic emissions: NO 10^{-9} mol/mol/sec.

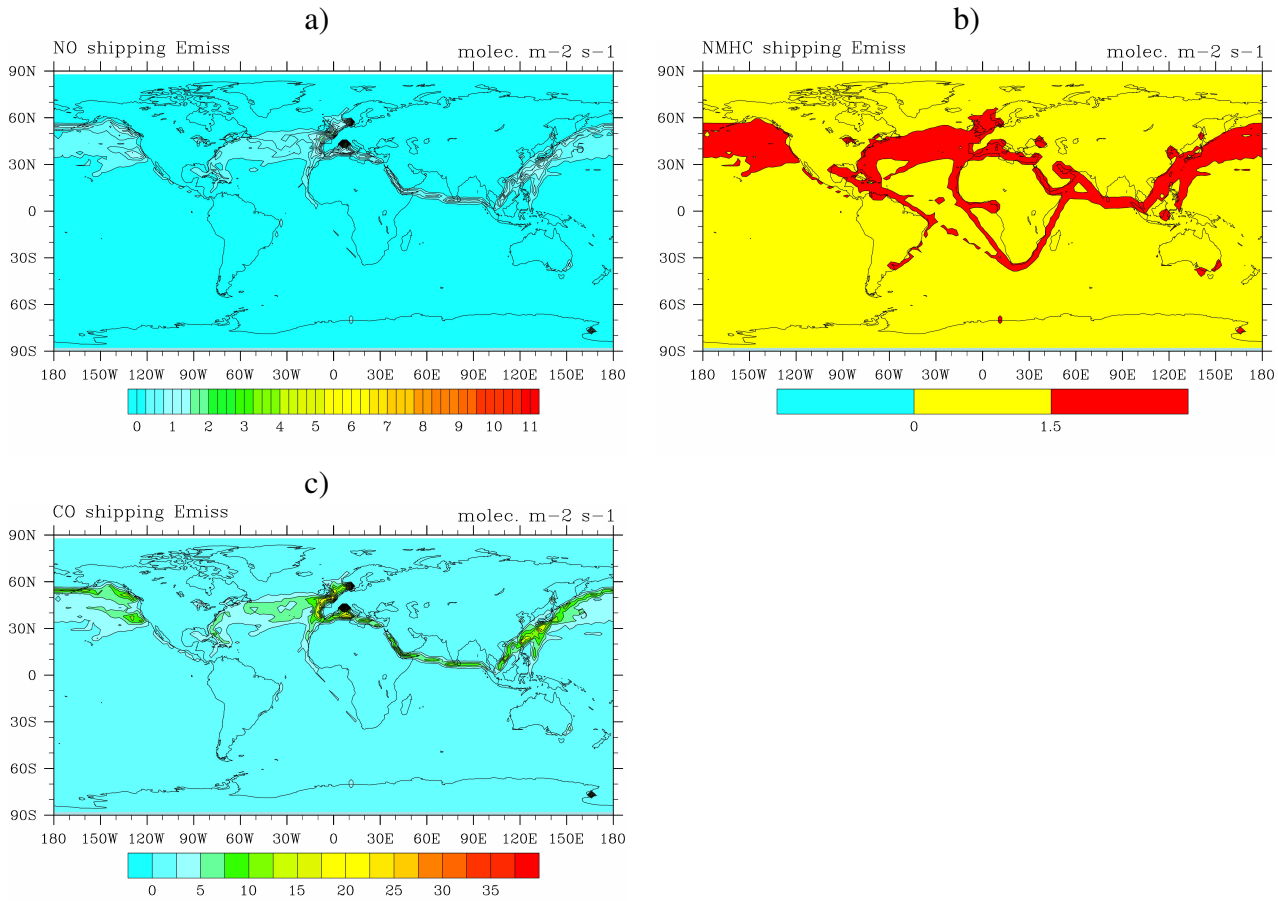

Figure C.2: Shipping emissions: a) NO 10^{-14} , b) NMHC and c) CO 10^{-12} mol/mol/sec.

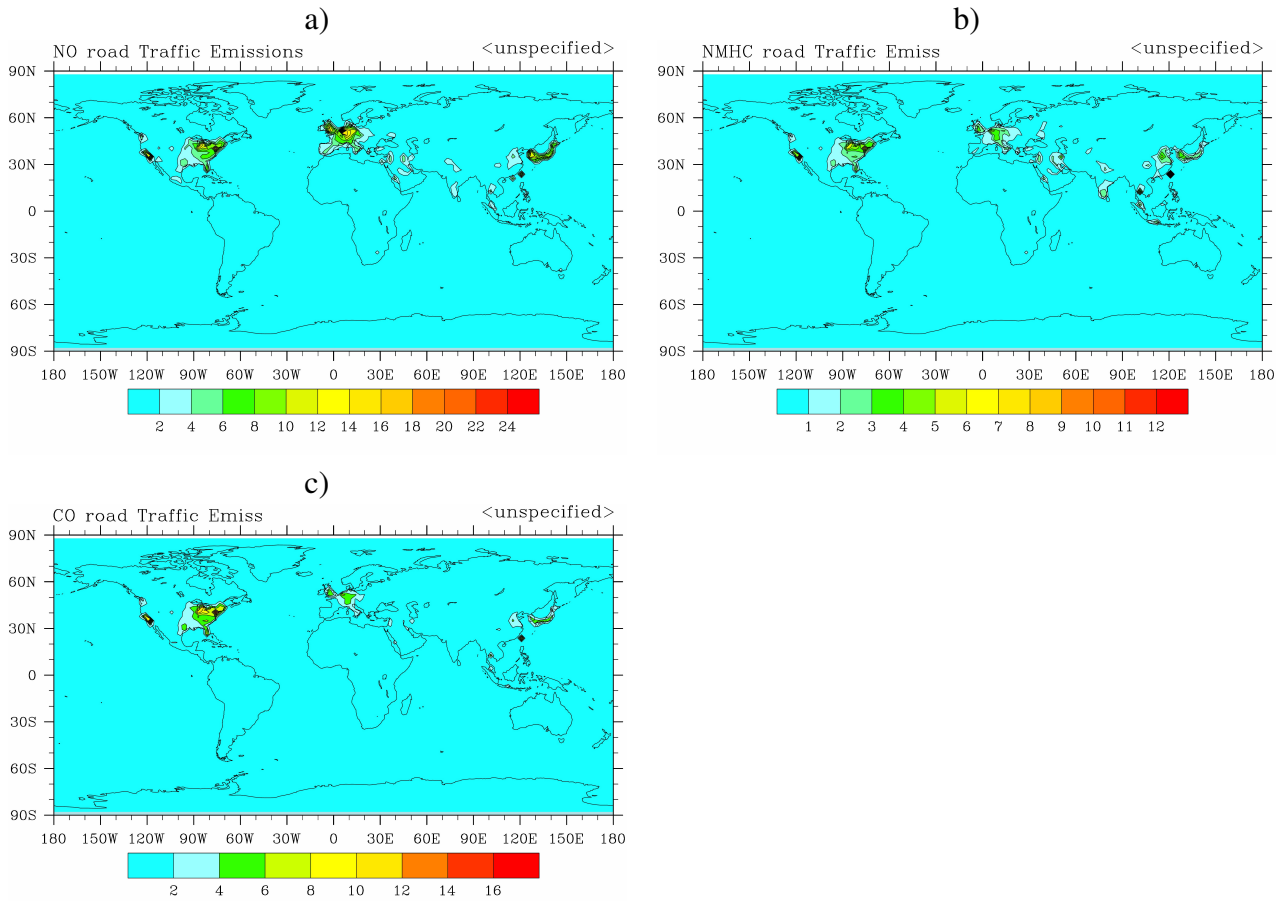

Figure C.3: Road traffic emissions: a) NO 10^{-14} , b) NMHC 10^{-14} and c) CO 10^{-15} mol/mol/sec.

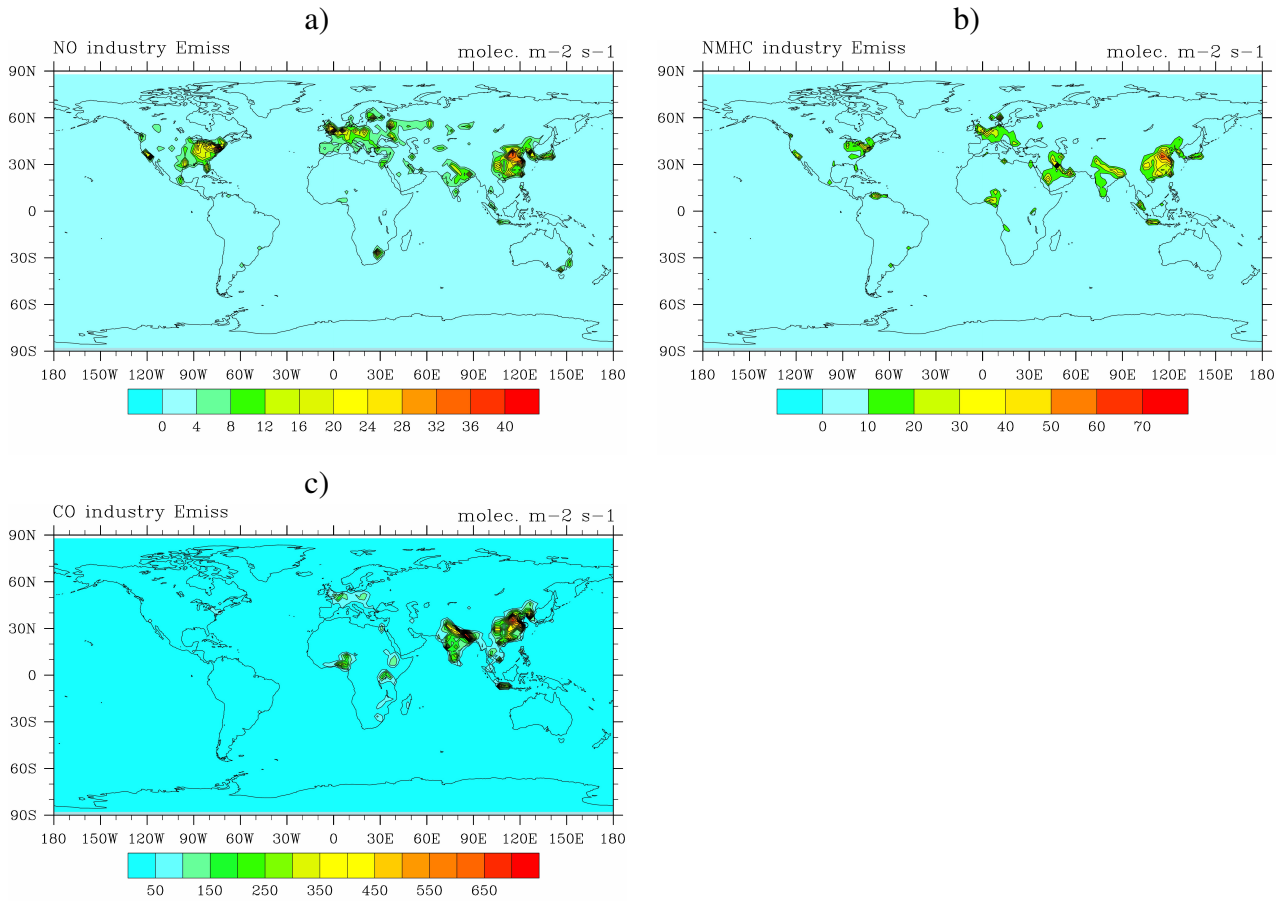

Figure C.4: Industry emissions: a) NO, b) NMHC and c) CO 10^{-13} mol/mol/sec.

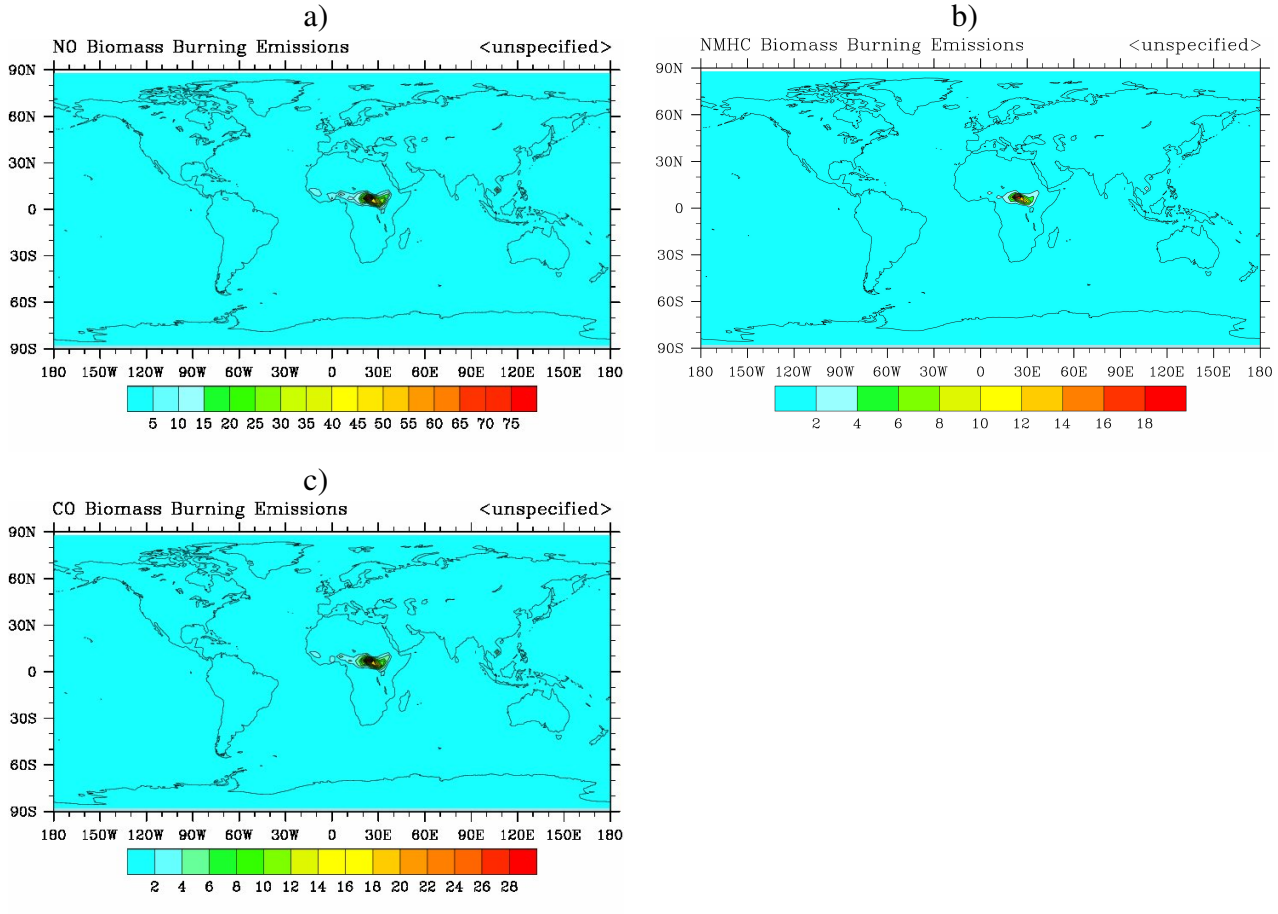

Figure C.5: Biomass burning emissions: a) NO 10^{-10}, b) NMHC 10^{-11} and c) CO 10^{-12} mol/mol/sec.

Bibliography

Atkinson, R. (1990). Gas-phase tropospheric chemistry of organic compounds. *Atmospheric Environment*, 24A, No 1.:1–41.

Atkinson, R., Baulch, D., Cox, R., Crowley, J. N., Hampson, R., Hynes, R., Jenkin, M., Rossi, M., and Troe, J. (2003). Evaluated kinetic and photochemical data for atmospheric chemistry: Volume i - gas phase reactions of ox, hox, nox and sox species. *Atmospheric Chemistry and Physics*, 3:6179–6699.

Blinova, E. N. (1943). Hydrodynamic theory of pressure waves, temperature wave and atmospheric actions centers. *Doklady Akademii nauk SSSR*, 39:284–287.

Bojkov, R. (1988). Ozone changes at the surface and in the free troposphere, in tropospheric ozone: Regional and clobal scale interactions. *I.S.A. Isaksen, Ed., D. Reidel Publishing Company*, pages 83–96.

Borken, J., Steller, H., Meretei, T., and Vanhove, F. (2007). Global and country inventory of road passenger and freight transportation-their fuel consumption and their emissions of air pollutants in the year 2000. *Transport. Res. Rec.*, doi:10.3141/2011-14,2007.

Brewer, A. (1949). Evidence for a world circulation provided by the measurements of helium and water vapour distribution in the stratosphere. *Quarterly Journal of the Royal Meteorological Society*, 75:351–363.

Butler, T., Lawrence, M., Taraborrelli, D., and Lelieveld, J. (2011). Multi-day ozone production potential of volatile organic compounds calculated with a tagging method. *Atmospheric Environment*, 45:4082–4090.

Crutzen, P. (1973). A discussion of the chemistry of some minor constituents in the stratosphere and troposphere. *Pure and Applied Geophysics*, 106-108:1385.

Crutzen, P. (1974). Photochemical reactions initiated by and influencing ozone in unpolluted tropospheric air. *Tellus*, 26:47.

Crutzen, P. (1979). The role of no and no2 in the chemistry of the troposphere and stratosphere. *Annual Review of Earth and Planetary Sciences*, 7:443.

Crutzen, P., Lawrence, M., and Pöschl, U. (1999). On the background photochemistry of tropospheric ozone. *TELLUS*, 51A-B:123–146.

Crutzen, P. and Zimmermann, P. (1991). The changing photochemistry of the troposphere. *Tellus*, 43AB:136–151.

Dahlmann, K., Grewe, V., Ponater, M., and Matthes, S. (2011). Quantifying the contributions of individual nox sources to the trend in ozone radiative forcing. *Atmospheric Environment*, 45:2860–2868.

Dameris, M., Grewe, V., Köhler, I., Sauen, R., Bruhl, C., Grooß, J.-U., and Steil, B. (1998). Impact of aircraft nox emissions on tropospheric and stratospheric ozone. part ii:3-d model results. *Atmospheric Environment*, 32:3185–3199.

Denman, K., Brasseur, G., Chidthaisong, A., Ciais, P., Cox, P., Dickinson, R., Hauglustaine, D., Heinze, C., Holland, E., Jacob, D., Lohmann, U., Ramachandran, S., da Silva Dias, P., Wofsy, S., and Zhang, X. (2007). *Couplings Between Changes in the Climate System and Biogeochemistry.* Climate Change 2007: The Physical Science Basis. Contribution of Working Group I to the Fourth Assessment Report of the Intergovernmental Panel on the Climate Change. Cambridge University Press, Cambridge, United Kingdom and New York, NY, USA.

Dentener, F., Van Weele, M., Krol, M., Houweling, S., and Van Velthoven, P. (2003). Trends and inter-annual variability of methane emissions derived from 1979-1993 global ctm simulations. *Atmospheric Chemistry and Physics*, 3:73–88.

Dobson, G. B. (1956). Origin of distribution of the polyatomic molecules in the atmosphere. *Proceedings of the Royal Society of London*, 236A:187–193.

Dobson, G. B., Harrison, D. N., and Lawrence, J. (1927). Measurements of amount of ozone in the earth's atmosphere and its relation to other geophysical conditions. *American Meteorological Society*, 55:364–365.

Emmons, L., Hess, P., Lamarque, J., and Pfister, G. (2012). Tagged ozone mechanism for mozart-4, cam-chem, and other chemical transport models. *Geoscientific Model Development*, 5:1949–1985, doi:10.5194.

Feister, W. and Warmbt, W. (1987). Long-term measurements of surface ozone in the german democratic republic. *Journal of Atmospheric Chemistry*, 5.

Finlayson-Pitts, B. and Pitts, J. N. (1997). Tropospheric air pollution: ozone airborne toxics, polycyclic aromatic hydrocarbons, and particulates. *Science*, 276:1045–1051.

Folkins, I. and Chatfield, R. (2000). Impact of acetone on ozone production and oh in the upper troposphere at high nox. *Journal of Geophysical Research*, 105:11,585–11,599.

Forster, P., Ramaswamy, V., Artaxo, P., Berntsen, T., Betts, R., Fahey, D., Haywood, J., Lean, J., Lowe, Myhre, G., Nganga, J., Prinn, R., Raga, G., Schultz, M., and Dorland, R. (2007). Climate change 2007: The physical science basis. contribution of working group i to the fourth assessment report of the intergovernmental panel on climate change. *Changes in Atmospheric Constituents and in Radiative Forcing. Cambridge University Press, Cambridge, United Kingdom and New York, NY, USA.*, pages 129–234.

Fowler, D., Flechard, C., Skiba, U., Coyle, M., and Cape, J. (1998). The atmospheric budget of oxidized nitrogen and its role in ozone formation and deposition. *New Phytologist*, 139:11–23.

Fuglestvedt, J., Berntsen, T., Myhre, G., Rypdal, K., , and Skeie, R. (2008). Climate forcing from the transport sectors. *Proceedings of the National Academy of Sciences. USA*, 105(2):454–458.

Granier, C. and Brasseur, G. (2003). The impact of road traffic on global tropospheric ozone. *Geophysical Research Letters*, 30:1086, doi:10.1029/2002GL015972.

Grewe, V. (2007). Impact of climate variability on tropospheric ozone. *Science of the Total Environment*, 374:167–181.

Grewe, V. (2009). Impact of lightning on air chemistry and climate in h.d. betz, u. schumann und p. laroche, eds, 'lightning: Principles, instruments and applications review of modern lightning research. *Springer Verlag*, pages pp.524–551.

Grewe, V., Dahlmann, K., Matthes, S., and Steinbrecht, W. (2012). Attributing ozone to nox emissions: Implications for climate mitigation measures. *Atmospheric Environment*, 59:102–107.

Grewe, V., Dameris, M., Fichter, C., and Lee, S. (2002a). Impact of aircraft nox emissions. part 2: effects of lowering the flight altitude. *Meteorologische Zeitschrift*, 3:197–205.

Grewe, V., Dameris, M., Fichter, C., and Sausen, R. (2002b). Impact of aircraft nox emissions. part 1: Interactively coupled climate-chemistry simulations and sensitivities to climate-chemistry feedback, lightning and model resolution. *Meteorologische Zeitschrift*, 11:177–186.

Grewe, V., Frömming, C., Matthes, S., Brinkop, S., Ponater, M., Dietmüller, S., Jöckel, P., Garny, H., Tsati, E., Dahlmann, K., Søovde, O., Fuglestvedt, J., Berntsen, T., Shine, K., Irvine, E., Champougny, T., and Hullah, P. (2014). Aircraft routing with minimal climate impact: the react4c climate cost function modelling approach (v1.0). *Geoscientific Model Development*, 7, 175-201:doi:10.5194.

Grewe, V., Tsati, E., and Hoor, P. (2010). On the attribution of contributions of atmospheric trace gases to emissions in atmospheric model applications. *Geoscientific Model Development*, 3:487–499.

Gromov, S., Jöckel, P., Sander, R., and Brenninkmeijer, C. (2010). A kinetic chemistry tagging technique and its application to modelling the stable isotopic composition of atmospheric trace gases. *Geoscientific Model Development*, 3:337–364.

Grooß, J., Bruhl, C., and Peter, T. (1998). Impact of aircraft emissions on tropospheric and stratospheric ozone. part i: Chemistry and 2-d model results. *Atmospheric Environment*, 32:3173–3184.

Hansen, J. and Lacis, A. (1990). Sun and dust versus greenhouse gases: an assessment of their relative roles in global climate change. *Nature*, 346:713.

Hansen, J., Sato, M., Ruedy, R., Nazarenko, L., Lacis, A., Schmid, G., Russell, G., Aleinov, I., Bauer, M., Bauer, S., Bell, N., Cairns, B., Canuto, V., Chandler, M., Cheng, Y., Del Genio, A., Faluvegi, G., Fleming, E., Friend, A., Hall, T., Jackman, M., Kelley, M., Kiang, N., Koch, D., Lean, J., Lerner, J., Lo, K., Menon, S., Miller, R., Minnis, P., Novakov, T., Oinas, V., Perlwitz, J., Perlwitz, J., Rind, D., Romanou, A., Shindell, D., Stone, P., Sun, S., Tausnev, N., Thresher, D., Wielicki, B., Wong, T., Yao, M., and Zhang, S. (2005). Efficacy of climate forcing. *Journal of Geophysical Research*, 110:D18104, doi:10.1029/2005JD005776.

Holton, J., Haynes, P. H., Mclntyre, M., Douglass, A., Rood, R., and Pfister, L. (1995). Stratosphere-troposphere exchange. *Reviews of Geophysics*, 33,4:403–439.

Hoor, P., Borken-Kleefeld, J., Caro, D., Dessens, O., Endressen, O., Gauss, M., Grewe, V., Hauglustaine, D., Isaksen, I., Jöckel, P., Lelieveld, J., Myhre, G., Meijer, E., Olivie, D., Prather, M., Schnadt Poberaj, C., Shine, K., Staehelin, J., Tang, Q., Van Aardenne, J., Van Velthoven, P., and Sausen, R. (2009). The impact of traffic emissions on atmospheric ozone and oh: results from quantify. *Atmospheric Chemistry and Physics*, pages 3113–3136.

Horowitz, L. and Jacob, D. (1999). Global impact of fossil fuel combustion on atmospheric nox. *Journal of Geophysical Research*, 104(D19):23823–23840.

IPCC (2001). A report of working group i of the intergovernmental panel on climate change. Technical report, ¡http://www.ipcc.ch/¿.

IPCC (2013). Climate change, the physical science basis of the intergovernmental panel on climate change. Technical report, ¡http://www.ipcc.ch/¿.

Jacob, D. (2004). *Introduction to Atmospheric Chemistry*.

Janach, W. (1989). Surface ozone: trend details, seasonal variations, and interpretations. *Journal of Geophysical Research*, 94:18289.

Jeffries, H. and Crouse, R. (1990). Scientific and technical issues related to the application of incremental reactivity. *Dept. Environmental Sciences and Engineering , Univ. North Carolina, Chapel Hill, NC*.

Jöckel, P., Sander, R., Kerkweg, A., Tost, H., and Lelieveld, J. (2005). Technical note: the modular earth submodel system (messy) - a new approach towards earth system modelling. *Atmospheric Chemistry and Physics*, 5:433–444.

Jöckel, P., Tost, H., Pozzer, A., Brühl, C., Buchholz, J., Ganzeveld, L., Hoor, P., Kerkweg, A., Lawrence, M., Sander, R., Steil, B., Stiller, G., Tanarthe, M., Taraborrelli, D., van Aardenne, J., and Lelieveld, J. (2006). The atmospheric chemistry general circulation model echam5/messy1: consistent simulation of ozone from the surface to the mesosphere. *Atmospheric Chemistry and Physics*, 6:5067–5104.

Johnston, H., Kinnison, D., and Wuebbles, D. (1989). Nitrogen oxides from high altitudes aircraft: an update of potential effects on ozone. *Journal of Geophysical Research*, 94:16,351–16,363.

Karnosky, D., Skelly, M., Percy, K., and Chappelka, A. (2007). Perspectives regarding 50 years of research on effects of tropospheric ozone air pollution on us forests. *Environmental Pollution*, 147:489–506.

Kerkweg, A., Sander, R., Tost, H., and Jöckel, P. (2006). Technical note: Implementation of prescribed (offlem), calculated (onlem), and pseudo-emissions (tnudge) of chemical species in the modular earth submodel system (messy). *Atmospheric Chemistry and Physics*, 6:3603–0609.

Kirner, O., Ruhnke, R., Buchholz-Dietsch, J., Jöckel, P., Brühl, C., and Steil, B. (2010). Simulation of polar stratospheric clouds in the chemistry-climate-model emac via the submodel psc. *Geoscientific Model Development*, 4:169–182.

Kley, D., Geiss, H., and V.A., M. (1993). Concentrations and trends of tropospheric ozone and precursor emissions in the united states and europe. *Atmospheric Environment*.

Koffi, B., Szopa, S., Cozic, A., Hauglustaine, D., and Van Velthoven, P. (2010). Present and future impact of aircraft, road traffic and shipping emissions on global tropospheric ozone. *Atmospheric Chemistry and Physics*, 10:11681–11705.

Kraus, A., Rohrer, F., Grobler, E., and Ehhalt, D. (1996). The global tropospheric distribution of nox estimated by a three-dimensional chemical tracer model. *Journal of Geophysical Research*, 101:18,587–18,604.

Lacis, A., Wuebbles, D., and Logan, J. (1990). Radiative forcing of climate by changes in the vertical distribution of ozone. *Journal of Geophysical Research*, 95:9971–9981.

Lamarque, J.-F., Bond, T., Eyring, T., Granier, C., Heil, A., Klimont, Z., Lee, D., Liousse, C., Mieville, A., Owen, B., Schultz, M., Shindell, D., Smith, S., Stehfest, E., Van Aardenne, J., Cooper, O., Kainuma, M., Mahowald, N., McConnell, J., Naik, V., Riahi, K., and van Vuuren, P. (2010). Historical (1850-2000) gridded anthropogenic and biomass burning emissions of reactive gases and aerosols: Methodology and application. *Atmospheric Chemistry and Physics*, 10:7017–7039,doi:10.5194/acp–10–7017–2010.

Landgraf, J. and Crutzen, P. (1998). An efficient method for online calculations of photolysis and heating rates. *Journal of the Atmospheric Science*, 55(5):863–878.

Lee, D. S., Owen, B., Graham, A., Fichter, C., Lim, L. L., and Dimitriu, D. (2005). Allocation of international aviation emissions from scheduled air traffic-present day and historical. *Final Report to DEFRA Global Atmosphere Division, Manchester Metropolitan University, Centre for Air Transport and the Environment*, Manchester, UK.

Lerdau, M. and Keller, M. (1997). Control on isoprene from trees in a subtropical dry forest. *Plant, Cell and Environment*, 20:569–578.

Logan, A., Prather, J., Wofsy, S., and McElroy, M. (1981). Tropospheric chemistry: A global perspective. *Journal of Geophysical Research*, 86:7210–7254.

London, J., S. and Lui (1992). Long-term tropospheric and lower stratospheric ozone variations from ozone sonde observations. *Journal of Atmospheric and Solar-Terrestrial Physics*, 54:599.

Matthes, S. (2012). Climate-optimised flight planning - react4c in innovation for a sustainable aviation in a global environment proceedings of the sixth european aeronautics days 2011. *IOS Press & European Union*, ISBAN:978–92–79–22968–8.

Matthes, S., Grewe, V., Sausen, R., and Roelofs, G.-J. (2007). Global impact of road traffic emissions on tropospheric ozone. *Atmospheric Chemistry and Physics*, pages 1707–1718.

Matthes, S., Schumann, U., Grewe, V., Frömming, C., Dahlmann, K., Koch, D., and Mannstein, H. (2012). Climate optimized air transport edited by: Schumann u. *Springer , Heidelberg New York, Dordrecht, London*, ISBAN 978 3 642 30182 7:doi: 10.1007–978–3–642–30183–4.

McConnell, J. and Jin, J. J. (2008). Stratospheric ozone chemistry. *Atmosphere-Ocean*, 46:69–92.

McMurry, J. (1984). *Organic Chemistry*. BROOKS/COLE, CENGAGE Learning.

Monks, P. (2005). Gas-phase radical chemistry in the troposphere. *Chemical Society Reviews*, DOI:10.1039/b307982c.

Myhre, G., Shine, K., Rädel, G., Gauss, M., Isaken, I., Tang, Q., Prather, J., Williams, J., Van Velthoven, P., Dessens, O., Koffi, B., Szopa, S., Hoor, P., Grewe, V., Borken-Kleefeld, J., Berntsen, T., and Fuglestvedt, J. (2011). Radiative forcing due to changes in ozone and methane caused by the transport sector. *Atmospheric Environment*, 45:387–394.

Myhre, G., Shine, K., Radel, G., Gauss, M., Isaksen, I., Tang, Q., Prather, M., Williams, J., Van Velthoven, P., Dessens, O., Koffi, B., Szopa, S., Hoor, P., Grewe, V., Borken-Kleefeld, J., Berntsen, T., and Fuglestvedt, J. (2010). Radiative forcing due to changes in ozone and methane caused by the transport sector. *Atmospheric Environment*, pages 387–394.

Olson, J. R., Crawford, J. H., Chen, G., Brune, W. H., Faloona, I. C., Tan, D., Harder, H., and Martinez, M. (2006.). A revaluation of airborne hox observations from nasa field campaigns. *Journal of Geophysical Research*, 111:doi:10.1029.

Oltmans, S., Lefohn, A., Harris, M., Galbally, I., Scheel, H., Bodeker, G., Brunke, E., Claude, H., Tarasick, D., Johnson, B., Simmonds, P., Shadwick, D. anf Anlauf, K., Hayden, K., Schmidlin, F., Fujimoto, T., Akagi, K., Meyer, C., Nichol, S., Davies, J., Redondas, A., and Cuevas, E. (2006). Long-term changes in tropospheric ozone. *Atmospheric Environment*, 40:3156–3173.

Oltmans, S., Lefohn, A., Scheel, H., Harris, M., Levyll, H., Galbally, I., Brunke, E., Meyer, C., Lathrop, J., Johnson, B., Shadwick, D., Cuevas, E., Schmidlin, F., Tarasick, D., Claude, H., Kerr, J., Uchino, O., and Mohnen, V. (1998). Trends of ozone in the troposphere. *Geophysical Research Letters*, 24:139–142.

Roberts, J. (1990). The atmospheric chemistry of organic nitrates. *Atmospheric Environment*, 24:243–287.

Roeckner, E., Arpe, K., Bengtsson, L., Christoph, M., Claussen, M., Dümenil, L., Esch, M., Giorgetta, M., U., S., and Schulzweida, U. (1996). The atmospheric general circulation model echam4: Model description and simulation of present-day climate. report 218. Technical report, Max Planck Institut für Meteorologie, Hamburg. Germany.

Roeckner, E., Bäuml, G., Bonaventura, L., Brokopf, R., Esch, M., Giorgetta, M., Hagemann, S., Kirchner, I., Kornblueh, L., Manzini, E., Rhodin, A., Schlese, U., Schulweida, U., and Tompkins, A. (2003). The atmospheric general circulation model echam5, part i. Technical report, Max-Planck-Institut für Meteorologie.

Roeckner, E., Brokopf, R., Esch, M., Giorgetta, M., Hagemann, M., Kornblueh, L., Manzini, E., Schlese, U., and Schulzweida, U. (2006:). Sensitivity of simulated climate to horizontal and vertical resolution in the echam5 atmosphere model. *Journal of Climate*, 19:3771–3791.

Rossby, C. (1939). Relation between variabiations in the intensity of the zonal circulation of the atmosphere and the displacement of the semipermanent centers of action. *Journal of Marine Research*, 2:38–55.

Sander, R., Kerkweg, A., Jöckel, P., and Lelieveld, J. (2005). Technical note: The comprehensive atmospheric chemistry module mecca. *Atmospheric Chemistry and Physics*, 5:445–450.

Schmitt, A. and Brunner, B. (1997). Emissions from aviation and their development over time, in : Pollutants from air traffic - results of atmospheric research 1992-1997. final report on the bmbf verbundprogramm "schadstroffe in der luftfahrt". *Tech. Report, DLR- Mitteillung*, 97-04:1–301.

Schumann, U. (1997). The impact of nitrogen oxides emissions from aircraft upon the atmosphere at flight altitudes - results from the aeronox project . *Atmospheric Environment*, 31:1723–1733.

Schumann, U. and Wurzel, D. (1994). Impact of emissions from aircraft and spacecraft upon the atmosphere. *DLR-Mitteilung*, 94-06:ISSN 0939–298X.

Seinfeld, J. and Pandis, S. (2006). *Atmospheric chemistry and physics, from air pollution to climate change*. A WILEY-INTERSCIENCE PUBLICATIONS.

Simmons, A., Burridge, D., Jarraud, M., Girard, C., and Wergen, W. (1989). Development of the numerical formulations and the impact of increased resolution. *Meteorology and Atmospheric Physics*, 40:28–60.

Staehelin, J. and Schmid, W. (1991). Trend analysis of tropospheric ozone concentrations utilizing the 20-year data set of balloon soundings over payerne (switzerland). *Atmospheric Environment*, 25A:1739.

Stevenson, D., Dentener, F., Schultz, M., Ellingsen, K., Van Noije, T., Wild, O., Zeng, G., Amann, M., Atherton, S., Bell, N., Bergmann, D., Bey, I., Butler, T., Cofala, J., Collins, W., Derwent, R., Doherty, R., Drevert, J., Eskes, H., Fiore M., Gauss, M. H. D. H. W., Isaken, I., Krol, M., Lamarque, J., Lawrence, M., Montanaro, V., Müller, J., Pirati, G., Prather, M., Pyle, A., Rast, S., Rodriguez, M., Sanderson, M., Savage, N., Shindell, D., Strahan, S., Sudo, K., and Szopa (2006). Multimodel ensemble simulations of present-day and near-future tropospheric ozone. *Journal of Geophysical Research*, 111:1029.

Stevenson, D., Young, P., Naik, V., Lamarque, J., Shindell, D., Voulgarakis, A., Skeie, R., Dalsoren, S., Myhre, G., Berntsen, T., Folberth, G., Rumbold, S., Colins, W., MacKenzie, I., Doherty, R., Zeng, G., Van Noije, T., Strunk, A., Bergmann, D., Cameron-Smith, P., Plummer, D., Strode, S., Horowitz, L., Lee, Y., Szopa, S., Sudo, K., Nagashima, T., Josse, B., Cionni, I., Righi, M., Eyring, V., Conley, A., Bowman, K., Wild, O., and Archibald, A. (2013). Tropospheric ozone changes, radiative forcing and attribution to emissions in the atmospheric chemistry and climate model intercomparison project (accmip). *Atmospheric Chemistry and Physics*, 13:3063–3085.

Tost, H. (2006). Global modelling of cloud, convection and precipitation influences on trace gases and aerosols,. *Ph.D thesis, Rheinischen Friedrich-Wilhelms-Universität Bonn*.

Tost, H., Jöckel, P., Kerkweg, A., Sander, R., and Lelieveld, J. (2006). Technical note: A new comprehensive scavenging submodel for global atmospheric chemistry modelling. *Atmospheric Chemistry and Physics*, 6:565–574.

Tost, H., Lawrence, M., Brühl, C., Jöckel, P., Team, T. G., and Team, T. S.-O.-D. (2010). Uncertainties in atmospheric chemistry modelling die to convection parameterisations and subsequent scavenging. *Atmospheric Chemistry and Physics*, 10:1931–1951.

Van der Werf, G., Randerson, J., Giglio, L., Collatz, G., Mu, M., Kasibhatla, P., Morton, D., DeFries, R. S., Jin, Y., and Van Leeuwen, T. T. (2010). Global fire emissions and the contribution of deforestation, savanna, forest, agricultural, and peat fires (1997-2009). *Atmospheric Chemistry and Physics*, 10, doi:10.5194/acp-10-11707-2010:11707–11735.

Vingarzan, R. (2004). A review of surface ozone background levels and trends. *Atmospheric Environment*, 38:3431–3442.

Von Kuhlmann, R. (2001). *Tropospheric Photochemistry of Ozone, its Precursors and the Hydroxyl Radical: A 3D-Modeling Study Considering Non-Methane Hydrocarbons.* University of Mainz, Dissertation.

Wang, W.-C., Shi, G.-Y., and Kiehl, J. (1991). Incorporation of the thermal radiative effect of ch4, n2o, cfcl3 and cf2cl2 into the ncar community climate model. *Journal of Geophysical Research*, 96:9097.

Wang, Z., Chien, C.-J., and Tonnesen, G. (2009). Development of a tagged species source apportionment algorithm to characterize three-dimensional transport and transformation of precursors and secondary pollutants. *Journal of Geophysical Research*, 114:D21206, doi:10.1029.

Wege, K., Claude, R., and Hartmannsgruber (1989). "several results from 20 years of ozone observations at hohenpeissenberg", in ozone in the atmosphere. *Deepak Publishing*, pages 109–112.

Acknowledgements

First of all, I would like to thank Prof. Dr. Martin Dameris for his support and helpful advice for entire course of this work. All his comments have improved this thesis and are greatly appreciated.

I also would like to thank Prof. Dr. Bernhart Mayer for being the second corrector of my PhD thesis.

Specially thanks go to my supervisor Dr. Volker Grewe for accepting me at the German Aerospace Center (DLR) and thus giving me the great opportunity to write my PhD thesis at the Institute for Atmospheric Physics (IPA), Oberpfaffenhofen, Germany. Many thanks for your great help, support and time to discuss my work, which made it possible to accomplish it.

I would like to thank Dr. Patrick Jöckel for his significant help with the EMAC model. I thank Dr. Sigrun Matthes for her help and support not only in science but for also other aspects of my life. I thank my roommate Roland Eichinger for the great moments we had during our PhDs. I thank Dr. Mattia Righi for his help in NCL. Also, I would like to thank the whole department "Erdsystem-Modellierung" for the nice moments I had during all these years.

I also acknowledge Prof. Dr. Robert Sausen, Prof. Dr. Markus Rapp and Prof. Dr. Urlich Schuhmann for gave me the opportunity to work at the Institute for Atmospheric Physics (DLR-IPA).

I would like to thank my parents: Ourania and Dimitris and my lovely brothers: Stratos and Angelos for their constant love and support throughout my life.

Last but not least, I would like to express my deepest gratitude to all my friends: Vassiliki, Guillermo, Ingo, Sanne, Basti, Nantia and Antigoni for their support in all aspects of my life and being by my side whenever I need them!